POLITECNICO DI TORINO

Ph.D. in Electrical, Electronics and Communications Engineering

Doctoral Thesis

Carbon-based materials for desalination and energy harvesting from salinity gradients

Supervisors:
Prof. Andrea Lamberti
Prof. Candido Fabrizio Pirri

Candidate:
Alessandro Pedico

June 2021

Abstract

Carbon-based materials have been developed, characterized and tested for desalination and energy harvesting application. In particular, novel functionalized graphene oxide has been synthesized by steps of reduction and functionalization with charged acrylate monomers (both positive and negative) and mixed with activated carbon to obtain novel capacitive electrodes.

The materials have been fully characterized by scanning electron microscopy, thermogravimetric techniques, infrared spectroscopy, energy dispersive x-ray analysis and other characterization techniques, including electrochemical ones.

These materials have been successfully employed in electrodes used to produce desalinated water through capacitive deionization, showing an improved desalination efficiency. The same materials have also been employed to harvest energy from salinity gradients through capacitive mixing, a novel technique recently proposed in literature.

Table of contents

1. Introduction

1.1 Overview

Worldwide, there is an always increasing demand of freshwater. Human settlements, industries, animal farms and agriculture put a challenge to engineers and material scientists to provide always larger amount of freshwater in the most efficient and economical way.

Since the freshwater on the Earth is only 3% of the total water (Fig. 1) and, even worse, the available surface freshwater (mostly lakes and rivers) is less than 1% of the previous [1], the necessity of new ways to produce freshwater becomes evident.

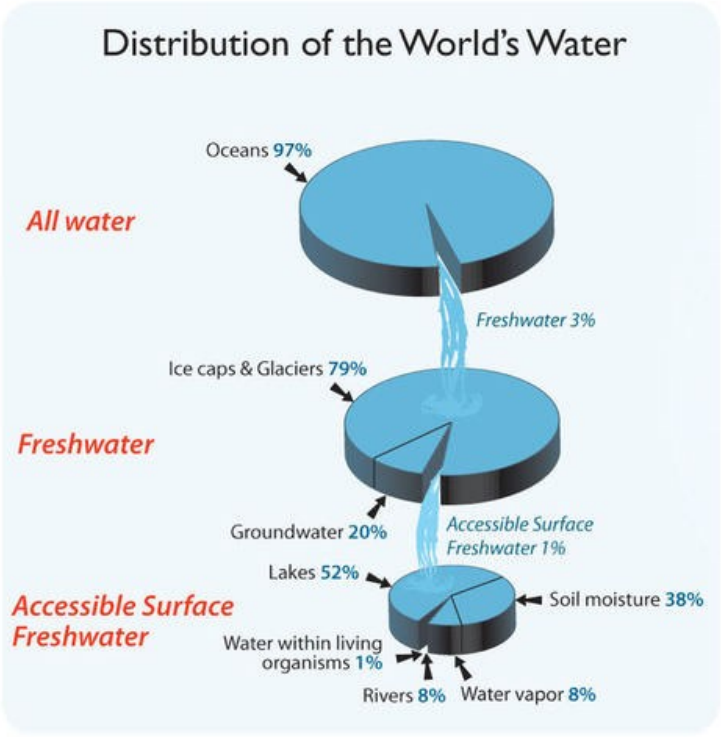

Fig. 1: Distribution of water on Earth [2]. From top to bottom: the total amount of water on Earth, the distribution of freshwater, the distribution of accessible surface freshwater.

Desalination of seawater is the most feasible solution, even the only way to supply drinkable water to cities, factories and cultivated land for countries suffering the scarcity of freshwater. Actually, the most widespread technology for water desalination is the reverse osmosis [3], which is based on membranes.

Countries like Israel and Saudi Arabia have large plants able to produce up to 10^7 litres of freshwater per hour. However, the power consumption of these plants is in the order of 30~100 MW. Such an energy consumption is related mostly to the fact that seawater

has to be pressurized up to 60~80 bar to allow the permeation of water through the membranes, while rejecting the salt.

To lower the energy amount required by the whole desalination process, the researchers are working also on other techniques, like membrane distillation [4] and capacitive deionization [5]. The last technique is based on a totally different approach. Instead of physically separating the water from the salt by means of membranes and applying a pressure, the salt is instead removed by an electrical field and stored in a porous media to produce freshwater. This mechanism allows to remove the salt from the water without applying any overpressure, leading to less maintenance due to the absence of mechanical moving components. However, the state of the art of this technology [6] [7] is still far from the performance of the more mature reverse osmosis and that's where the scientific effort goes into. An assessment of the actual desalination technologies is reported in Tab. 1.

Desalination technology	Water type	Electrical energy (kWh/m^3)	Thermal energy (kWh/m^3)	Operating temperature (°C)
Multi-stage flash distillation	Seawater, Brackish water	2.5-3.5	12	90-110
Multi-effect distillation	Seawater, Brackish water	1.5-2.5	6	70
Thermo-vapor compression	Seawater, Brackish water	1.6-1.8	14.6	63-70
Membrane distillation	Seawater, Brackish water	0.6-1.8	54-330	80
Reverse osmosis	Seawater, Brackish water	3.5-5.0	-	Ambient
Electrodialysis	Brackish water	1.5-4.0	-	Ambient
Nanofiltration	Brackish water	2.6-3.4	-	Ambient
Mechanical vapor compression	Seawater, Brackish water	7.0-12.0	-	-

Tab. 1: Performance assessment of desalination technologies [8].

Simultaneously with the increasing need of freshwater, the world has seen over the years a rapid increase in the demand of energy [9]. Cities keep growing, the lifestyle of the people has changed, always connected, with jobs becoming more dynamic. Contemporarily, the energy requirements of emergent countries are rapidly increasing, together with the growth of industries and the increasing welfare.

It's been many years since the scientists started saying that such a growth is not sustainable if our sources of energy are non-renewable, like oil, coal and nuclear energy (see Fig. 2). In this sense, the only choice to keep growing in a sustainable way for the planet is to increase drastically the contribute from renewable sources, like solar and wind. There are two ways to do so. First, spreading these technologies worldwide, increasing their diffusion and employment. Second, keep researching to improve their efficiency, reduce their cost and maybe find new solution to harvest energy from renewable sources.

This is indeed the case of the so called "Blue Energy" [10], which is drawing the attention of the scientific community because of its great potential. As the name suggests, this energy is related to the water and, in particular to the sea. Every time freshwater mixes with seawater, energy is released in form of heat. Nowadays, few technologies have been studied to harvest this energy, but they are still far from reaching an energetic efficiency sufficient to candidate them for industrial and large-scale application [11]. And that's where the scientific goes into. The exploitation of this new source of energy would lead to a new era for the renewable technologies.

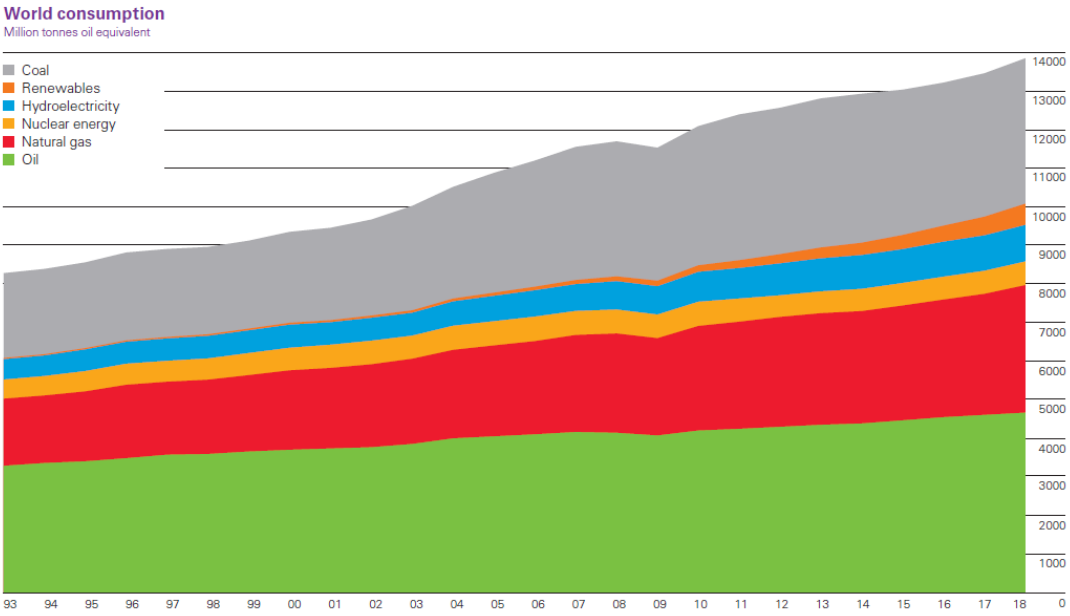

Fig. 2: Energy consumption in million tonnes oil equivalent as function of the years [12].

1.2 Thesis objective

The goal of this thesis is to develop and characterize new materials for desalination and energy harvesting application, pushing forward the research in this field to find new solutions to provide freshwater and energy from renewable sources.

In particular, the context of this thesis work is set in two of the sustainable development global goals defined by the United Nations. The Goal 6: Clean Water and Sanitation, whose first target is "Achieve universal and equitable access to safe and affordable drinking water for all". The Goal 7: Affordable and Clean Energy, whose first target is "Ensure universal access to affordable, reliable and modern energy devices" and second target is "Increase substantially the share of renewable energy in the global energy mix".

Most of thesis work (included research, fabrication and measurements) was carried out at the Department of Applied Science and Technology (DISAT) c/o Politecnico di Torino, Turin, Italy. Few material characterizations were carried out at the Center for Sustainable Future Technologies (CSFT) of the Istituto Italiano di Tecnologia (IIT) c/o Environment Park, Turin, Italy.

2. Capacitive technology

Alessandro Volta, at the end of 18th century, performed many experiments in the field of electrochemistry and electrostatic. Renown worldwide for the discovery of the voltaic pile, he also described what he called the "electrical condenser", i.e. the modern parallel-plate capacitor.

In the following centuries, the capacitor became a constituting element of electrical circuits and, thus, kept evolving. From parallel plate configuration to wrapped design, from ceramic capacitors to electrochemical capacitors, from macroscale to nanoscale.

Even though design and materials can vary a lot, the fundamental working principle is the same. When a voltage is applied to the capacitor, charges accumulates to the surface of the two electrodes. The physical quantity relating the applied voltage and the accumulated charge is the capacitance:

$$Q = CV \tag{1}$$

Where Q is the accumulated charge (C), C is the capacitance (F) and V is the applied voltage (V). For a parallel-plate capacitor, the capacitance can be calculated as described in Eq. 2:

$$C = \frac{\varepsilon A}{d} \tag{2}$$

Where ε is the electric permittivity of the material between the plates (F/m), A is the area of one electrode (m^2) an d d is the distance between the electrodes (m).

In the last century, the world has seen the rise of a new type of device: the supercapacitor [13]. In 1954, Howard Becker described for the first time an "electrolytic capacitor with porous carbon electrodes". He discovered that replacing the metallic electrodes of an electrolytic capacitor with porous ones, the final device was showing a capacitance order of magnitude higher. The idea behind that is pretty simple: moving from a flat metallic surface to a porous carbon surface, the A factor increases by order of magnitude and so does the C.

However, this is not completely true. Indeed, to take advantage of the boosted area provided by porous carbon, the ions of the electrolyte solution must be able to access such pores. Therefore, not only the presence of pores, but also their size distribution plays a key role in supercapacitors [14].

From a circuital point of view, a real supercapacitor and a real capacitor have the same representation. Indeed, both of them can be schematized as an ideal capacitor in series with a resistance, usually called “equivalent series resistance” (ESR).

What differs between the two technology is the energy storage mechanism. Indeed, a supercapacitor can store energy in two ways: by means of both Faradaic and non-Faradaic processes. In the first case, we speak of “pseudocapacitance”, in the second case we talk about “electrical double layer capacitance”. Both contributions can be present in the same device and they are better described in the following sections.

The supercapacitors have risen the interest of the research and industrial communities because of the behavior in between a standard capacitor and battery. Indeed, a supercapacitor can store more energy than a capacitor and release it faster than a battery. To represent this behavior, a Ragone plot is commonly used (Fig. 3). The Ragone plot was proposed by David Ragone in 1986 [15]. It is commonly used for comparing energy density and power density for various energy storage devices.

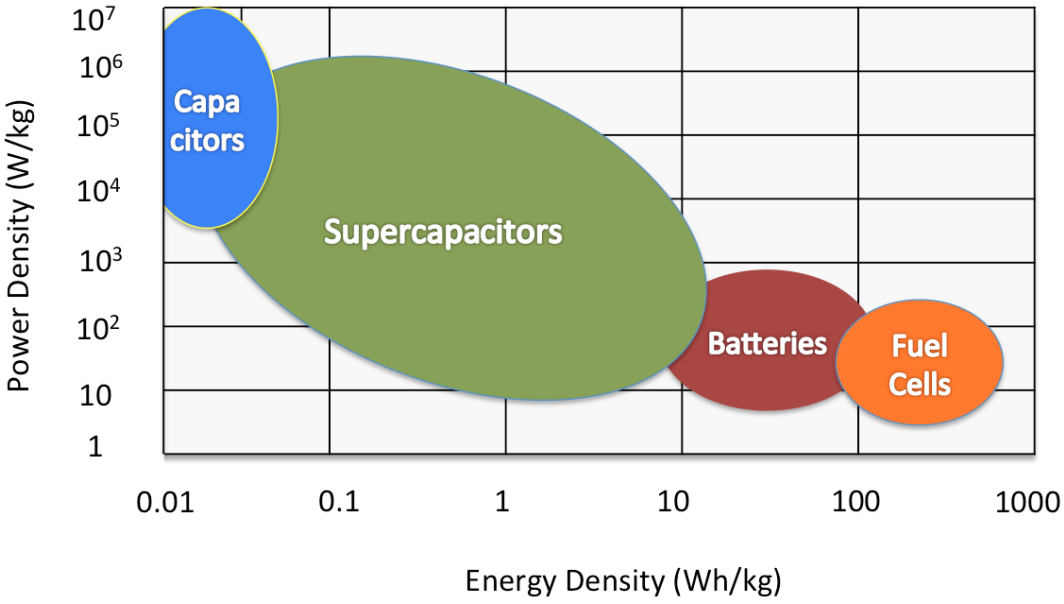

Fig. 3: Ragone plot comparing different energy storage devices.

Nowadays, supercapacitors usually find application together with rechargeable batteries [16]. However, supercapacitors are not the only devices taking advantage of porous carbon-based electrodes. Capacitive deionization cells, for instance, are the case. In these cells, two porous electrodes are employed to remove salt from water by means of an applied electrical field, thus producing freshwater. The working principle is exactly the same as charging a supercapacitor. For these reason, materials employed in capacitive deionization and capacitive mixing are commonly characterized in terms of capacitance, coulombic efficiency and ESR.

2.1 Electrical double layer

A voltage difference applied to the two electrodes of a supercapacitor generates an electric field able to move the charges present inside the electrolyte. Negative ions travel to the positive electrode, while positive ions travel to the negative one, creating in both the electrodes a double layer of charges, as described by the DBM model [17]. The DBM model describes the formation of the electrical double layer as the contribution of many effects.

Focusing the attention on one electrode, a charged layer forms at the surface of the electrode, while another layer, with opposite sign, forms at the surface of the electrolyte. The latter is called "Outer Helmholtz Plane" (OHP). Between the two layers, there is the so-called "Inner Helmholtz Plane" (IHP). The IHP is a layer of strongly oriented neutral molecules of the solvent adsorbed at the surface of the electrode. Between the OHP and the bulk of the electrolyte, a diffuse layer of charges is present (Fig. 4).

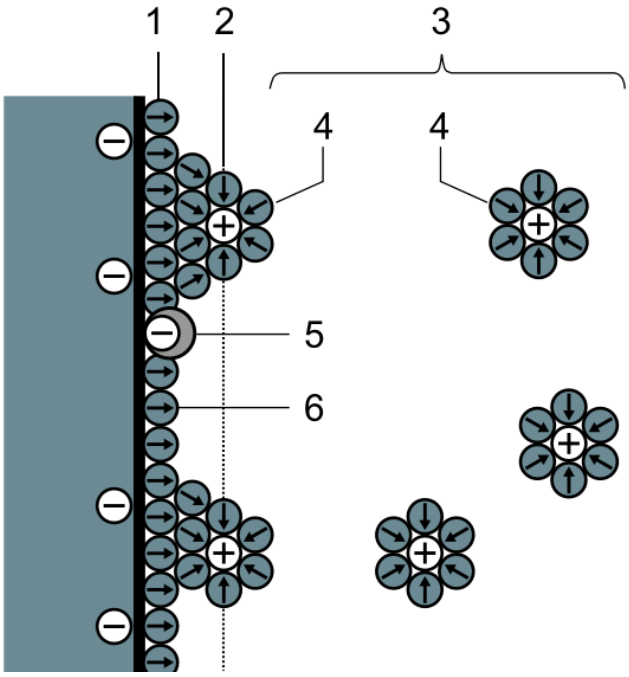

Fig. 4: Schematic representation of a double layer on an electrode. [18]
1. Inner Helmholtz plane. 2. Outer Helmholtz plane. 3. Diffuse layer. 4. Solvated ions. 5. Specifically adsorbed ions (redox ion, which contributes to the pseudocapacitance, as described in chapter 2.2). 6. Molecules of the solvent.

The ions in solution are attracted by electrostatic forces to the electrodes that keep them there until the voltage difference is maintained. The charges accumulated in this way on the Helmholtz plane play a key role in determining the capacitance of the device. The capacitance originated by the accumulation of charges as described above is called

"electrical double layer capacitance". It can be evaluated as the capacitance of a parallel plane capacitor:

$$C = \frac{\varepsilon A}{d} \tag{2}$$

Where C is the capacitance of the single electrode (F), ε is the permittivity of the IHP, d is the thickness of the IHP (m) and A is the surface area of the electrode (m^2). Being the IHP really small (its thickness is of the order of one solvent molecule) and the surface area of the electrode very large (thanks to the presence of materials of high degree of porosity), the final capacitance can be very high (hundreds of farad per gram of material).

By the way, in a supercapacitor two electrodes are present, each of them having its own IHP and therefore its own C. Follows that the final capacitance of the device is the series of the capacitances of the single electrodes. The same applies to capacitive deionization cells.

Ideally, no charges are transferred from the electrolyte to the electrodes and then in the external circuit. Indeed, in presence of charge transference, a leakage current is established, leading to a reduction of the number of accumulated charges. This is the primary cause of self-discharging of these kind of devices. The presence of redox reactions at the surface of the electrodes can involve the ions in solutions or simply the molecules of the solvent. Such redox reactions make the electrodes non-ideally polarizable, originating therefore a leakage current causing the self-discharge of the electrodes. For carbon electrodes, a source of self-discharge is the oxygen dissolved in water, causing the oxidation of the carbon through irreversible redox reactions [19].

When an electrode is immersed in a solution in open circuit condition, after a certain time an equilibrium is reached and the potential of the electrode is stable. Such potential is called "spontaneous potential" (V_s). When the electrode is polarized at a potential V, the potential will vary over time following the law:

$$\frac{dV}{dt} = \frac{1}{C}\left(I + \frac{V_S - V}{R}\right) \tag{3}$$

Where R is the parasitic leakage resistance (ohm), I is the electronic current (A) and C is the capacitance of the electrode (F). From the Eq. 3, it is possible to see that the potential will vary even if no current is flowing. Indeed, greater the difference between V_s and V, more intense is the self-discharge. Therefore, working at a potential V_s is to be preferred when aiming to minimize the leakage.

The presence of the diffuse layer of charges inside the electrolyte is directly responsible of other properties of the device, which are of interest for capacitive

deionization and capacitive mixing. Such properties become even more important in presence of functionalized materials, therefore a brief insight of the related theory is herein provided.

The capacitive deionization rely on the adsorption of ions at the surface of the electrodes to remove them from the water stream (see section 3.3.3 for further details). When charging the electrodes, counter-ions move from the bulk of the solution to the proximity of the electrodes, creating the diffuse layer.

Every electrode has its own potential of zero charge (V_{pzc}). This is the potential at which no charges are adsorbed on the electrode surface. It can be either positive or negative, depending on the nature of the electrode, its state of oxidation, etc. Polarizing an electrode will lead to a potential of $|V - V_{pzc}|$ used to attract the counter ions. However, if V and V_{pzc} have the same sign, a part of the energy will be spent to repel the co-ions naturally adsorbed on the surface of the energy [20]. The co-ions expulsion is also reducing the useful voltage window, because only $(V - V_{pzc})$ is used to adsorb counter-ions, while $(V_{pzc} - 0)$ is used to expel the co-ions, thus lowering the efficiency of the system.

The presence of functionalization on the surface of the electrodes provides a net charge that is able to shift this potential. Positively charged electrodes will have their $V_{pzc} < 0$, while negatively charged electrodes will have their $V_{pzc} > 0$. Therefore, polarizing the electrodes with a potential V with opposite sign with respect to V_{pzc}, will lead to $|V - V_{pzc}| > |V|$. This will highly increase the amount of stored counter-ions (refer to Eq. 4 below) and nullify the co-ions expulsion, yielding to improved adsorption capacity.

In capacitive mixing experiments, the voltage rise is the key feature. It is due to an expansion of the diffuse layer driven by diffusion forces caused by a concentration gradient (for further details see section 3.3). This voltage rise can be expressed as a function of the salinity of the solution and the potential applied. This property can be directly deduced from the Gouy-Chapman-Stern (CGS) theory. To do that, it is necessary to define a certain number of physical quantities, which are schematically represented in Fig. 5.

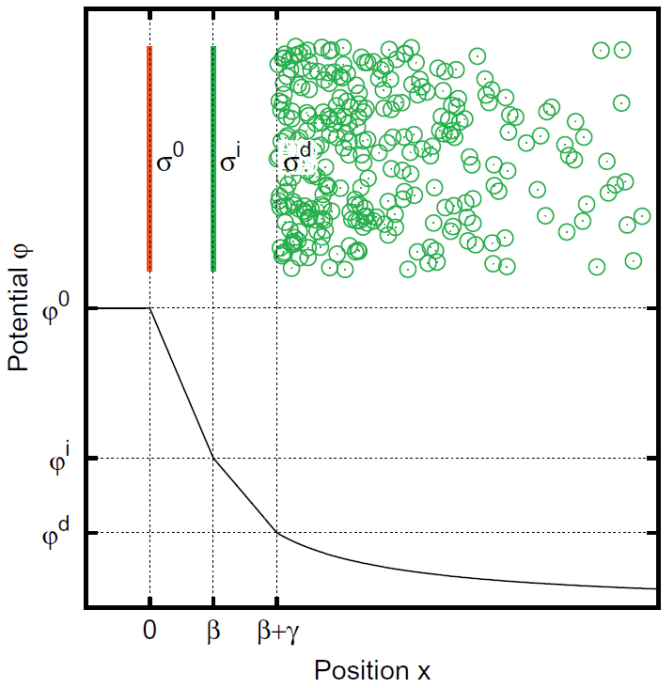

Fig. 5: Schematic representation of the potential and charges distributions in proximity of the electrode. The origin of the x axis is set at the electrode's surface. [19]

The potential φ^0 is the potential at the surface of the electrode due to the presence of the charge σ^0. The potential φ^i is due to the presence of the functionalized materials containing the charge σ^i. This charge is placed at a distance β from the electrode. Finally, at the distance β + γ is the potential φ^d due to the presence of the charged ions (σ^d) of the electrolyte. In the CGS model, the charges inside the electrolyte are not localized, but they constitute the "diffuse layer". In this model, the relation between φ^d and σ^d can be written in the following way:

$$\varphi^d = -\sqrt{8\varepsilon MRT}\sinh\left(\frac{zF\sigma^d}{2RT}\right) \tag{4}$$

Where ε is the permittivity of the solvent, M is the molarity of the electrolyte (mol/l), R is the universal gas constant (8.31441 N m mol^{-1} K^{-1}), T is the absolute temperature (K), z is the number of charges in which the salt dissociates (2 for NaCl) and F is the Faraday constant (96485 C mol^{-1}).

From the electroneutrality it is possible to estimate σ^d:

$$\sigma^d = -\left(\sigma^0 + \sigma^i\right) \tag{5}$$

Since the potential decreases linearly from 0 to β (Eq. 6) and from β to β + γ (Eq. 7), the equations in these regions can be easily written:

$$\varphi^i = \varphi^0 - \frac{\beta}{\beta+\gamma}\frac{\sigma^0}{C} \tag{6}$$

$$\varphi^d = \varphi^i - \frac{(\sigma^0+\sigma^i)}{C}\frac{\gamma}{\beta+\gamma} \tag{7}$$

$$C = \frac{\varepsilon}{\beta+\gamma} \tag{8}$$

Where C is the capacitance of the electrode. Now, combining the equations 6 and 7, the relation between φ^0 and φ^d can be obtained:

$$\varphi^0 = \varphi^d + \frac{\sigma^0}{C} + \frac{\sigma^i}{C}\frac{\gamma}{\beta+\gamma} \tag{9}$$

From this equation, it is immediately clear how the potential at the electrode strictly depends on the potential at the surface of the diffuse layer (which, by extension, depends on the charges in this layer through Eq. 4).

Finally, the equation describing the voltage rise can written:

$$\Delta\varphi = \varphi^0(\sigma^0, M^L) - \varphi^0(\sigma^0, M^H) \tag{10}$$

Where the superscripts L and H refer to low and high salinity solutions respectively. The term $\varphi^0(\sigma^0, M^H)$ is often written in the simple form of φ^H and it is called "base potential". The term "base" refers to the fact that this is the potential of the electrode in the high salinity solution, before the potential rise takes place. As for the voltage rise, the base potential is also function of the state of charge of the electrode. From Eq. 10, the condition $\Delta\varphi = 0$ is always verified if the base potential is set at the potential of zero charge. In this case, the absence of an electrical double layer prevents its expansion.

It is interesting to note how the presence of a functionalization charge σ^i provides a constant shift to the base potential of the electrode (refer to Eq. 4, Eq. 5 and Eq. 9). Depending on the sign and module of this charge, completely different values of the voltage rise can be obtained (Fig. 6).

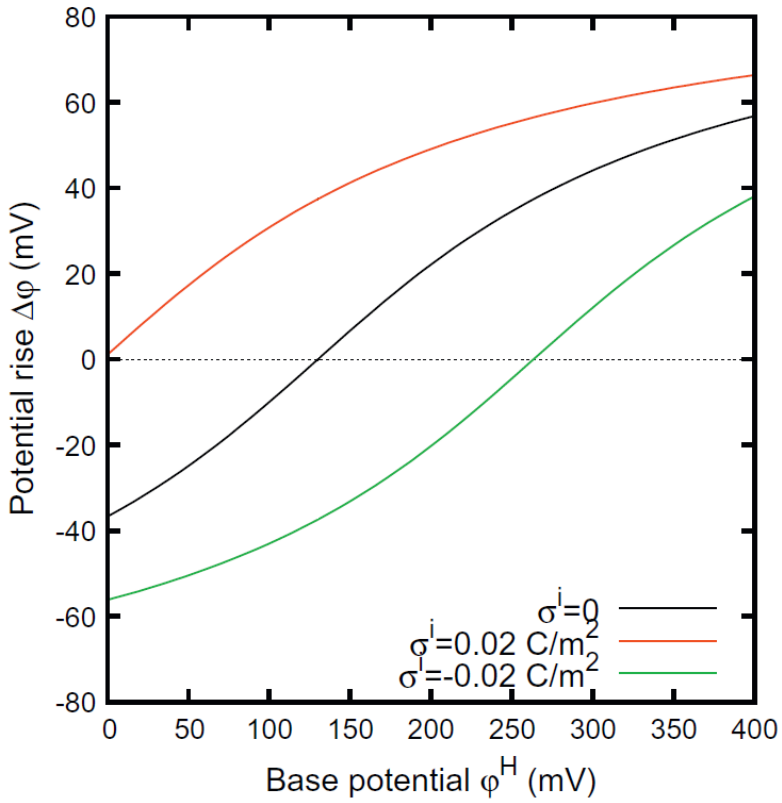

Fig. 6: Effect of functionalization on potential rise. Positively charged layers shift the curves to the left. On the contrary, negatively charged layers shift the curve to right. For the same base potential, a totally different voltage rise is obtained in these three cases. [19]

2.2 Faradaic processes

Faradaic processes are the phenomena linked to reversible redox reactions taking place at the surface of the electrodes (see Fig. 7). These reactions are the origin of the so-called "pseudocapacitance".

Ions of the electrolyte transfer electrons to materials like transition-metal oxides (e.g. RuO_2, MnO_2, MoO_3) through redox reactions without forming chemical bonds with them. Until the voltage is applied, the transferred charge will be trapped due to the presence of the electrostatic double layer. This charge transfer is fully reversible and, if the electrodes are symmetric, it can be observed both with positive and negative voltage applied, being the electrodes interchangeable.

Since the presence of the electrical double layer is a necessary condition to observe these reactions, pseudocapacitance directly contributes to the capacitance of the device, allowing for more charges to be stored.

Pseudocapacitance is also observed in the presence of intercalation processes. Ions coming from the electrolyte can intercalate inside the electrodes under an applied voltage. It also involves a redox reaction between them.

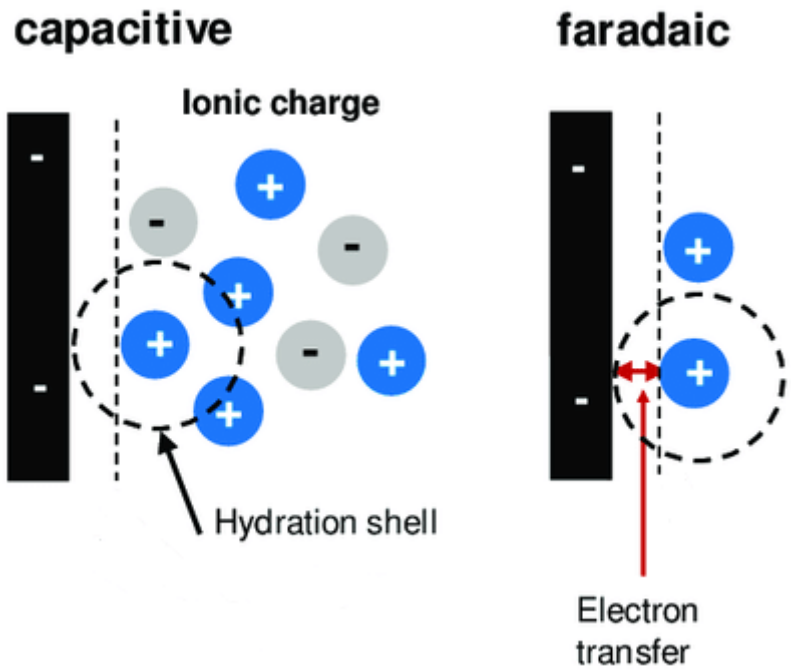

Fig. 7: Comparison between a faradaic reaction involving an electron transfer (right) and the electrical double layer formation (left).

2.3 Capacitive electrodes

When talking about capacitors (or supercapacitors in our case), there is a vastness of possible materials, configuration and technologies. From now on, the focus shifts to the electrodes, thus excluding from this dissertation the electrolyte, the separator and the packaging.

The reason for this choice is that this work is focused on finding new and efficient materials for water desalination and energy harvesting, without investing time on optimizing the setup. The package and the separator are typically investigated when optimizing a setup or a device. For what concerns the electrolyte, few can be done since the goal is to simulate seawater and freshwater. Therefore, the other elements will not be investigated nor discussed.

Any capacitive electrode is composed of 2 main elements: the current collector and the active material. The current collector, as the name suggests, is the part of the device in which the electron current flows. Its function is to provide an electrical contact between the active material and the external circuit. For this reason, it is usually a metal. The advantage of using this kind of materials is the ability of a metal of managing a high amount of current in short times, thanks to its low resistance and capacitance.

The active material is the part of the device which is responsible for storing the charges. Historically, carbon-based materials have always been employed for this purpose because of their high specific surface area, almost inert behaviour in water and their different allotropic forms, making them suitable for flat, curved and even flexible devices [21]. The first supercapacitor featuring carbon-based active material was made by Howard Becker, in 1954 [13]. His device was simply composed of two parallel plates immersed in an aqueous electrolyte.

Nowadays, the most common material employed as active material is the activated carbon. Activated carbons are manufactured on large scale by carbonization of natural precursors like wood, nutshells, coconuts, crops, etc. [22]. Activated carbons are a large family of carbon-based materials whose common denominator is being electrically conductive and having a structure with a high degree of porosity, making them suitable for application in which a high surface area is required.

Together with activated carbons, biochar and carbon black are porous carbon-based materials often employed for the production of capacitive electrodes. Biochars usually exhibit a lower specific surface area respect to activated carbon and carbon black, but they are attracting interest because they are obtained from food waste, making them promising for circular economy [23]. Carbon black is often used stand-alone [24] or as additive with other carbon-based materials [25] [26]. The reason of this choice is due to the size of the carbon black particles. While activated carbon and biochar are made of bulky, large particles, carbon black trades a bit of surface area for a much smaller particle

dimension (Fig. 8), resulting in a good filler to create electrical connection patterns on the electrodes and thus reducing the parasitic resistance [27].

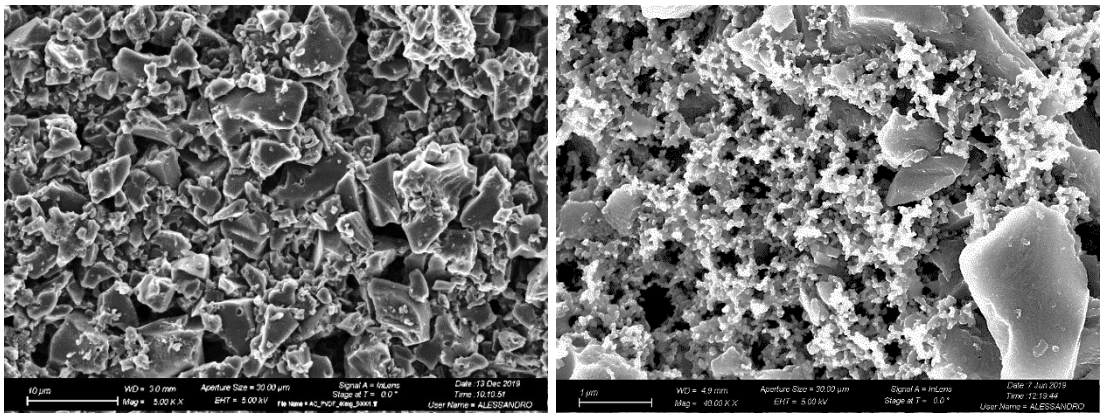

Fig. 8: On the left, activated carbon coating. On the right, carbon black smaller particles inside a larger activated carbon matrix.

Another class of materials which is attracting the interest of the scientific community is the family of 2D materials. The so-called "2D materials" are the materials whose thickness is just one atom (like graphene) or few atoms (like graphene oxide, MXenes, MoS_2, etc.).

Features of these materials are the remarkably high specific surface area (2630 m^2/g for graphene, almost the double of a common activated carbon) and the nanometric thickness, while having peculiar chemical, electrical and physical properties. Graphene, for instance, is electrically conductive, flexible and chemically inert, making it a good candidate for flexible electronic [28]. Graphene oxide can be easily functionalized and its structure makes this material promising for application like water purification [29]. MoS_2 is chemically reactive and can be exploited for energy storage [30]. All these materials are also studied as active materials for capacitive electrodes [31] [32], both as additive or self-standing.

The materials described above constitute the working core of the active material, but they are not the only ones which the active material is composed of. Being most of those materials in form of powder, a binder agent is usually required to obtain the cohesion necessary to create a uniform, continuous layer of active material.

For this purpose, polymeric binders have always been employed in supercapacitors. The features of a binder are the chemical and electrical stability, the high adhesion on the current collector and the good binding properties, of course. The most diffused binders present in literature are polytetrafluoroethylene (PTFE), polyvinylidene fluoride (PVDF) and carboxymethylcellulose (CMC). While often not investigated, the choice of the proper binder can improve both physical and electrical properties of the final device [33].

2.4 Ion exchange membranes

An ion exchange membrane (IEM) is a semipermeable membrane allowing the passage of only one type of charged solute while rejecting the opposite charged species [34]. There are different types of IEMs [35]. The most renowned are the cation exchange membranes (selective for positive charged species) and the anion exchange membranes (selective for negative charged species).

The structure of IEMs is constituted by a polymeric matrix to which ionizable groups are covalently bound. These groups dissociate in presence of water, leaving charged groups bound to the matrix which are responsible for the charge selectivity. The ion exclusion is described in thermodynamics terms by the Gibbs-Donnan equilibrium. The consequence is that IEMs can convey a high flux of ions through their structure. This can happen in presence of a concentration gradient or with an applied electric field.

The concept of IEM was born at the end of the XIX century. In that time, W. Ostwald was studying semipermeable membranes while he discovered that a membrane can be impermeable for any electrolyte if its impermeable either for its cation or its anion [36]. However, the world had to wait 20 years before this phenomenon was rigorously explained. In 1911, Frederick Donnan described through its famous equation the concentration equilibrium and the membrane potential (from that moment on called "Donna potential"), that builds in between a membrane and its surrounding solution [37].

However, the first experiment on an IEM as we intend it nowadays, was carried out by Michaelis and Fujita in 1925 [38]. In the following years, many experiments were carried out to study the IEMs. The first commercial product arrived on the market 5 decades later. In the 1970s, the company DuPont started selling on the market the Nafion, their registered trademark for a CEM largely employed in the chlor-alkali production and in fuel cells [39].

Nowadays, there are few companies worldwide selling IEMs, while the research is focusing on studying solutions which can improve stability [40], efficiency [41] and antifouling properties [42], together with reducing the cost of this membranes [43], a key point to make their application feasible in emerging sectors like energy harvesting.

2.4.1 Cation exchange membranes

A cation exchange membrane (CEM) is made of a polymer having on its backbone a series of negatively charged groups (typically sulfonated groups) responsible for the conduction of cations.

The most famous example of CEM is the Nafion, a commercial name for a sulfonated tetrafluoroethylene-based fluoropolymer-copolymer [44]. This kind of membrane, even if been costly due to the presence of many fluorinated groups in its structure, has been largely employed as proton exchange membrane in fuel cells and as CEM in chlor-alkali cells [45]. Indeed, the presence of sulfonated groups allows protons to hop from one site to another, while also allowing the movement of cations through pores. Anions and electrons, instead, are not conducted. For this reason, Nafion also found application in the chlor-alkali production, in which Na^+ and K^+ must be separated from Cl^- to produce respectively NaOH and KOH.

A part from Nafion, many other CEMs have been investigated. Sulfonated poly(ether ether ketone), commonly known as SPEEK, has attracted the attention of the community [46] [47] due to its chemical and thermal stability [48], ease of preparation [49] and reduced costs compared to Nafion.

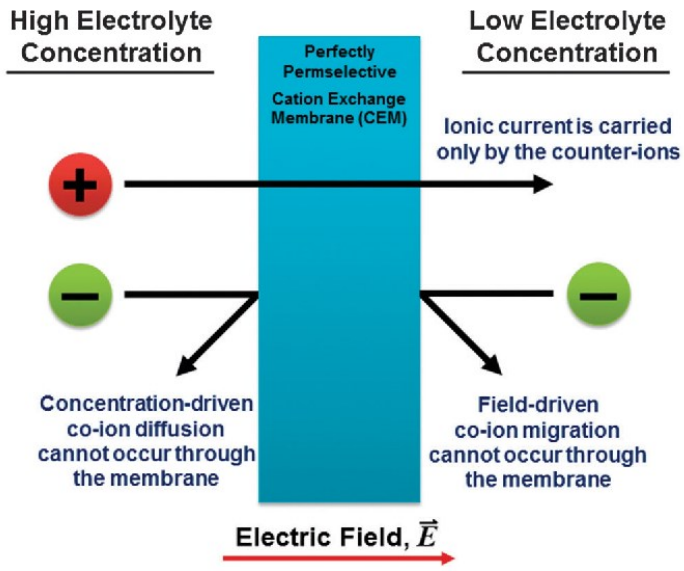

Fig. 9: CEM working principle [50].

2.4.2 Anion exchange membranes

An anion exchange membrane (AEM) is made of a polymer having on its backbone a series of positively charged groups (typically ammonium groups) responsible for the conduction of anions.

Unlike what happened for the CEM counterpart, AEMs have not seen a wide diffusion due to the absence of a top selling membrane like Nafion. The cause of that lays in their lower stability and in the complexity of the preparation process [35]. Historically, AEMs found application initially in alkaline fuel cells [51], in which their adoption allowed to reduce the costs while contemporarily improve the overall stability of the system. Indeed, the presence of amine groups allows hydroxides to hop from one site to another, while also allowing the movement of anions through pores. Cations, instead, are rejected.

Nowadays, AEMs are used coupled with CEMs in a vast range of application, like capacitive deionization [52], reverse electrodialysis, redox flow batteries [53], etc.

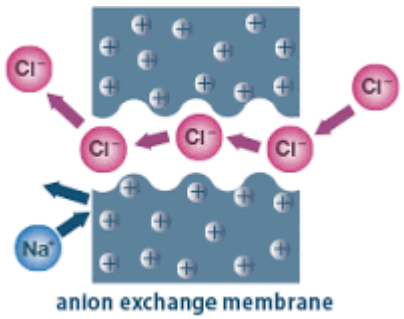

Fig. 10: AEM working principle [source: http://www.astom-corp.jp].

2.4.3 Other ion exchange membranes

The most renown type of IEMs are surely CEMs and AEMs. However, in literature it is possible to find also other kind of IEMs [35], like bipolar IEMs, mosaic IEMs and amphoteric IEMs. The latters, were proposed almost one century ago by Sollner, in 1932 [54].

The bipolar IEMs are characterized by a layered structure composed of a cation selective layer and an anion selective layer. To visualize the structure, it is possible to image this kind of membranes like a CEM coupled with an AEM (see Fig. 11). They find application in the electrodialysis industry for the production of acid and bases through water splitting starting from their salt [55].

Mosaic IEMs, instead, consist of a set of anion and cation exchange sites arranged in parallel. The result is a membrane constituted by a series of channels, each of them with a well-defined charge, providing a pathway for the matching ion. Such membranes allow both species of ions to flow through their structure, without violating the macroscopic electroneutrality. Because of the circulation of current which establishes is presence of a potential applied or a concentration gradient, mosaic IEMs show negative osmosis and high salt permeability. This behaviour cannot be observed in common IEMs [56].

Finally, amphoteric IEMs are a class of IEMs constituted by a random arrangement of weak acidic groups and weak basic groups. Because of the presence of opposite charged weak groups, they can behave both as CEM or AEM depending on the pH of the solution in which they are immersed. This peculiar property makes them interesting as chemical switches in systems in which the flow of ions can be easily pH-controlled [57].

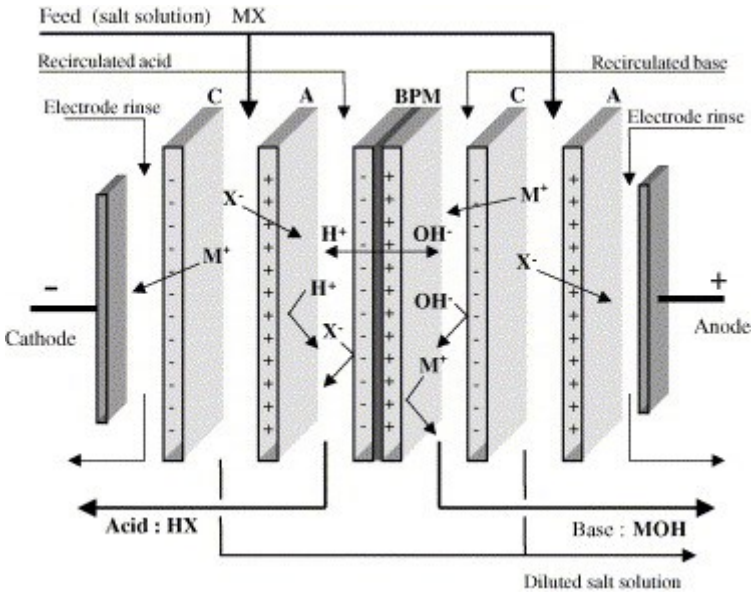

Fig. 11: Electrodialytic production of acid and bases by means of bipolar IEM [55].

3. Energy harvesting from salinity gradients

The first person who described the possibility to extract energy from salinity gradients was Richard Pattle, in 1954 [58]. He was able to experimentally prove the feasibility of his theory, even though it was not economically convenient at that time.

Only 20 years later, in 1974, Richard Norman took back this idea, theorizing the possibility to harvest energy from the osmotic pressure generated when two solutions of different concentration are put in contacts [59]. He estimated that 1 m^3 of freshwater poured into the ocean is releasing an energy equal to 2.24 MJ as heat. This energy comes from an increase of entropy happening when two solutions with different concentrations are mixed together. Practically speaking, this is the same energy released by a waterfall 225 m high.

In terms of power, taking into account the global freshwater discharge originated by rivers each second, the power at stake is of the order of 2 TW [60]. In 2018, the global energetic requirement was 18.4 TW [12]. Considering that only 11% of this power came from renewable resources, it becomes immediately clear how important such a source of energy can be. At the moment, there are no industrial plants in the world taking advantage of this phenomenon to produce clean and renewable energy.

The key requirement to harvest energy from salinity gradients is having access contemporarily to both low and high salinity sources. The mouth of rivers is a perfect candidate, but it is not the only one. Brines, originated as a byproduct of desalination plants, can be exploited as well. Moreover, larger the concentration difference between the two solutions, higher the theoretical energy that can be harvested.

Three are the technologies reported in literature able to harvest energy from salinity gradients: Pressure Retarded Osmosis, Reverse Electrodialysis and Capacitive Mixing.

3.1 Pressure retarded osmosis

Pressure retarded osmosis (PRO) is a process able to harvest energy from salinity gradients. PRO was invented by Sidney Loeb, in 1975 [61]. Together with Norman, Loeb described the feasibility of this technique, both from an engineering and an economical point of view [62].

However, the world had to wait until 2009 to see the first pilot plant based on PRO [63]. The Starkraft company built a small-scale prototype in Tofte, Norway. This pilot plant was able to produce an output power of 10 kW by mixing 20 litres of seawater and 13 litres of freshwater per second [64].

Unfortunately, the project was closed only 5 years later, in 2014. As declared by Starkraft, they were forced to take this decision because of the poor efficiency of the membranes commercially available at that time. To reach economical break-even, membranes had to guarantee a power density of 5 W/m^2. Even if in literature membranes able to go above 5 W/m^2 are reported [65], the membranes available on market barely reached 1 W/m^2 [64]. The gap between research level investigation and large-scale commercialization forced the Starkraft company to invest in different technologies and shut down the PRO pilot plant.

Sadly, Starkraft was both the first and the last company to fund such a project. Actually, there are no plants based on PRO technology running all over the world.

3.1.1 Working principle

The working principle of PRO, as the name suggests, is based on the forward osmosis. Osmosis is the phenomenon in which a solvent is spontaneously moving from a diluted solution towards a more concentrated solution.

The driving force of this phenomenon is a pressure difference which establish between the two solutions in presence of a semipermeable membrane. Such a pressure is the osmotic pressure π described by the van't Hoff equation:

$$\pi = icRT \tag{11}$$

where c is the molar concentration (mol/l), R is the universal gas constant (8.31441 N m mol^{-1} K^{-1}), T is the absolute temperature (K) and i is the number of osmotically active particles in the solution.

The resulting unit for π in Eq. 11 is the kPa. For seawater, where the NaCl concentration is around 0.6 M, the osmotic pressure is roughly 29 bar, for a temperature

of 25 °C. For freshwater, where the NaCl concentration is below 0.02 M, the osmotic pressure is lower than 1 bar at 25 °C.

The idea of PRO is to exploit this osmotic pressure to power a hydraulic turbine to generate electric power from mechanical work. To do so, it is necessary to provide a constant flux of both diluted and concentrated solutions in two chambers separated by a semipermeable membrane allowing only water to pass through. A scheme is reported in Fig. 12.

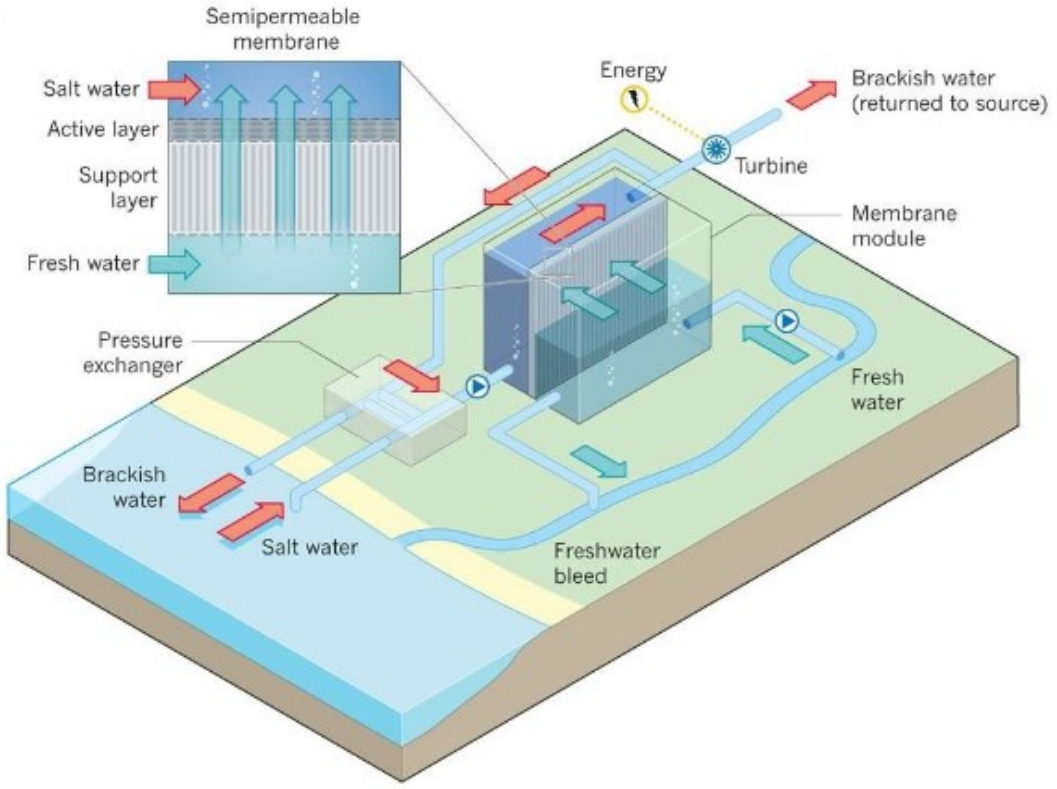

Fig. 12: Scheme of PRO power plant [66].

Another feature of PRO is, as the name suggests again, the need of an overpressure applied on the concentrated side. This requirement comes from the necessity of a constant flux of water to keep stable the concentration difference between the two compartments and, therefore, to keep constant the power generated. This overpressure must be enough to push the water in, but contemporarily as low as possible to minimize the reduction of pressure difference between the two solutions.

Combing all the previous requirements, it is possible to demonstrate that maximum power can be extracted when the system works with an overpressure equal to half of the pressure difference between the two compartments [67].

A key element of a PRO plant is the pressure exchanger [68]. A pressure exchanger is a rotating cylinder connecting the pressurized stream with the low pressure one. The cylinder houses one or more pistons which allow to change the internal volume of the

device. The pistons are actuated by the pressurized solution, allowing to transfer pressure to the other solution thanks to a change in the volume.

Without a pressure exchanger, it will be impossible to have an energy gain from this process, due to the power consumption of the hydraulic pumps which have to pressurize the water up to the working pressure.

3.1.2 State of the art

The research on PRO field is mainly focusing on the membranes, since the Starkraft's project highlighted the necessity of better performing ones. In particular, it is mandatory to improve the power density. One possibility is to further enhance the membranes properties, increasing the water flux and salt rejection, however this route is self-limiting, since the two parameters are in contraposition [69] [70].

On the other hand, if the actual technology does not allow to reach the break-even employing seawater, a possible way would be exploiting a more concentrated solution. Brines coming from desalination plants, saltworks, or high-salinity places like the Dead Sea provide a much higher output power [71]. There are many experimental works showing promising results in this sense, with membranes showing energy density well above 10 W/m^2 [65] [67]. However, the initial cost of the plant increases due to the much higher pressure and water flux that pumps have to provide, together with an intensified corrosion phenomenon that pipelines have to endure. Furthermore, the membranes have to sustain pressure differences of tens of bar. Finally, such membranes have to keep their cost low and have to be produced on large-scale, otherwise the price of the energy cannot be competitive with other technologies actually on the market.

From an engineering point of view, there are a few technical areas of improvement towards reducing the costs of osmotic power. The following considerations are the result of the experience gained in the Starkraft project [72]. First, membrane stack must be able to accommodate about 5000 m^2 of membrane area. Then, the system efficiency must be increased with the development of low energy-intensive systems for water conveyance and treatment, and minimizing the energy losses in the piping system. The latter can be achieved using pressure exchangers, devices able to recover mechanical energy with an efficiency above 90% [73]. Finally, the system must be scaled up into commercial production to further reduce costs.

In conclusion, with improved membranes, optimized flows and minimized energy losses, an efficiency of 70% for a terrestrial sea-level plant with pressure exchangers can be achieved [74].

For what concerns the research, for the moment, recent works are focusing on improving the membrane performances, while reducing the production cost.

3.2 Reverse electrodialysis

Reverse electrodialysis (RED) is the first process ever described to harvest energy from salinity gradients [58]. In 1954, Richard Pattle assembled a lab-scale device able to produce a power of 15 mW employing a solution of NaCl 0.5 M and tap water.

However, the invention of the RED technology comes 2 decades later. Sidney Loeb, in 1979, deposited a patent in which described in details the working principle of this technique [75], anticipating the possibility of using also concentrated solutions instead of simply seawater.

Like for the PRO technology, the world had to wait 35 years to see the first pilot plant based on RED [76]. In 2014, the REDstack company built a small-scale prototype in the Afsluitdijk dam, Netherlands. Unlike conventional dam, this one was built to subtract portions of land from the sea.

This pilot plant is still running, producing an output power of 50 kW by mixing 55 litres of seawater and freshwater per second [76]. The system is employing ion exchange membranes supplied by Fujifilm.

The abundance of both freshwater and seawater, combined with the absence of differences in height on the landscape, led the Netherlands to be the first country to invest in RED for energy production. If this technology will reach the large-scale development, in the future the country will be able to achieve electrical independence from fossil fuels.

A more recent pilot plant was built in 2015 in Marsala, Italy [77]. While REDstack provided the technology and Fujifilm the membranes, the aim of this project is completely different from the previous. In the framework of the REAPower project, RED technology is being tested to recover energy from brines produced by saltworks. This plant is running 1125 cell pairs, providing an output power of 330 W (1.4 W/m^2 cell pair), mixing 33 litres of brines and 48 litres of seawater per minute [78].

3.2.1 Working principle

The working principle of RED, as the name suggests, is based on the electrodialysis. Electrodialysis is a process in which an electrical potential is used to move ions from a diluted solution to a concentrated solution by means of ion exchange membranes. Electrodialysis finds application in brackish water desalination, water reuse and food and chemical purification.

Reverting the process, ions of the proper charge sign will cross the matching ion exchange membrane, moving from the concentrated solution towards the diluted solution. Due to the unpaired movement of ions across the membranes, an electrical potential rises across each membrane, as described by the Donnan-Gibbs law. This potential, combined

with the electrical current associated to the spontaneous flow of the ions, can be exploited to harvest energy.

In practical devices, a RED cell is constituted by a stack of alternated anion and cation exchange membranes. In between them, a separator is placed in which water is flowing. The alternation of concentrated and diluted water flowing in opposite directions is granting a constant concentration of ions in each compartment. Such a configuration (Fig. 13) is responsible for a flow of net charges, granting a constant current and a constant potential, resulting in a constant output power.

Thanks the potential difference that builds up across the stack, redox reactions are exploited at the electrodes to convert the chemical energy into electrical one. A circulation of the external electrolyte solution is required to move the redox species and keep redox reactions happening.

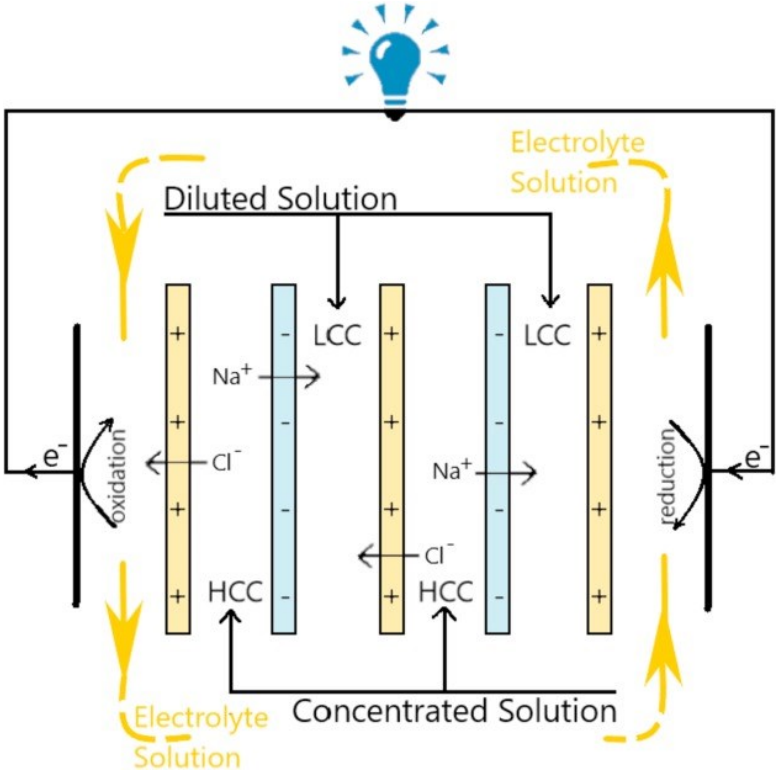

Fig. 13: Scheme of RED cell [79].

3.2.2 State of the art

Recent studies highlighted how the efficiency of RED drops drastically when passing from artificial solutions (lab scale) to real applications (pilot plants) [78]. The reasons of this worsening are many.

In the lab, artificial solutions are usually made of NaCl and deionized water. In real applications, there are many other salts dissolved in water [80] [81]. Among them, divalent ions are known to be responsible for lowering the performances of ion exchange membranes [82]. Due to the strong interaction with the active sites of the membranes, their presence results in a shielding effect which is reducing the permselectivity of the membranes themselves. The final outcome is a lowering of the Donnan potential and, therefore, a reduction of the output power of the system.

Fouling is causing high energy losses, strongly affecting in particular the anion exchange membranes [83]. While organic larger particles can be easily removed from water with a simple pre-treatment step (filtration, mostly), inorganic or organic smaller particles are a completely different cup of tea [84]. Many studies address the cause of fouling mainly to silica particles and humic acid [85] [86]. To solve the problems, a great effort has been requested to researchers. Actually, two approaches seem to be the most effective. The first one is periodically switching the feed waters, in such a way to force the ions to move in the opposite directions across the membranes [87]. The second one consists in employing functionalized membranes. In particular, adding a proper surfactant with a fixed charge on the surface of the membranes can both reduce fouling while increasing selectivity towards monovalent ions [88].

A part from improving the actual polymeric membranes, the research is also focusing on new materials, both for electrodes [89] and membranes [90] [91] [92]. Actually, electrodes are commonly made of an inert material working with a redox couple (usually Fe^{2+}/Fe^{3+}). In literature are reported electrodes able to work with different redox couples or making use of high surface area materials to store the charges [93], thus avoiding the presence of redox couples. For what concerns the membranes, while the majority of the studies still focus on polymer-based materials, there are new emerging trends in research. 2D materials are attracting the interest of many researchers and companies because of their unique properties [94]. In particular, in the membrane field, they show to be promising because of their minimal thickness, thus reducing hydrodynamic resistance, while providing good selectivity. Efforts in this sense are towards improving selectivity and mechanical strength, while contemporarily finding cheap and large-scale production method to make them attractive (from an economical point of view) respect to the well-known and consolidated polymer-based technology [95].

As commonly done, RED devices are tested at lab level using artificial solution, typical NaCl 500 mM to simulate seawater and NaCl 10 mM for freshwater. It is also often

reported a series of tests using higher concentrations, from 1 M up to saturation. The purpose of these experiments, even if apparently far from reality, is to study the efficiency of system or investigate the membranes' performance. However, such tests are motivated by the possibility of employing brines [78] [96] to increase the output power of the system thanks to the larger salinity difference and, therefore, a higher theoretical energy at stake. Of course, such a choice is only feasible for saltworks realities or for systems coupled with desalination plants, from which a huge amount of brine is constantly provided.

Nowadays, one weak point of RED technology is still the cost of the ion exchange membranes required [43]. However, the research keeps working to find cheaper and more performant membranes, while contemporarily on the international scene, the first pilot plants are running to prove the feasibility of RED technology.

3.3 Capacitive Mixing

Capacitive Mixing (CapMix) is a quite recent technique. Invented by Doriano Brogioli in 2009 [97], CapMix has been inspired by an experiment performed by Michael Faraday in the first decades of the 19th century [98].

Faraday observed that once a parallel-plate capacitor is charged, it is necessary to provide mechanical work to increase the distance between the plates. He discovered, therefore, that was possible to convert mechanical energy into stored electrical energy.

Starting from this concept, Brogioli proved that it was possible to use a supercapacitor to harvest energy [97]. This can be achieved forcing the charges stored near the surface of the electrodes to move far away. If this is done increasing the distance between these charges and the surface of the electrode without releasing them (i.e. without discharging the device), the capacitance of the device will decrease and the voltage will rise (refer to Eq. 1-2 in section 2).

The idea, therefore, is to charge a supercapacitor up to a certain voltage and discharge it at a higher voltage. If the leakage is negligible, during the discharge step the amount of charges will be roughly the same provided during the charge, thus the energy released will be higher than the energy required to charge the device (Eq. 12-13). The energy gain therefore is directly proportional to the voltage difference that can be achieved (Eq. 14).

$$E_{in(out)} = \frac{1}{2} Q_{ch(dch)} V_{ch(dch)} \tag{12}$$

$$E_{out} = E_{in} \frac{V_{dch}}{V_{ch}} \qquad \text{if} \qquad Q_{dc} \approx Q_{dch} \tag{13}$$

$$\Delta E = \frac{1}{2} Q \Delta V \tag{14}$$

Where E is the provided/extracted energy (J), Q is the charge accumulated/released (C) and V is voltage at the end/beginning of the charge/discharge step (V).

3.3.1 Working principle

The working principle of CapMix, as the name suggests, is based on the mixing of two solutions. The alternation of a solution at high salinity (for example seawater) with a solution at low salinity (freshwater, for instance) at the surface of the electrodes of a

supercapacitor is the key point to harvest energy. The origin of this energy harvesting is the presence of a voltage rise across the device.

The whole process can be divided into 4 steps:

1. In open circuit condition, the space between the electrodes is filled with solution at high concentration.
2. An external power source provides electrical energy to charge the electrodes up to a fixed voltage.
3. The eternal power source is disconnected and the solution is replaced with the one at low concentration.
4. The device is discharged on a load and the procedure is repeated.

An example of this cycle is shown in Fig. 14, where a CapMix cell is charged at a fixed voltage of 0.2 V.

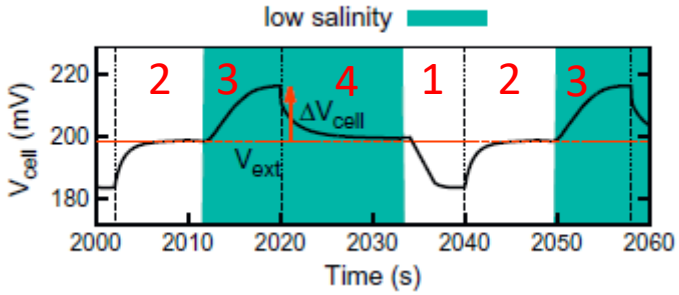

Fig. 14: Example of CapMix cycle [19]. The cell is charged up to a voltage of 0.2 V during step 2. In step 3 there is a voltage rise due to the injection of the low salinity water. Step 4 corresponds to the cell discharge and the harvested energy is recovered. The high salinity water is injected during step 1 and the process is repeated.

During step 3, the injection of low salinity water is causing an expansion of the electrical double layer. This expansion, located in the diffuse part of the electrical double layer [19] (refers to chapter 2.1 for further details), is responsible for the voltage rise, as already described. Analogously, during step 1, a contraction of the electrical double layer is caused by the injection of the high salinity water. This effect results in a decrease of the potential difference across the cell.

During step 2, the solution gets partially deionized due to the potential applied, as in capacitive deionization. During step 4, instead, the concentration of the solution is increased because of the release of the ions. The consequence is that this process performs a controlled mixing of the solutions.

Thus, at each cycle, a portion of Gibbs free energy [99] is lost due to this mixing, leading on one side to a dilution of the more concentrated solution and on the other to a

concentration of the less concentrated solution. Contemporarily, part of this energy is harvested in form of electrical energy due to the voltage rise as described in Eq. 13.

Without entering too deeply in the thermodynamic description which was thoroughly described by Brogioli [100], in the following are summarized the equations involved in this phenomenon.

The Eq. 15 assesses the Gibbs free energy that can be extracted by mixing two solutions at different concentrations.

$$\Delta G = RTn \log \frac{c_{low}}{c_{high}} \tag{15}$$

Where G is the Gibbs free energy (J), R is the universal gas constant (8.31441 N m mol^{-1} K^{-1}), T is the absolute temperature (K), n is the number of moles of salt transferred (mol), and c is the starting concentration of the two solutions (M).

Combining the Eq. 15 with Eq. 14, it is also possible to show how the voltage rise strictly depends on the concentration of the initial solutions and the desalination efficiency of the electrodes.

$$\Delta V = \eta \frac{2RT}{F} \log \frac{c_{low}}{c_{high}} \tag{16}$$

where V is the voltage difference across the device (V), F is the Faraday constant (96485 C mol^{-1}) and η is the desalination efficiency of the active material, representing the number of salt molecules captured over the total number of molecules which crossed the device. In the case of a redox reaction, η = 1, thus obtaining the Nernst law, representing a thermodynamic limit for the method.

3.3.2 State of the art

Since the dawn of the CapMix, this technique has faced rapid improvements. The first attempts were performed with symmetric, uncharged materials [97]. The results were enough to prove the potentiality of this technique, even though they were obtained in a microfluidic cell. The energy extracted at each cycle was only 5 μJ, with a power output of roughly 7 mW/m^2.

In the following years, many experiments were run to improve the efficiency of this technique. Work has been made on the design of the cell [101], on the possible combinations of different activated carbons [60] and also on the application of charged

coatings on the surface of the electrodes to exploit their spontaneous potential difference [102]. All these works go under the category of the membrane-less CapMix.

Another family of materials that have recently attracted the interest of the scientific community are the electrodes coupled with ion exchange membranes. In this frame, the membrane-based CapMix find application because of the exploitation of the Donnan potential which builds up thanks to the presence of ion exchange membranes, providing a stable, net bias to the cell [103]. Even more, the entire cycle can be performed without providing electrical energy to the cell, thus strongly increasing the efficiency of the whole process [104]. Also for the membrane-based CapMix, engineered electrodes have been proposed, coupling flow electrodes with ion exchange membranes [105]. Another variation on the theme consists in the exploitation of the industrial waste heat to enhance the energy harvesting process [106].

A totally different approach to CapMix has been proposed by La Mantia et al. in 2011 [107]. In their work, they used a battery instead of a supercapacitor to harvest energy from salinity gradients. Such battery exploited a silver electrode to capture the Cl ions, while a sodium manganese oxide was responsible for the capture of Na ions. Being the equilibrium potential a function of the NaCl concentration in solution, they proved that this kind of system is able to harvest energy when performing a CapMix cycle. The power obtained in this way was 105 mW/m^2, with an energy conversion efficiency of roughly 75%. They called this device “mixing entropy battery”. From that moment on, other research groups started working on this kind of devices. Improvements of the system have been proposed in literature to increase the efficiency of the process [108].

Few years later, published works in this field described the possibility of using hexacyanoferrate salts in mixing entropy batteries. Copper [109], cobalt [110], nickel [111] and iron [112] hexacyanoferrate have been proposed as active materials for the positive electrode, showing good results in term of density of power and efficiency. In particular, Ye et al. [112] investigated the possibility of coupling the Prussian Blue with polypyrrole to obtain a battery which is able to harvest energy without supplying any electrical energy to it.

This scenario shows how the CapMix is a very recent technique which is still under study at the laboratory scale, keeping high interest among the scientific community. Efforts are still in the direction of improving the efficiency of the whole cycle, to reach output power which can compete with more mature techniques, aiming for larger scale applications.

3.3.3 Capacitive deionization

Capacitive deionization (CDI) is a technique able to remove ions from water. While it can be employed to remove any kind of ions, CDI commonly finds application in removing salt from brackish water to produce freshwater.

CDI was first proposed by Blair and Murphy in 1960 [113]. They used activated carbon to fabricate the electrodes and they called such technique "electrochemical demineralization". In the following decade, many experiments were run to investigate its working principle [114] and to prove the feasibility of this technique [115]. In the very beginning, it was thought that this technique was relying on the ability of porous materials to chemisorb ions present in solution by means of redox reactions [116]. Only at the beginning on '70 became clear that the working principle of CDI was relying mainly on the formation of the electrical double layer on the porous carbon [117]. Contemporarily, it was also proved how irreversible redox reactions would bring to a degradation of the electrodes and thus must be avoided.

The following 2 decades had seen an increasing scientific effort to push forward the CDI towards large-scale application, including efficient ways to separate deionized water from concentrated water after each desalination cycle [118].

Starting from the '90, the interest of the scientific community in CDI has grown fast, thanks to the diffusion of new performing materials like activated carbons with high surface area [119], carbon aerogels [120], carbon nanotubes [121], graphene [122], zeolites [123] and the diffusion of theoretical models and new, promising technologies [5], like membrane capacitive deionization (MCDI) [124].

3.3.3.1 Working principle

The working principle of CDI is essentially the same of a supercapacitor and can be seen as the counterpart of the CapMix. The CDI cell is made of two electrodes, in which a porous material is used to store ions taken from the electrolyte. In this case, the electrolyte is a stream of brackish water. A cyclic operation mode is required to release the salt that has been adsorbed when the electrodes reach the saturation point.

In general, a standard operation cycle for a CDI device is the following. First, the cell is filled with a stream of brackish water. Then, a voltage is applied to the cell and the deionization process begins. In this step, freshwater is produced. When the electrodes saturate, the voltage is reversed and the electrodes start releasing ions in solution. In this step, brine is produced. When the discharge is complete, production of freshwater starts again and the cycle is repeated. This working mechanism is sketched in Fig. 15.

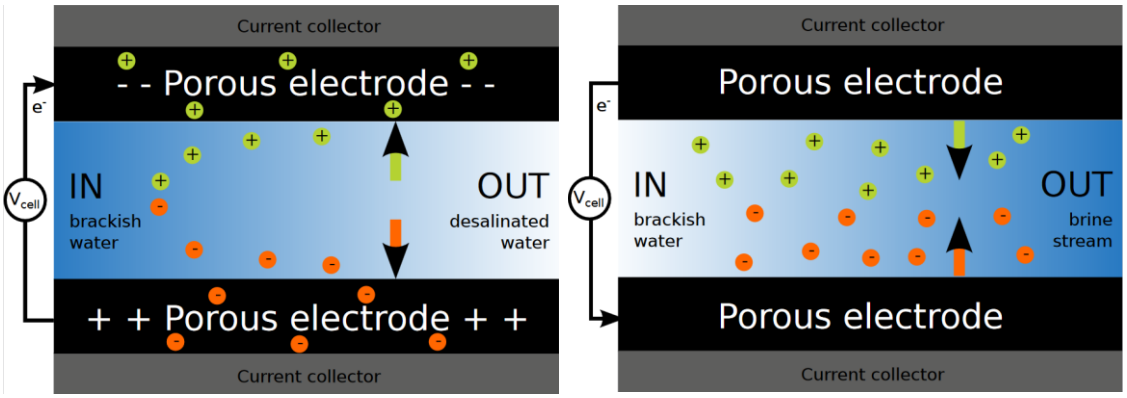

Fig. 15: Working principle of CDI [125]. On the left, the charge step with the corresponding production of freshwater. On the right, the discharge step and the production of brine.

There are many variations of the cycle described above. One of them consists in short-circuiting the electrodes during the discharge step instead of reversing the polarity [126]. This allows to drastically reduce the incidence of the re-adsorption phenomenon of released ions on the oppositely charged electrodes.

A different approach consists in applying a constant current to the electrodes, while measuring the potential. When a certain voltage difference is reached (usually 1.2 V to minimize the water electrolysis), the current is reversed and the discharge begins. This method, in certain conditions [127], can be useful to save energy and preserve the electrodes from degradation.

Another variation on the theme is the employment of ion exchange membranes, which are used to reduce the energy provided during the charging step [128] and contemporarily increasing the efficiency of the desalination process because of the negligible adsorption of counter ions on both the electrodes [129]. A graphical representation of the MCDI working principle is provided in Fig. 16.

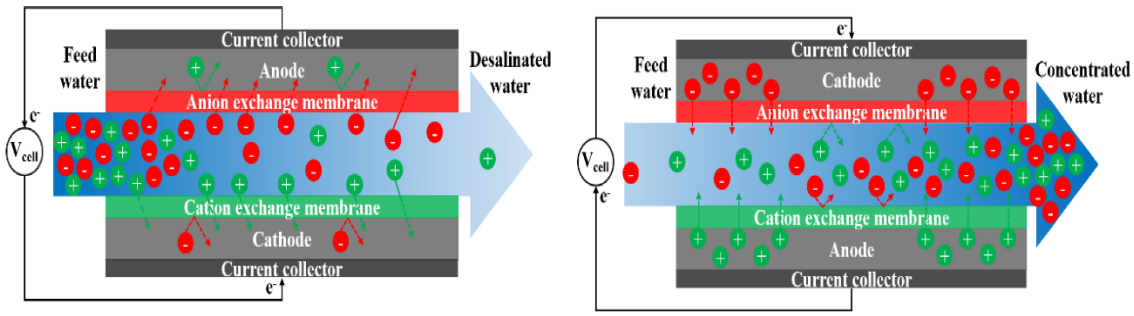

Fig. 16: Working principle of MCDI [130]. On the left, the charge step with the corresponding production of freshwater. On the right, the discharge step and the production of brine.

The processes described above are referring to a particular operation condition of the CDI cell, the so-called "flow-by" operation mode, in which the stream of water is passing between the electrodes. However, there is another setup often employed, the "flow-through" operation mode [131]. In this case, the water stream is crossing the porous electrodes which are placed perpendicularly to the stream. A scheme is reported in Fig. 17.

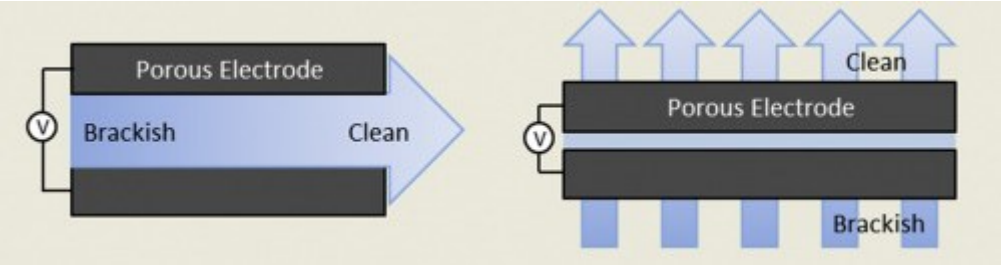

Fig. 17: Comparison of CDI operation modes [131]. On the left, flow-by process. On the right, flow-through process.

For what concerns the geometry of the electrodes, the planar configuration is the most commonly employed because of it is easy to handle, does not require complicated setup and it is fully compatible with rolled configuration. However, a different geometry can be found in literature, the so-called "flow-electrodes" [132].

The flow-electrodes are attracting the interest of the scientific community because they allow for a continuous operation of the CDI, thus avoiding the cycle previously described. The idea is that the fresh active material keeps flowing inside the electrodes, granting a constant desalination rate of the water stream. The regeneration (discharge) of the saturated material is deferred to a different device. To avoid loss of active material inside the water stream, ion exchange membranes are commonly employed [133]. A scheme of this configuration is shown in Fig. 18.

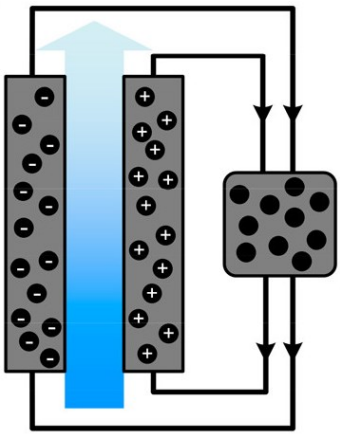

Fig. 18: Flow-electrodes CDI configuration [132]. The particles flow from a reservoir to the electrodes and vice versa while the desalination process in ongoing.

From the energetic point of view, every desalination process has to face a minimum energetic requirement which is given by the Gibbs free energy (see Eq. 15 in section 3.3.1 for further details). Indeed, the dissolution of salt in water is an exoenergetic process. Therefore, in compliance with thermodynamics, there is a certain amount of energy which must be provided to remove the ions from the water. This energy is estimated to be around 3600 J per liter of pure water obtained starting from seawater [134].

To this minimum amount of energy, it is necessary to sum the amount of energy required by the process of water pretreatment (removal of organic material, dispersed solids, etc.), by the pumping system and, of course, by the desalination process itself.

The strength of the CDI technique is its low energetic consumption. While not so much can be done about the pretreatment since it depends on the condition of the water source, the importance of the energetic efficiency becomes evident for the desalination process [135]. For the CDI process, no overpressure nor heating are required, but only electrical energy. This energy is initially provided during the charging step to remove the salt from the water. Then, it can be partially recovered during the regeneration step, in which the electrodes are discharged.

The energetic efficiency (η) of a whole desalination cycle is, therefore, defined as the ratio between the energy recovered during the regeneration step and the energy provided during the desalination step. This is represented by Eq. 17.

$$\eta = \frac{W_{discharge}}{W_{charge}} \tag{17}$$

The possibility of recovering even partially the energy provided is the reason of such a low energetic consumption, in combination to a potential applied to the CDI cells that is usually around 1 V. A similar principle is used in reverse osmosis, where pressure exchangers are used to pressurize the incoming streaming of water. However, in that case, the pressure drop across the membrane stack drastically lowers the η of the system.

In the frame of efficiency, there is another kind of efficiency parameter that can be defined, the so-called "charge efficiency" (Λ). First introduced by Johnson and Newman in 1971 [117], this parameter represents the amount of ions stored into the double layer over the number of electronic charges provided by the external circuit.

$$\Lambda = \frac{mSAC \cdot F \cdot m}{10^3 \cdot MM \cdot Q} \tag{18}$$

Where MM is the molar mass of the removed salt (58.44 g/mol for the NaCl), F is the Faraday constant (96485 C/mol), m is the mass of the active material (g), Q is the electronic charge (C) and $mSAC$ is the maximum salt adsorption capacity (mg/g).

The mSAC represents the maximum amount of salt that the active material is able to adsorb at a fixed voltage. This value can be measured only when the equilibrium is reached, thus constant current methods cannot be used. The mSAC is normalized by the weight of the active material. Together with the mSAC, other parameters are often reported in CDI experiments [7]. The percentage of salt removal (%) is commonly found in CDI papers, even though it is a meaningless parameter when provided without any information about the total volume of desalinated solution and/or the amount of active material.

The average salt adsorption rate (ASAR) is a parameter linked to both the architecture of the cell and the electrode material. It represents the rate of salt adsorption on the electrodes (mg g^{-1} min^{-1}). It can be evaluated as the mSAC divided by the time required to adsorb that amount of salt. The importance of this parameter was highlighted by Xu et al. in 2008 [136], showing how the mSAC was influenced by the setup and the flow rate. A comprehensive study on a CDI plant or device should pay attention to the ASAR, since it's providing a measure of the adsorption capability of the system and, thus, of its efficiency. However, this parameter is not recommended when confronting different studies on active materials, because it is strongly affected by the flow rate, cell geometry, etc. Moreover, the definition of time over which the mSAC should be normalized is not univocal. It can be the time to reach the mSAC or the time of the full cycle [7].

Finally, a parameter often reported in literature is the electrode capacity (F/g). Commonly used when characterizing supercapacitors, it is a measure of the number of charges that the material is able to store at a certain voltage. It is normalized by the electrode mass or the electrode area. In CDI, it is usually evaluated through electrochemical methods (see section 4.1.3.1) employing high salinity solutions (for instance NaCl 1 M).

3.3.3.2 State of the art

The established desalination technology is nowadays the reverse osmosis. It has become the conventional system for most of the desalination plants all over the world, followed by multistage flash distillation which is still employed in a certain number of plants in the Middle East [137].

Even though there are many patents related to CDI [138] [139] [140], this technology is still far from reaching the mass production and large scale diffusion. However, studies have shown how, at low salinity, the CDI can be more efficient than reverse osmosis because of its low energy consumption [141]. In the recent years, projects involving the development of CDI pilot plants have been funded all over the world. While most of the studies are exclusively theoretical [142] [143] [144] [145], few example are reported in literature of small CDI pilot plants.

Ahmad et al. [146] tested activated carbons mixed with TiO_2 initially in a single cell for a proof of principle. Then, they moved to a laboratory-scale system made of a stack of 6 cells. Finally, they built a pilot scale device working with a stack of 20 cells. They used artificial solutions of NaCl 35~50 mM, achieving an mSAC of 11.2 mg/g and a salt removal of 70% at 1.8 V.

Kim et al. [147] used a pilot plant made of a stack of 50 cells, each 100 cm^2. They tested the performance of activated carbon coated with ion exchange membranes in a real case study with municipal wastewater. The results show a charge efficiency of ~ 73% at 1.2 V. For each ion specie found in solution, they also reported the adsorption capability.

Tan et al. [148] designed, constructed and operated a 1 kW CDI pilot plant. To verify their model, they built a pilot plant coupling an MCDI system with a photovoltaic power source. The CDI unit (comprised of pumping system, reservoir tanks and CDI cells) was provided by an industrial company. To guarantee a 24 h operational condition, a battery system has been added to store the excess of energy produced by the solar cells during the daytime and to use this energy during the night. A production of 5 m^3/day of freshwater has been achieved starting from an artificial solution of NaCl 20 mM. The results obtained in their study allowed to validate their model and to demonstrate the feasibility of coupling a solar power source with a CDI desalination system.

For what concerns the field of application of CDI, the target is commonly brackish water with a low salinity content. However, other applications seem feasible. It's the case reported by Lado et al. [149], in which they employed the CDI to remove salt from concentrated brackish water (thus increasing the desalination efficiency of the plant) and to release this salt in a brine stream. A part from the added value of concentrated brines in raw materials recovery [150], discharging the CDI electrodes in a highly concentrated solution increases the efficiency of the energy recovery [151].

The most common architecture of the cell is a stack made of current collector, active material and separator. However, there are studies in literature reporting the possibility of using interconnected structures both as current collector and active material [152] [153], thus removing the metal component from the cell, making it lighter and thinner.

Finally, for what concerns the salt adsorption reported in literature, the numbers vary a lot. Confronting more than 200 values reported in 5 different reviews [5] [6] [126] [154] [155], it is possible to observe that the majority of the materials show a salt adsorption below 10 mg/g. Among them, there is a non-negligible portion below 1 mg/g. The remaining part of the materials show a salt adsorption above 10 mg/g, with just a few above 20 mg/g. However, it is mandatory to put in evidence the total absence of a standardized method. Each experiment has been run in a different condition and the data are often reported in different manners, making a comparison almost impossible. For the CDI technique, this fact is surely one of the causes behind its struggling in scaling-up and emerging in the large-scale market. To resolve this issue, Hawks et al. [156] have recently proposed to report the results in term of volumetric energy consumption (Wh/m^3) and throughput productivity ($L\ h^{-1}\ m^{-2}$), with a standard water recovery of 50 % and a starting concentration of NaCl 5~20 mM.

4. Experimental

In this chapter are reported in details the experimental procedures adopted during the research activity. In particular, for both capacitive deionization and capacitive mixing, a list of materials and methods is provided, together with a description of the experimental setups. Finally, an overview of the characterization techniques is provided.

4.1 Capacitive deionization

Capacitive deionization (CDI) is the starting point of this research activity. All the materials which have been lately employed for capacitive mixing, have been previously characterized and tested for CDI. The reason for this choice is straightforward: a material which cannot efficiently remove and store ions from water, cannot be suited to harvest energy from salinity gradients.

4.1.1 Materials and methods

In this section, the materials tested for CDI are listed, together with a description of the experimental setup and the procedure adopted to assemble the device.

4.1.1.1 Active material

The active material plays a key role in CDI. Responsible for the formation of the electrical double layer (EDL), it has to provide a large surface area to store a great number of ions.

Moreover, it must be conductive to minimize the voltage drop between the current collector and the surface of the electrolyte. To account for that, the active material is usually made of a thin layer (tens or hundreds of μm) of carbon-based material directly coated onto the metallic current collector.

There are many coating procedures reported in literature. Above them, dip coating [157], spray coating [158], doctor blade method [159], spin coating [160] and screen printing [161] must be mentioned because of their scalability which allowed them to be scaled in the past years to industrial application.

For all the preparation methods cited above, a liquid phase is mandatory. Therefore, the preparation of the related slurry with a proper density is a crucial step to obtain a performing device. The choice of an adequate solvent, a functional mass ratio of active

material, additive and binder, and finally a proper mixing procedure are the keys to achieve a composition that can work for the purpose.

In this work, I decided to work with activated carbon, since it is mass-produced, it is highly conductive, it is providing a high surface area and can be easily dispersed in many solvents. Activated carbon YP-50F manufactured by MIT Corporation was selected for this thesis activity. This activated carbon is specifically designed for supercapacitor electrodes, the datasheet reports a nominal surface area of 1666 m^2/g and the dominant impurities are declared to be K (167 ppm), Na and Fe (both ~35 ppm).

For what concerns the binder, among the vastness of possible polymers, I decided to use the polyvinylidene fluoride (PVDF, M_w 534000, Sigma Aldrich), since it provides good adhesion over the current collector and it is insoluble in water, while being easier to solubilize in organic solvents and cheaper than its fully fluorinated counterpart, the polytetrafluoroethylene (PTFE). With the aim of furtherly reduce the cost of the final device while contemporarily improve the performances, the sulfonated poly(ether ether ketone) (SPEEK) exchanged with Na^+ ions was tested as a binder. The SPEEK was synthetized in the Center for Sustainable Future Technology of the Istituto Italiano di Tecnologia (IIT) in Turin (https://www.iit.it/it/csft-polito) and provided as a membrane.

The exchange procedure here described was always the same, regardless of the final use of the SPEEK (membrane, coating or binder). The SPEEK membrane as-provided was first washed in deionized water (DI H_2O) to remove impurities. Then, it was immersed for 2 hours in HCl 0.5 M to provide H^+ to the active sites of the polymer. After that, it underwent another washing step in DI H_2O and then it was immersed in a NaCl 1 M solution for 24 h for allow for the $H^+ \rightarrow Na^+$ exchange. The membrane was finally rinsed in DI H_2O to remove the excess of salt. HCl (fuming, 37%) and NaCl (≥ 99% purity) were both supplied by Sigma Aldrich.

As a solvent for the slurry preparation, dimethyl sulfoxide (DMSO, ≥99.5% purity, Sigma Aldrich) was selected because of its ability to disperse PVDF, activated carbon and graphene oxide (GO), together with its high boiling point and low vapour pressure. Moreover, the DMSO is also able to quickly solubilize the SPEEK membranes. The PVDF was dispersed in a concentration of 4 mg/ml, the GO in a concentration of 10 mg/ml, while the SPEEK in a concentration of 40 mg/ml.

The last component of the active material is the additive. In this research activity, the additives employed were all based on GO, with the only exception of MXenes. GO (Single layer GO, 300-800 nm of lateral dimension, Cheap Tubes Inc.) was used as it is for negatively charged electrodes or functionalized (fGO) for positively ones. The functionalization of GO flakes was based on a modification of the method described by Roppolo et al. [162].

Briefly, GO flakes were dispersed in N,N-dimethylformamide (DMF, ≥ 99% purity, Sigma Aldrich) in a concentration of 1 mg/ml. The dispersion was sonicated for 30 min

at 40 kHz. Then, 4-hydroxybenzophenone (HBP, 98% purity, Sigma Aldrich) was added to the dispersion in an amount triple with respect to the mass of the GO. The dispersion obtained in this way was stirred and bubbled with N_2 for 30 min. At this point, it was exposed to UV radiation (UV solar simulator, Newport) for 5 min with an intensity of 200 mW/cm^2 while stirring. After this treatment, the result was a reduced graphene oxide (rGO) functionalized with the HBP.

Subsequently, the dispersion was centrifuged (IEC CL10, Thermo Scientific) at 4000 rpm for 20 min. The precipitate was washed in ethanol (anhydrous, ≥99.5% purity, Carlo Erba) and centrifuged. This step was repeated 3 times to separate the unreacted material. The functionalized GO obtained in this way (fGO-Step I) was dispersed again in DMF in a concentration of 1 mg/ml. To achieve the final desired functionalization, the proper amount of (2-(acryloyloxy)ethyl)trimethylammonium chloride solution (80% in H2O, Sigma Aldrich) was added to the dispersion in the mass ratio 15:1 with respect to fGO-Step I. The solution was stirred, degassed by nitrogen bubbling, exposed to UV, centrifuged and washed like before. The only difference is that the exposition time was 15 min in this case. After the final washing, the fGO-Step II was obtained and it was stored in ethanol in a concentration of 5 mg/ml.

The same procedure has also been adopted to functionalize GO with 3-sulfopropyl acrylate potassium salt (anhydrous, ≥99% purity, Sigma Aldrich) and 2-Acrylamido-2-methyl-1-propanesulfonic acid (anhydrous, ≥99% purity, Sigma Aldrich).

For what concerns the MXenes, they are a class of 2D inorganic materials obtained from a combined chemical etching and exfoliation of MAX phases [163]. Among the many chemical compositions available, the MXenes used during this thesis are of the form Ti_2C_3X, where X is a halogen impurity coming from the etching of the Al. It is mainly F and Cl. The MXenes are supplied by partner research lab in Grenoble (INP, NanoMat research group).

Independently on the final composition of the active material, the slurry preparation followed always the same procedure, here described. First, the binder and the DMSO are put in beaker and sonicated for 10 min at 59 kHz in an ultrasonic bath (LBS2, FALC INSTRUMENTS SRL). After that, the activated carbon is slowly added while contemporarily stirred. The slurry is then stirred for 1 h. At this point, depending on the slurry composition, the additive material previously prepared is added to the slurry, together with its own solvent. No other solvents are added to the slurry. Finally, the slurry is stirred overnight and stored in sealed vials. The mass ratio of components in each slurry was 9:1 for activated carbon and binder, respectively. In presence of any additive, the ratio was changed to 9:0.5:0.5.

In Tab. 2 is reported a summary of all the combination of materials tested for CDI, together with a brief description of their features.

Material	Positive electrode	Negative electrode
AC	Activated carbon: 90% PVDF: 10%	Activated carbon: 90% PVDF: 10%
AC-SPEEK	Activated carbon: 90% PVDF: 10%	Activated carbon: 90% SPEEK: 10%
GO-$GONH_3$	Activated carbon: 90% PVDF: 5% GONH3: 5%	Activated carbon: 90% PVDF: 5% GO: 5%
GOPSS-$GONH_3$	Activated carbon: 90% PVDF: 5% GONH3: 5%	Activated carbon: 90% PVDF: 5% GOPSS: 5%
MX-$GONH_3$	Activated carbon: 90% PVDF: 5% GONH3: 5%	Activated carbon: 90% PVDF: 5% MXenes: 5%

Tab. 2: Summary of the materials tested for CDI.

4.1.1.2 Device fabrication

In this work, the doctor blade method was selected because of its simplicity and scalability. It is commonly used in industrial roll-to-roll applications [164] where many meters of membranes or coatings can be stacked in a small volume to meet certain requirements, like in the case of desalination plants.

This method consists in coating the current collector by means of tool like a blade, a rod, a bar or anything similar to it, which allows to spread out the slurry in a uniform way. To do so, the tool is moved at a constant speed and direction over the current collector. Such tool has a spacer granting a fixed thickness of the final dried coating.

In this work, a rod featuring a metallic spire on its surface was used for this purpose. Such rod is designed to produce a coating of nominal thickness equal to 150 μm. The system was manually operated.

An insulating Kapton tape is applied on the edge of the current collector to define a fixed geometry and to avoid lateral leakage of solution from the CDI cell. The active area of each electrode is 64 cm^2.

The slurry is poured on the current collector and spread on the surface by means of the doctor blade method described above. The excess of material is removed during the coating procedure and then the electrode is dried at 50 °C for 15 min on a hotplate. Finally, the electrode is weighted to check the amount of active material deposited on its surface.

A sketch of the whole electrode fabrication is reported in Fig. 19.

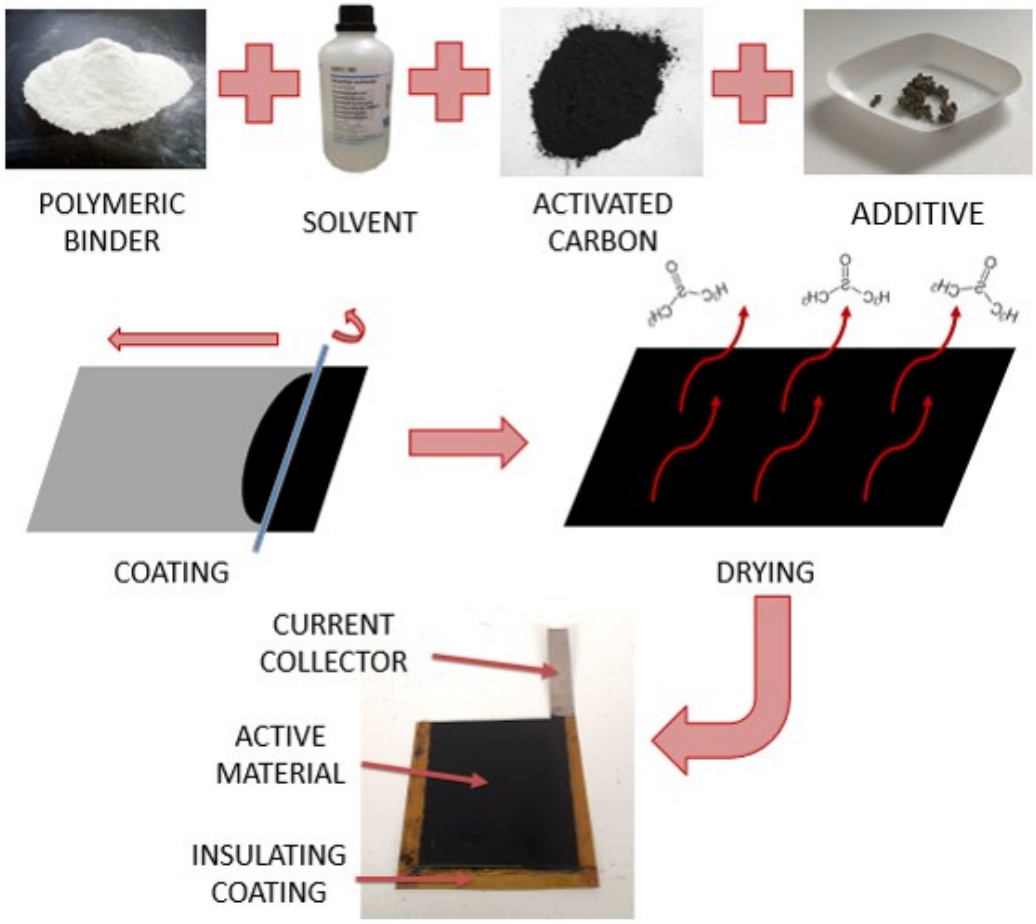

Fig. 19: Scheme of electrode fabrication, showing the components of the active material, the coating procedure and the final electrode.

The CDI tests were performed in a homemade cell (Fig. 20). The walls are made of poly(methyl methacrylate), while the sealing is made of polydimethylsiloxane. These materials are both transparent and chemical inert. The first one is rigid, the second is flexible and perfectly fits as sealer.

The whole cell is kept together by a series of 4 screws and bolts. On the walls of the cell, the two electrodes are kept in place by the sealing, at a fixed distance of 1 cm. The metallic finger of the electrodes is used to connect each of them to the potentiostat. The inlet tube is placed on top left corner of the cell, while the outlet tube on the bottom right corner. This positioning allows a uniform mixing of the solution in the whole cell, even if the squared design is not optimized for fluidic applications.

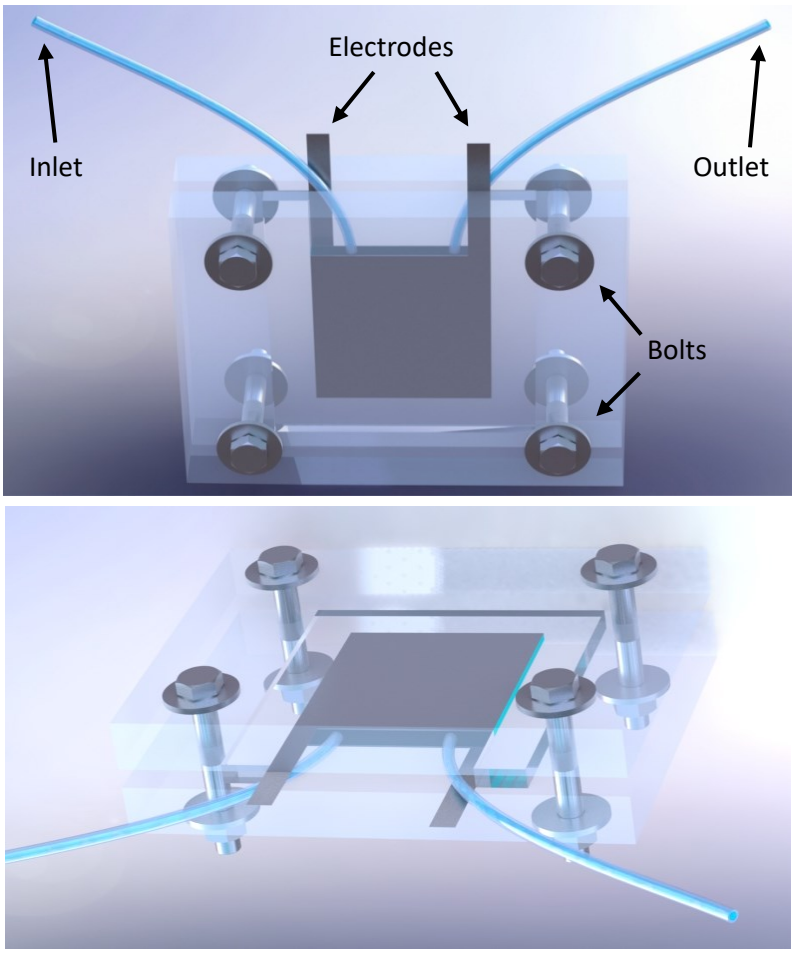

Fig. 20: On the top, front view of the CDI cell. On the bottom, top view of the cell. It is possible to see the clamping system, the polymeric sealing, the electrodes and tubes.

A different cell is used when characterizing the active materials, before testing them for CDI (Fig. 21). Two smaller electrodes (5 x 2 cm) with a coating of 1 cm^2 of active material are facing each other inside a beaker containing few ml of electrolytic solution. A polymeric spacer is used to keep them at a fixed distance of 1 cm, to mimic the CDI setup. The potentiostat is directly connected to the electrodes.

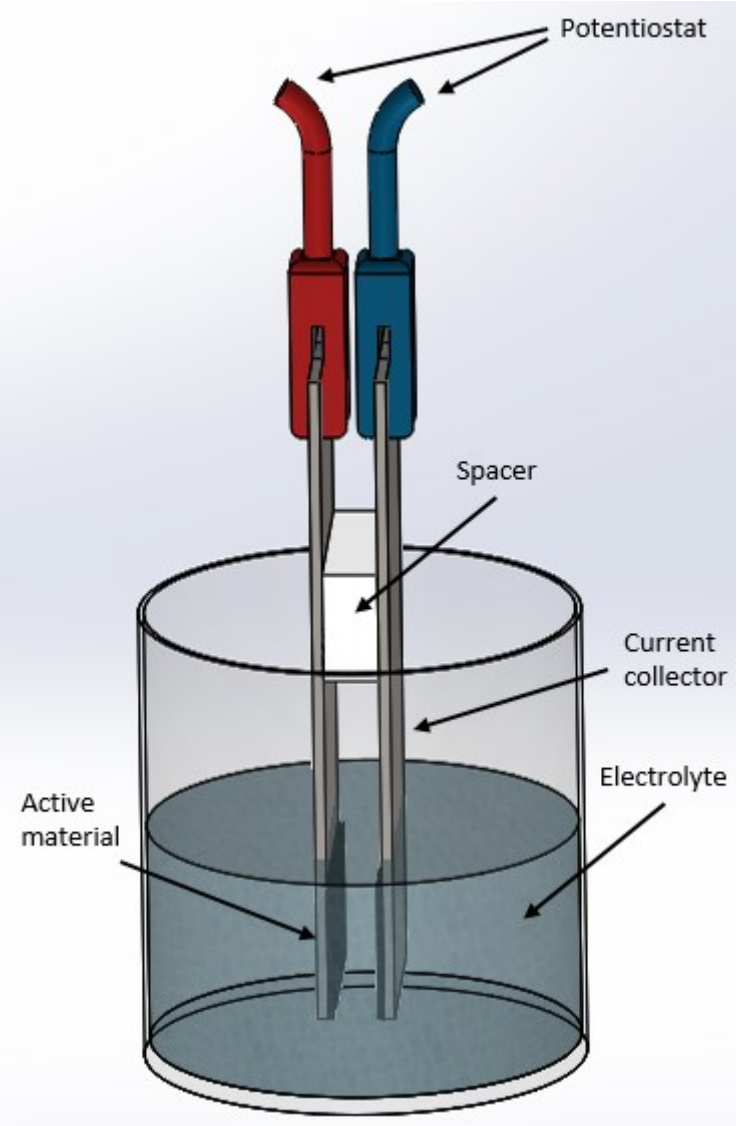

Fig. 21: Scheme of the cell employed for the electrochemical characterization of the active materials.

4.1.1.3 Experimental setup

The experimental setup for CDI experiments is composed of five elements (Fig. 22). The CDI cell, described in section 4.1.1.2. A peristaltic pump (Reglo Pump, Ismatec), providing a fast circulation of the water from the CDI cell to the conductivity meter and vice versa. A thermostatic bath (Omnicool unit 62 Plus, LAUDA), in which the conductivity is measured at a constant temperature while the solution is contemporarily stirred. A conductivity meter (Edge, Hanna Instruments), featuring an automatic temperature control and equipped with an internal memory for the automatic acquisition of up to 1000 measurements. A potentiostat (Autolab, Metrohm), powering the CDI cell. A computer, with the Reglo software for the remote control of the pump and the Nova 2.1 software controlling the potentiostat.

For all the CDI experiments, the water was pumped at a fixed speed of 20 ml/min. The total volume of the solution in the circuit (CDI cell + tubes + reservoir for conductivity measurements) was 80 ml. The solution employed was NaCl 10 mM, each time freshly prepared. The conductivity of the solution was measured every minute for the whole duration of each experiment. In every experiment, the cell was charged and discharged 5 times between 1.2 V and 0 V, without switching the polarity of the cell.

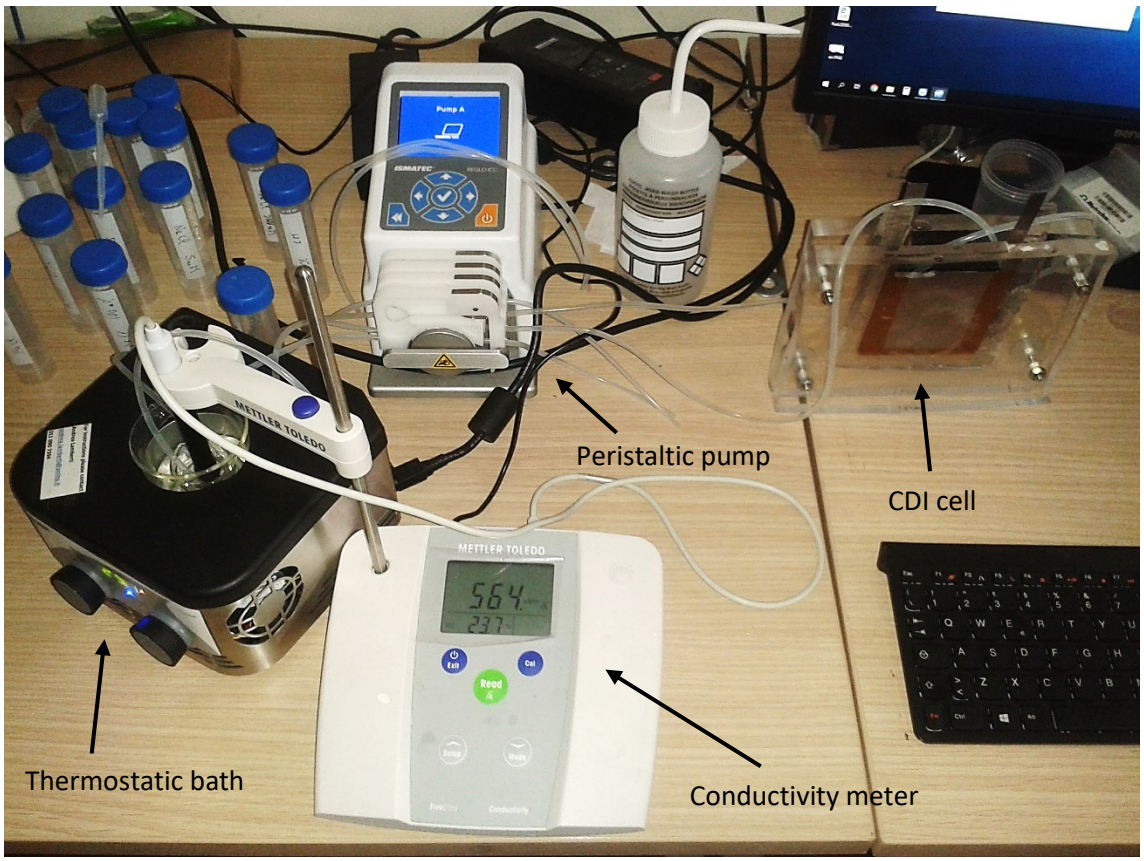

Fig. 22: Experimental setup for capacitive deionization. Out of the image, the potentiostat powering the deionization cell.

4.2 Capacitive Mixing

Capacitive Mixing (CapMix) is the final goal of this research activity. All the materials which have been previously employed for capacitive deionization, have been then tested for CapMix.

4.2.1 Materials and methods

In this section, the materials tested for CapMix are listed, together with a description of the experimental setup and the procedure adopted to assemble the device. While most of the characterization methods are in common with capacitive deionization and have been previously described, here are, therefore, reported the procedures and methods strictly related to CapMix only.

4.2.1.1 Active material

The preparation of the active material followed the same procedure described for the CDI, in section 4.1.1.1. No changes are made to the slurry preparation and to the mass ratio of the components. In general, the materials already employed in CDI have also been tested for CapMix, with particular attention to the materials that already showed to be promising for CDI. There are few exceptions to this and will be described in chapter 5.2.

4.2.1.2 Device fabrication

The electrodes' fabrication resembles what described in chapter 4.1.1.2. The only difference is that the electrodes employed for CapMix are not the large ones, but the small ones (5 x 2 cm). The exposed area is ~1 cm^2. Consequently, the coating procedure underwent a slightly modification. To ensure repeatability, a plastic mask with a hole of 1 cm^2 was produced by cutting a polyethylene with a circular stamp. The mask is placed over the current collector and kept in place by means of a scotch tape. The doctor blade method described in section 4.1.1.2 is used to coat the active material over the current collector. Finally, the mask is removed and the final electrode is obtained. The result can be observed in Fig. 23.

The cell employed for CapMix, instead, is completely new. It was designed specifically for microfluidic application [165]. The cell is composed of two round-shaped resin caps, one featuring 2 inlets while the other 1 outlet. The two caps were made by 3D

printing in the scientific laboratory “ChiLab”, in Chivasso (TO), Italy. In between the two caps are placed the electrodes, separated by a polymeric spacer which is also working as cell itself, thanks to its drop-like design. The clamping system is composed of a set of 4 screws and bolts. A rendering of the cell is proposed in Fig. 23.

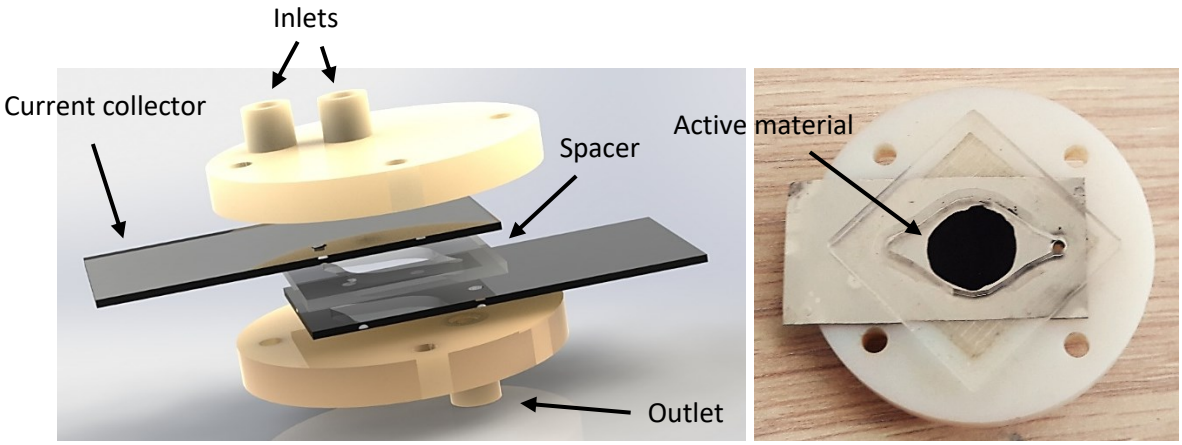

Fig. 23: On the left, exploded view of the CapMix cell. On the right, half-cell. It is possible to appreciate the design of the internal polymeric separator.

4.2.1.3 Experimental setup

The experimental setup for CapMix experiments is composed of five elements (Fig. 24). The CapMix cell, described in section 4.2.1.2. Two reservoirs containing, respectively, artificial seawater (NaCl 0.6 M) and artificial freshwater (NaCl 10 mM). A peristaltic pump (Reglo Pump, Ismatec), providing a fast circulation of the water from the two reservoirs to the CapMix cell. A potentiostat (Autolab, Metrohm), powering the CDI cell. A computer, with the Reglo software for the remote control of the pump and the Nova 2.1 software controlling the potentiostat.

During CapMix experiments, the water was pumped at a fixed speed of 10 ml/min, to allow for fast exchange of the water inside the internal volume of the cell. The volume of solution inside the cell was 0.25 ml.

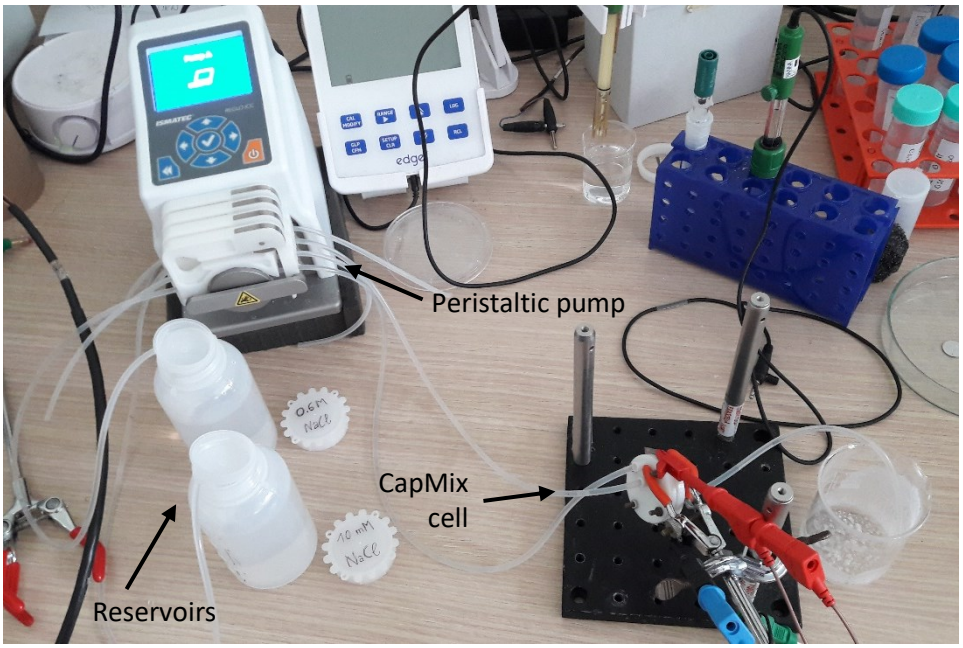

Fig. 24: Experimental setup for Capacitive Mixing. On the bottom right, the beaker collecting the mixed water and the CapMix cell, vertically housed in a clamping system and electrically connected to potentiostat (out of the image).

4.3 Characterizations

4.3.1 Physical and chemical characterizations

In this section, a description of the technologies involved in the physical and chemical characterizations of the materials is provided.

4.3.1.1 FESEM

Field Emission Scanning Electron Microscopy (FESEM) is a characterization technique used during the thesis work. The idea is to be able to see what an optical microscope cannot allow to see because of the diffraction limit of the visible light. This theoretical limit tells that a wave (visible light in this case) cannot be used to resolve details of the order of half its wavelength or below. However, this limit can be higher because non-ideal lens and other problems regarding the instrument. Practically speaking, with visible light is hard to resolve details of the order of few micrometers using a standard optical microscope.

To overcome the diffraction limit of visible light, Scanning Electron Microscopy employs electrons instead of visible light. Electrons have a wavelength depending on their energy (De-Broglie equation). In FESEM instruments, their wavelength can vary, but it is of the order of few picometres. The resulting resolution of these instruments is around few nanometres.

FESEM apparatus is made of a source of electrons, a column in which the electron beam is accelerated and focused, a chamber where sample and detectors are placed and a vacuum system.

In FESEM, as the name suggests, electrons are removed from a metal tip thanks to a high voltage applied (of the order of 10^5 V), generating an electric field sufficient to extract electrons from the material (field emission). An electric field accelerates them to the column.

Inside the column, magnetic lenses are used to focus and move the beam. After this stage, the electron beam reaches the chamber, impinging on the sample. The beam is used to scan the sample with parallel lines (from here, “scanning”), using a software to build the final image. When an electron reaches the sample, different types of interaction can take place.

The impinging electron, called “primary electron”, can be scattered back. In this case, its kinetic energy is not varied a lot (elastic scattering). This high-energy electron is not used for detection. If it is not the case, the primary electron will interact with the sample. It can collide with an electron of the sample’s atoms, transferring a part of its energy to

it. This energy can be enough to make this electron free. Such an electron is called "secondary electron". This electron can come from the surface, but it can have enough energy to let it escape the sample from below the surface. Secondary electrons have energies much lower than primary electrons. They are used for detection.

When a core electron is removed from an atom in the previously described way, an outer one will take its place. When this process takes place, it is possible that another electron will be released from the same atom. This electron is called "Auger electron". Its energy strictly depends on the element from which it comes from. Its energy is much lower than secondary electron's energy, so they cannot escape the sample unless they are emitted from the surface. Auger electrons are usually emitted by low atomic number elements. If an atom has a high atomic number, it is easier that it will release the excess of energy as an X-ray. X-rays, like Auger electrons, have different energies (and so different wavelengths) depending on the elements emitting them. Both are used for detections.

Due to the contemporary presence of all these phenomena, different types of sensors are present inside the chamber. Two secondary electron detectors are combined together to have information about the morphology of the sample. An Auger detector is usually close to the sample and it gives information about the elements on the surface. Finally, an X-ray detector gives information about the elements also below the surface of the sample and can give quantitative information like the relative percentage of the elements in the sample.

To make possible what described above, the system has to be in ultra-high vacuum (UHV) condition. This is required to grant the electrons a mean free path sufficiently long to let the primary electrons reach the sample and to let the secondary electrons and the Auger electrons to reach the detectors. UHV is necessary also to avoid ionization of gas molecules inside the chamber. To reach UHV, three different pumps are employed: a rotary pump, to bring the system from ambient pressure to high vacuum (HV), and a turbomolecular pump and an ionic pump to reach the UHV.

Electron microscopy characterization was carried out with a Field-Emission Scanning Electron Microscope (FESEM Supra 40, manufactured by Zeiss) equipped with a Si(Li) detector (Oxford Instruments) for Energy-Dispersive X-ray (EDX) spectroscopy.

Fig. 25: FESEM Supra 40 instrument.

4.3.1.2 EDX

Energy-Dispersive X-ray Spectroscopy (EDX) is a characterization technique used to identify the chemical elements present in a sample and to know approximately their relative atomic concentration.

This technique is based on the detection of X-rays coming from a sample. An atom can release an X-ray when an electron of the outer shells fills the vacancy left by a core electron. This process happens to balance the excess of energy inside the atom. The competing process can release an Auger electron instead.

For every atom, specific transitions can happen (called “K”, “L” and “M” and sub-divided in “α”, “β”, etc.). Every transition has a specific energy that depends both on the type of transition and on the chemical element.

Depending on the transition that an electron of the outer shells is subjected to, a different X-ray is emitted. The consequence is that this X-ray has a specific wavelength that can be directly linked to the chemical element that emitted it.

EDX detector must be able to measure the energy of the X-rays emitted from the sample. High precision is required to discriminate different elements that emit X-rays with wavelength close to each other.

EDX spectrum is a plot of the intensity of the detected radiation versus the energy. The FESEM apparatus described in chapter 4.3.3.1 performs the EDX measurements. The EDX detector is placed inside the FESEM chamber.

4.3.1.3 TGA

Thermal gravimetric analysis (TGA) is a destructive characterization technique in which a sample is heated under to induce thermal degradation. The mass of the sample is constantly measured during the process.

This technique is used to test the thermal stability of a sample, to know the kinetics of certain reactions, to study the thermal transition of a compound or to estimate its ignition temperature in different environmental conditions. A TGA plot is usually reporting the mass variation of the sample as a function of the temperature. Such technique is often coupled with other characterization techniques like IR to obtain information about the chemical composition of gas species evolving during the TGA.

TGA were carried out using a TG 209 F1 Libra (NETZSCH GmbH), at 20 °C min^{-1} heating rate, from 25 °C to 800 °C under nitrogen flow (40 cm^3 min^{-1}). Gas transmittance spectra of the evolved gasses were collected on a Bruker Tensor II equipped with IR gas cell (TGA–FTIR) heated at 200 °C to avoid condensation of degraded products.

Fig. 26: TG 209 F1 Libra instrument coupled with Bruker Tensor II instrument.

4.3.1.4 IR

Infrared spectroscopy is the analysis of the infrared radiation interacting with a sample. This can be analyzed in three ways by measuring absorption, emission and reflection. The main use of this technique is in organic and inorganic chemistry to identify specific functional groups.

Every chemical bond vibrating in the infrared spectrum can be excited only by a certain range of wavelengths. The intensity and the position of the peaks in the spectrum allow to identify each functional group. IR spectrum is a plot of the intensity of the detected radiation versus the wavenumber of the radiation.

The attenuated total reflection (ATR) configuration is a setup in which the infrared beam is directed with a certain angle to a crystal in contact with the sample. An evanescent wave forms at the surface of a crystal characterized by a high refractive index. This configuration is taking advantage of the interaction of the evanescent wave with the sample. The change in phase due to this interaction is detected by the instrument by means of a moving mirror. Then, through the Fourier transform the spectrum is reconstructed. Fourier Transform Infrared (FTIR) spectroscopy was performed in ATR configuration with the Bruker Tensor II coupled with the TGA, as described in section 4.1.2.3.

4.3.1.5 Z-potential

Z-potential measurement is a technique which allows to estimate the surface charge of particles in solution. Briefly, a diluted solution is placed between two electrodes and a varying electric field is applied. A light source and a detector are employed to count the amount of particles which are moving in solution due to the presence of the electric field.

Knowing the sign of the field, the optical properties of the solvent and measuring the speed and direction of the particles, the sign and magnitude of the surface charge can be estimated. Z-potential was measured by Zetasizer Nano ZS90 (Malvern) on solutions of with a concentration of 0.05 mg/ml.

Fig. 27: Zetasizer Nano ZS90 instrument.

4.3.2 Electrochemical characterizations

During the thesis activity, electrochemical characterizations were carried out to evaluate the performances of the many materials tested, extracting parameters such as their specific capacitance.

The electrochemical measurements were performed using the VMP3 potentiostat manufactured by BioLogic. The instrument offers a potential range of ±10 V, a maximum current of 400 mA, with a resolution of 5 μV at 760 pA. The accuracy is declared to be <0.1 % of the full scale range. The electrometer has an input impedance greater than 1 TΩ, a capacitance of less than 20 pF and a bias current lower than 5 pA.

4.3.2.1 Cyclic voltammetry

Cyclic voltammetry (CV) is an electrochemical method that requires a potentiostat sourcing a voltage ramp with a constant incremental value repeated forward and downward between two limits while contemporary measuring the current. It is called "cyclic" because the measurement requires repeating the ramp forward and downward until a stable voltammogram has been recorded.

The voltammetry can be performed at different "speeds", called scan rates. Higher the scan rate, lower the time required to perform a cycle. Scan rates chosen for the thesis activity are 5 mV/s, 10 mV/s, 50 mV/s, 100 mV/s, 500 mV/s. The capacitance is then calculated as shown in Eq. 19.

$$C = \frac{\int I(t)dt}{m\,\Delta V} \tag{19}$$

Where C is the total normalized capacitance of the cell (F/g), $I(t)$ is the current measured during a ramp by the voltmeter (A), integrated on the time required to perform the ramp. ΔV is the voltage difference between the last value of the ramp and the first one (V), m is the mass of the active material (g).

Capacitance values can vary significantly, depending on the device performance. The capacitance is defined as the ratio between the electrical charge stored inside a device and the potential difference required to store this charge. For what concerns the supercapacitors, the scan rate influences the capacitance, because the charges inside the electrolyte will require a not negligible time to reach the electrodes and find the best distribution inside the porous structure of the electrodes. Therefore, it is expected to observe higher capacitance values at lower scan rates.

Another parameter that can be easily extracted from CV is the coulombic efficiency (Eq. 20):

$$\mathrm{CE} = \frac{\mathrm{Q_{out}}}{\mathrm{Q_{in}}} \tag{20}$$

Where CE is the coulombic efficiency (also called faradaic efficiency) expressed in percentage (%), $\mathrm{Q_{in}}$ is the total charged injected by the potentiostat into the cell during the charge ramp (C), $\mathrm{Q_{out}}$ is the total charged extracted by the potentiostat from the cell during the discharge ramp (C). Values of CE close to the unit are linked to a proper working condition of the cell, with negligible self-discharge phenomena.

For the thesis activity, all the CV measurements have been run in a NaCl 1 M solution.

4.3.2.2 Charge-discharge (CDI)

Charge-discharge (CD) is the electrochemical method employed to run CDI measurements.

First, the CDI cell is charged with an applied constant voltage of 1.2 V. In this phase, the cell is charged removing ions from the solution. The current intensity provided by the potentiostat has the typical exponential decrease of a capacitor during the charging phase.

Then, the cell is discharged applying 0 V. As before, the characteristic behaviour of the current over time is obtained, just with the opposite sign. The duration of each charge and discharge phase was set to 30 min, to allow the cell to reach an equilibrium with the solution and, therefore, achieve the maximum desalination.

The CD characterization is the result of the alternation of charge and discharge phases. For every CD measurement, each phase was repeated 5 times, for a total of 5 hours. During this time, the solution's conductivity is constantly monitored once every minute.

For the thesis activity, all the CD measurements have been run in a NaCl 10 mM solution.

4.3.2.3 Open circuit voltage

Open circuit voltage (OCV), as the name suggests, is a measurement in which the potential across the cell is measured while no current flows through it. This measurement is typically employed to know the initial state of a device or a material.

In this particular case, OCV measurement was run while the cell was manually moved back and forth from a high salinity batch (NaCl 0.6 M) to a low salinity one (NaCl 10 mM). The aim was measuring the spontaneous voltage rise/drop when switching the salinity of the solution. This dynamic is the key feature for a material to be applied for CapMix. This kind of measurements is performed with 5 electrodes (Fig. 28). 2 of them are employed to provide a bias to the cell, while the other 3 are used to read the potential between each of the two electrodes and an Ag/AgCl reference electrode. The cell employed for the OCV was the small one described in section 4.1.1.2.

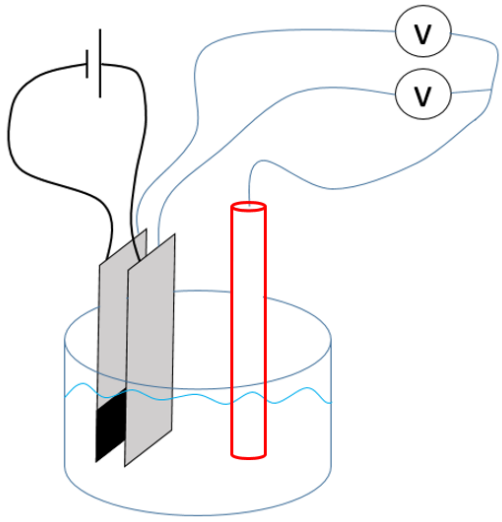

Fig. 28: Experimental setup for OCV measurements. On the left, the black wires connect the cell to the bias. On the right, the blue wires measure the potential difference between each electrode and the Ag/AgCl reference electrode, here represented in red.

4.3.2.4 Self-discharge

Self-discharge (SD) is a measurement in which the cell in charged up to a certain voltage and then it is let to rest in open circuit condition. The potential is monitored to quantify the importance of the SD phenomenon for each material.

Since in CapMix there is a dead time between the charge and the discharge of the device (see chapter 4.3.2.5 for further details), materials showing a moderate or negligible SD are preferred to maximize the energy gain.

For all the materials, SD measurements were performed charging the cell at a fixed voltage for 10 min, then let it rest for other 10 min while measuring the potential across it. The potentials applied started from 0.2 V and stopped at 1.2 V, with voltage steps of 200 mV. The maximum potential of 1.2 V was chosen to avoid the electrolysis of water (1.23 V for DI H_2O).

To be consistent with charge-discharge measurements, the SD measurements were run in a NaCl 10 mM solution.

4.3.2.5 Charge-discharge

As described in chapter 3.3.1, charge-discharge is the core of CapMix. The device is periodically charged and discharged to harvest energy at each cycle. This procedure is divided in 4 steps. The first is the charging step. The third is the discharging step. The second and the fourth are open circuit steps. To have a production of energy, the device is charged in a high salinity solution and discharged in a low salinity one. The solutions are switched during the 2^{nd} and the 4^{th} steps.

In this work, different ways to charge and discharge the device have been investigated. For the charging step, a constant current (CC) and a constant voltage (CV) methods have been tested with the purpose of verifying which one was less energy-consuming. For the discharging step, the CV method was used to estimate the maximum energy that can be extracted. This was done by short-circuiting the electrodes and measuring the current flowing. The CC and, even better, a constant load (CL) method were used for the discharge as being more representative for a real application of this technology.

Finally, the possibility of working from a state of fully discharged device up to a fixed state of charge has been investigated. This was done with the aim of increasing the harvested energy (Fig. 29). Indeed, in literature the CapMix cycle is always performed in a small voltage window around a fixed potential, thus limiting the theoretical amount of energy that can be extracted at each cycle.

For all the experiments, the solutions employed were 0.6 M and 10 mM NaCl, to simulate the seawater and the freshwater respectively.

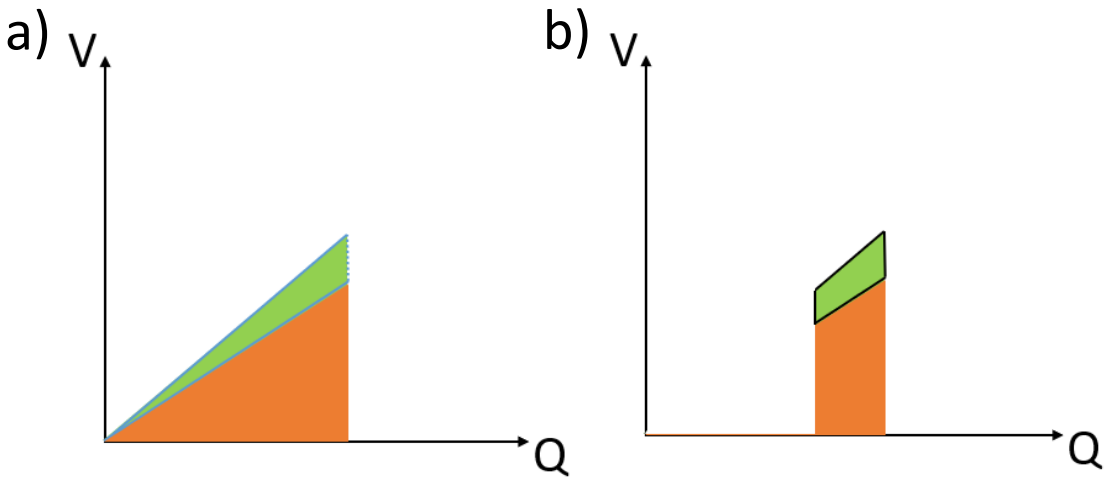

Fig. 29: Comparison of charge-discharge cycles. In green, the energy harvested at each cycle. In orange, the energy exchanged. a) Cycle performed from 0 V up to a maximum voltage. b) Standard cycle performed in a small voltage window around a set voltage.

5. Results and discussion

In this chapter are summarized all the relevant results achieved during this research activity. For both capacitive deionization and capacitive mixing, a discussion of the main achievements in also provided.

5.1 Capacitive deionization

In this section, the results of the CDI measurements are reported, together with the ones obtained from physical and electrochemical characterizations on each material.

5.1.1 Current collector

The very first set of measurements were run on bare current collectors. The purpose of these tests was to verify their stability in water. To do that, cyclic voltammetry (CV) technique was performed on 3 different samples: stainless steel (0.025 mm, Record), stainless steel 18Cr 9Ni (0.025 mm, Record) and titanium foil (0.2 mm thickness, Goodfellow).

The CV performed on stainless steel reported the presence of intense redox reactions starting around an applied voltage of 0.5 V and increasing in intensity with the voltage applied (Fig. 30). This behaviour is due to presence of iron atoms exposed to the solution, easily reacting with water and salt forming Fe^{2+}/Fe^{3+} oxides and chlorides, which are both easily solubilized. Indeed, after the CV, the electrodes clearly showed an onset of corrosion. For this reason, stainless steel electrodes were discarded for CDI application, even though their low cost.

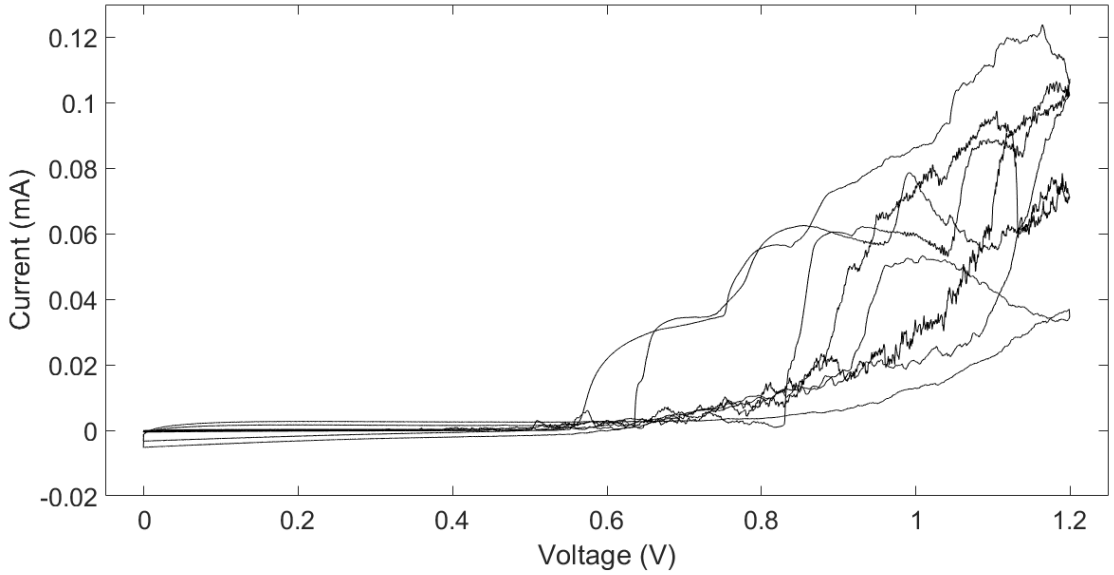

Fig. 30: CV on stainless steel. Intense redox reactions can be appreciated at any scan rate.

The stainless steel 18Cr 9Ni is particular steel developed for electrochemical applications. The heavy doping of chromium and nickel prevent the iron from reacting with dissolved species, or at least this phenomenon is strongly reduced. Indeed, the results show a peculiar behaviour (Fig. 31).

At high scan rates (50 mV/s, 100 mV/s, 500 mV/s) no redox reactions are appreciable. The CV curves have the typical rectangular shape of a capacitive, inert material. Instead, when lowering the scan rate (5 mV/s, 10 mV/s) redox peaks start showing above 0.6 V. Therefore, the Cr/Ni doping is effective if the contact time between ions from the solution and the current collector is relatively short. On the other hand, slowing down the dynamics of the process, the ions in solution can permeate through the steel and interact with Fe atoms, leading to irreversible redox reactions.

Even though in CDI measurements the current is coated with the active material, it is not possible to ensure perfect uniformity so that the solution will not find micrometric paths to the current collector. For this reason, it is not possible to employ such material for CDI, since the electrical double layer must be sustained for many minutes, i.e. orders of magnitude higher than the “fast” CV in which the electrodes proved to be stable.

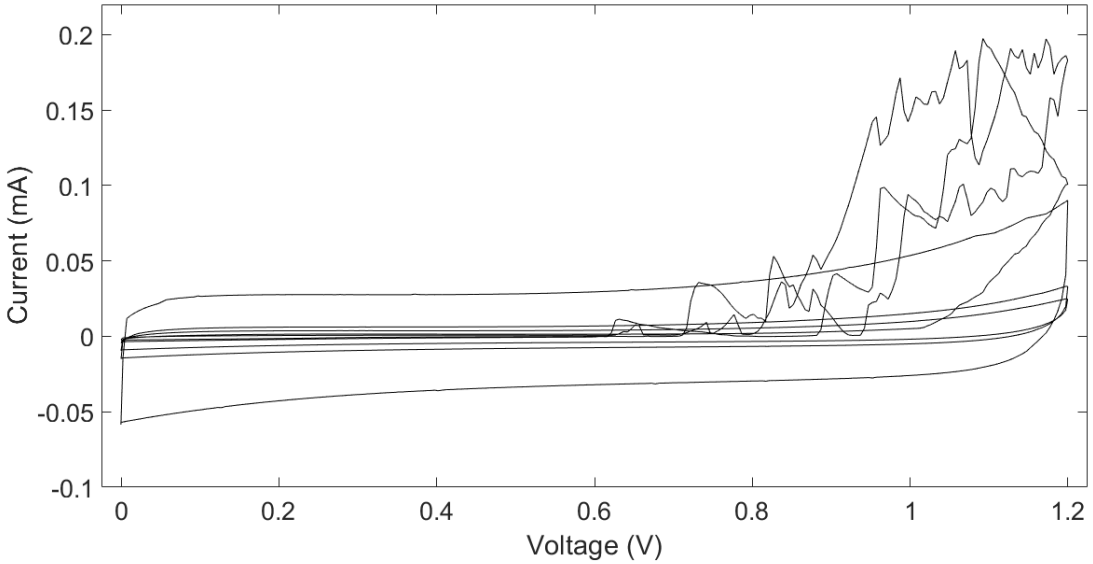

Fig. 31: CV on stainless steel 18Cr 9Ni. Redox reactions are observed only at low scan rates (5 mV/s and 10 mV/s).

The last material tested was titanium. This material is well-known for its chemical stability, mostly thanks to the presence of a thin native oxide on its surface which acts as a passive layer. The CV reported in Fig. 32 shows the absence or redox peaks in the voltage window examined.

The only appreciable effect, indeed, is an increase on the current when approaching the theoretical potential for the water electrolysis (1.23 V). However, this effect (starting around 1 V) will be strongly mitigated by the presence of the active material coating.

For what concerns the capacity of Ti electrodes, it is of the order of 10^{-3} F/g or, considering the area, 10^{-3} F/cm^2. Such values are both many orders of magnitude lower than to the ones obtained with the any of the active material. For this reason, any possible unwanted contribution coming from small uncoated regions of the current collector is totally neglected.

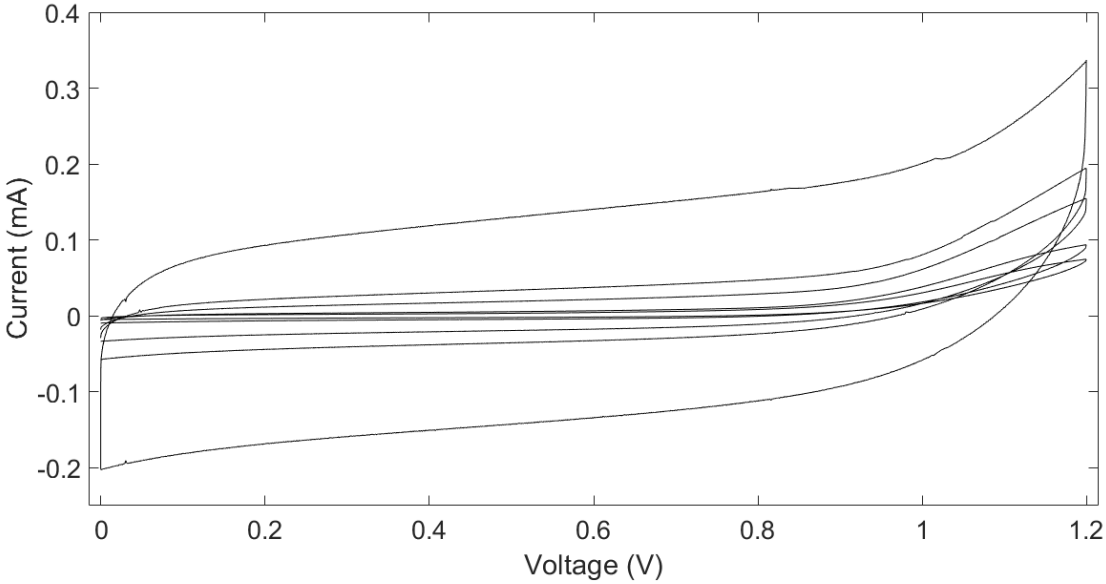

Fig. 32: CV on titanium. A beginning of redox reaction is observed above 1 V, but not dramatically intense as in the case of stainless steel.

In conclusion, among the current collectors tested for CDI, titanium was selected due to its inertness in the harsh salinity environment. Even if been more expensive than stainless steel, the electrochemical characterization proved the titanium to be the only feasible solution for long-term application in water.

Therefore, for all the other measurements reported in this thesis, titanium was always employed as current collector.

5.1.2 Active material

In this section is reported a series of characterizations performed on the materials employed for CDI.

5.1.2.1 Functionalized graphene oxide

The effectiveness of the two-steps functionalization procedure was verified performing TGA and IR characterization on pristine and functionalized GO.

The IR spectrum of pure GO sample has been compared with the spectra of the two samples of functionalized GO, obtained after the first functionalization step (fGO-Step I) and after the second functionalization step (fGO-Step II). All the samples have been dried in order to eliminate water interference.

The GO sample (Fig. 33) shows the typical spectrum of oxidized graphene consistent with literature [166]. The broad band (1) with a maximum near to 3400 cm^{-1} corresponds to the OH stretching vibration of hydroxyl of alcohol and carboxyl groups. The band at 1586 cm^{-1} (2) is due to the deformation vibration of aromatic C=C. Epoxy groups are present at 1224 cm^{-1} (3). Alkoxy C–O has a band at 1047 cm^{-1} (4). The band (5) with a maximum at 1718 cm^{-1} is assigned to the stretching carbonyl C=O mainly by carboxyl groups.

The fGO-Step I has a similar spectrum, where the presence of dimethylformamide is evidenced by the amide I and amide III stretching bands at 1629 cm^{-1} (6) and 1504 cm^{-1} (7), the bands at 1437 cm^{-1} (8) and the C-N at 1012 cm^{-1} (9) and the peak at 951 cm^{-1} (10). In the C-H stretching region the C-H absorption due to the $-CH_3$ of dimethylformamide between 3000 cm^{-1} and 2850 cm^{-1} are clearly visible.

The fGO-Step II has similar peaks but there are few differences due to the presence of the grafted monomer: the peak at 1012 cm^{-1} decreases for the degradation of the C-N group with the appearance of a C-O, at higher frequencies there is an increase of absorbance in the C-H stretching region due to the methyl linked to the nitrogen of the monomer.

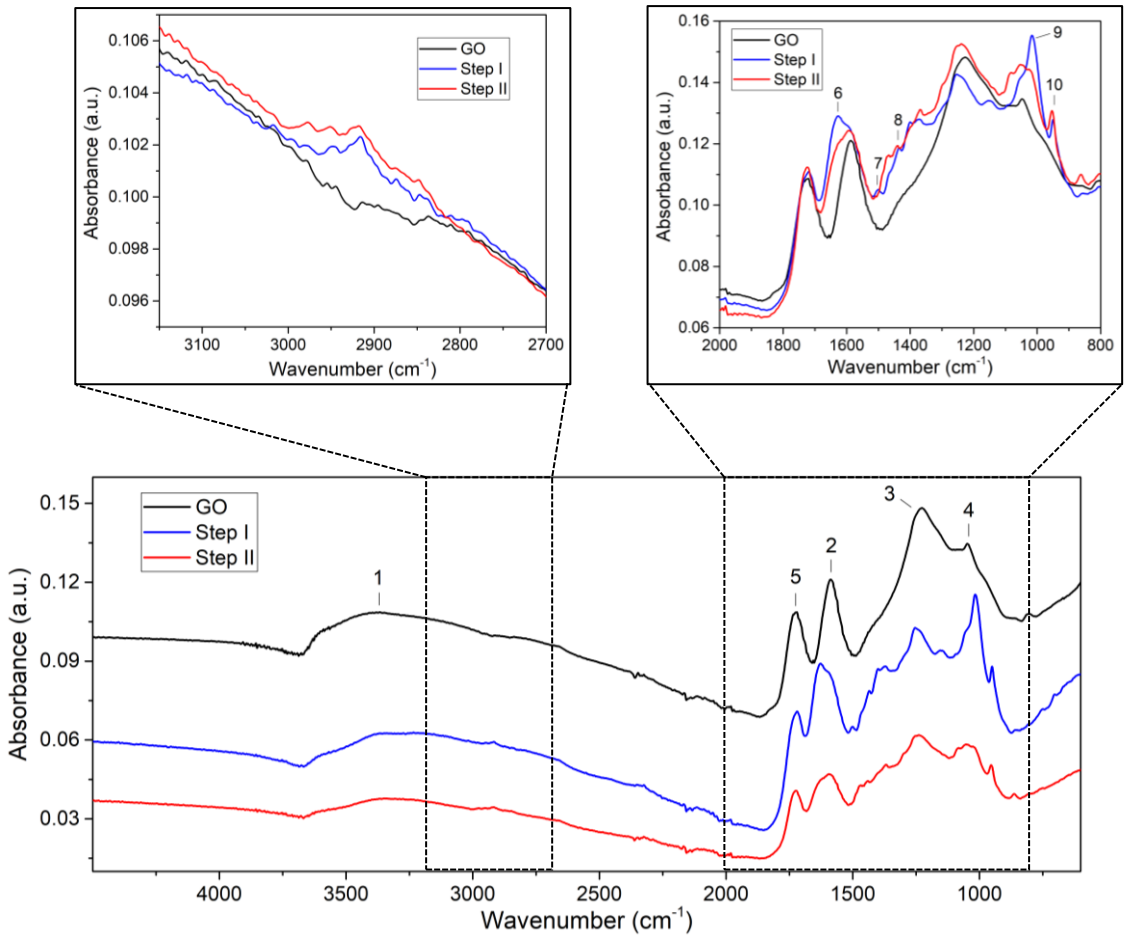

Figure 33: FTIR spectra in ATR configuration of GO, fGO-Step I and fGO-Step II.

To clarify the type of organic substituent linked to GO, a semiqualitative analysis has been performed by TGA.

The TGA of GO (Fig. 34) shows a main degradation peak at 220 °C, when the GO lost about 15% wt. For temperatures varying from 330 °C to 800 °C the GO slowly lost about 20% wt. with a final residue of about 65% wt.

The evolved gasses are composed by carbon dioxide, carbon monoxide and water; their relative intensity does not change during the whole degradation process and are similar to TGA 1st derivative.

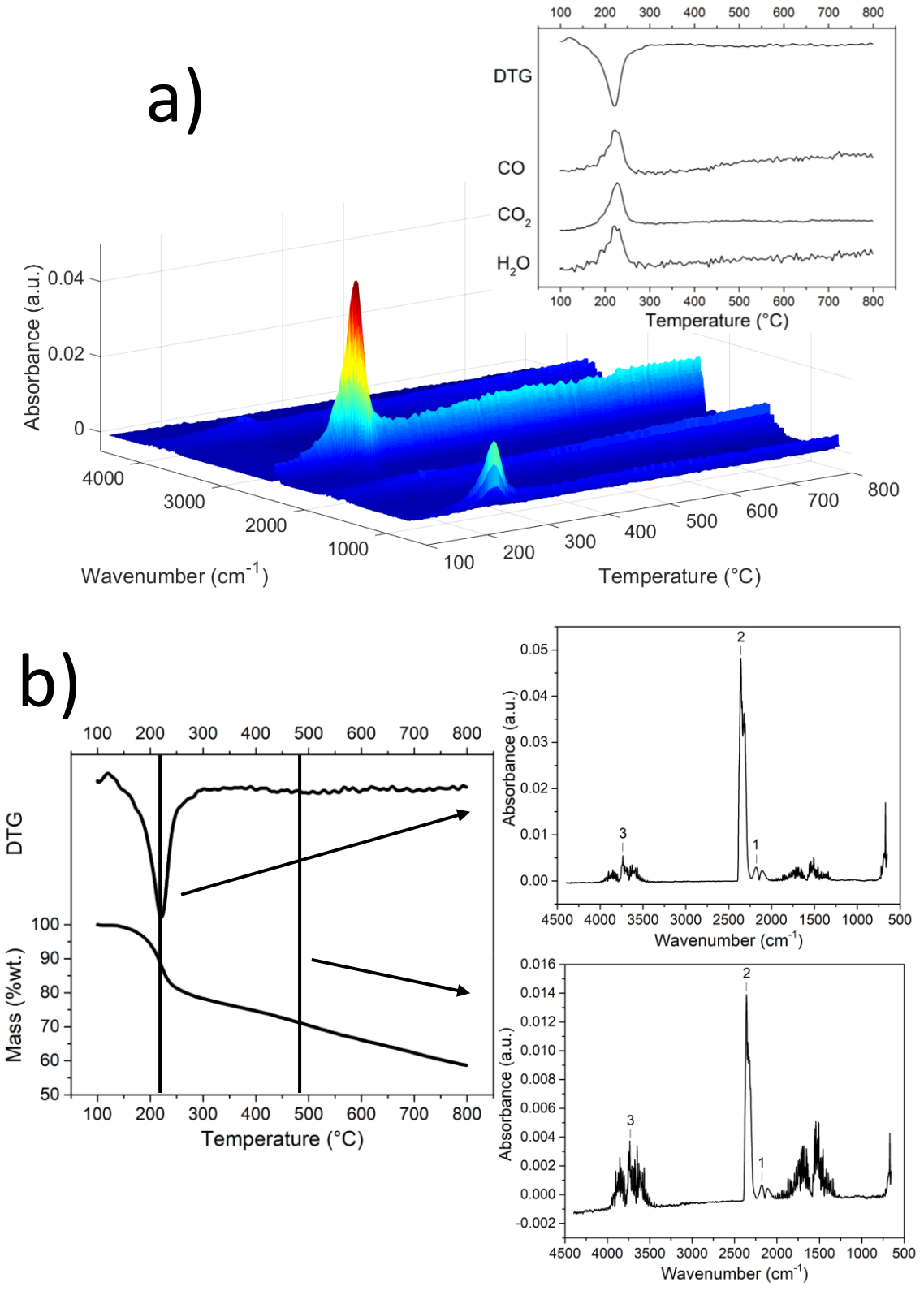

Fig. 34: TGA of GO. a) 3D IR adsorption as a function of temperature. In the inset, maximum adsorption for evaluated molecules compared with DTG: CO 2179 cm^{-1}, CO_2 2349 cm^{-1}, H_2O 3735 cm^{-1}. b) On the left, weight vs temperature (%wt. vs °C) and differential weight vs temperature (d%wt./d°C vs °C). On the right, FTIR of gasses developed at 220 ° C and 500 °C.

The thermogravimetric analysis of fGO-Step I (Fig. 35) shows two main degradation peaks at 190 °C and at 366 °C. The weight losses are respectively 24% wt. and 19% wt. Successively, in the temperature interval from 500 °C to 800 °C, fGO-Step I lost 8% wt. and the final residue is about 57% wt. with a difference respect to GO of about 15% wt. on dry bases.

Infrared analysis of the evolved gasses shows that the main products during the thermal degradation process are water, carbon monoxide, carbon dioxide and dimethylformamide used as solvent during the functionalization step I. The molecule was probably linked to the GO by the activation created from 4-hydroxy-benzophenone during the UV irradiation as in the case of the infrared analysis it is difficult to find traces of the 4HB formation and volatilization as reported from Roppolo et al. [162].

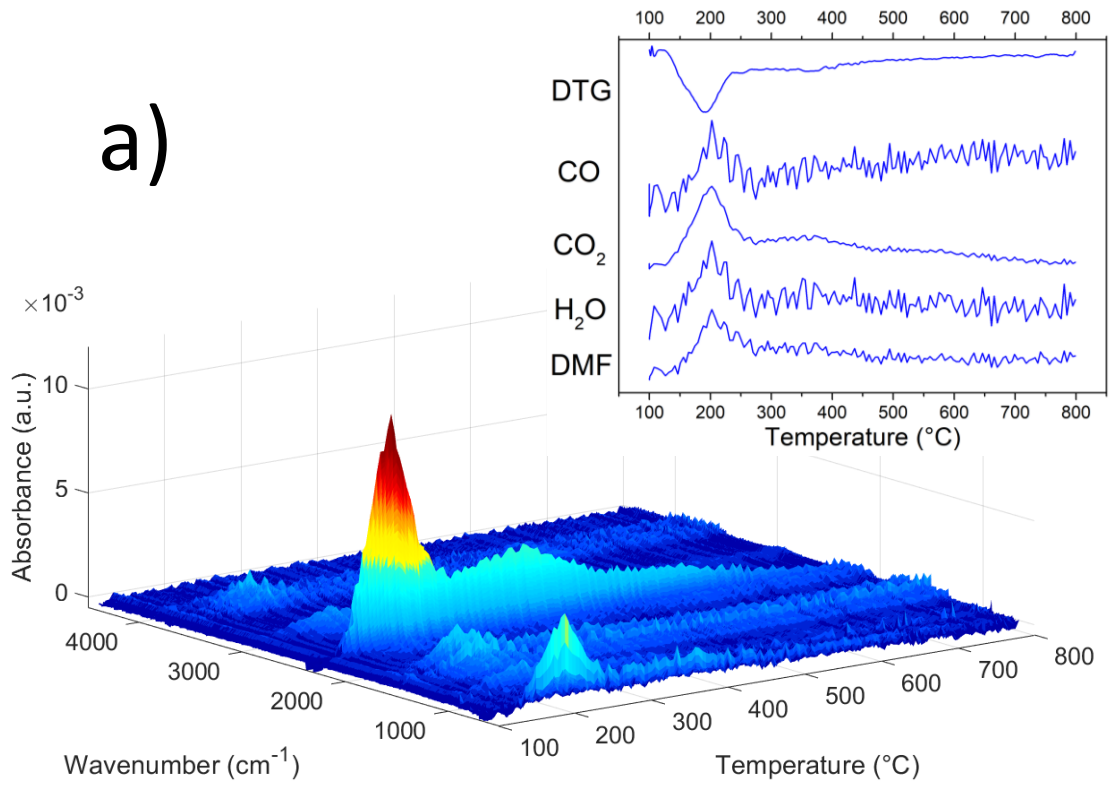

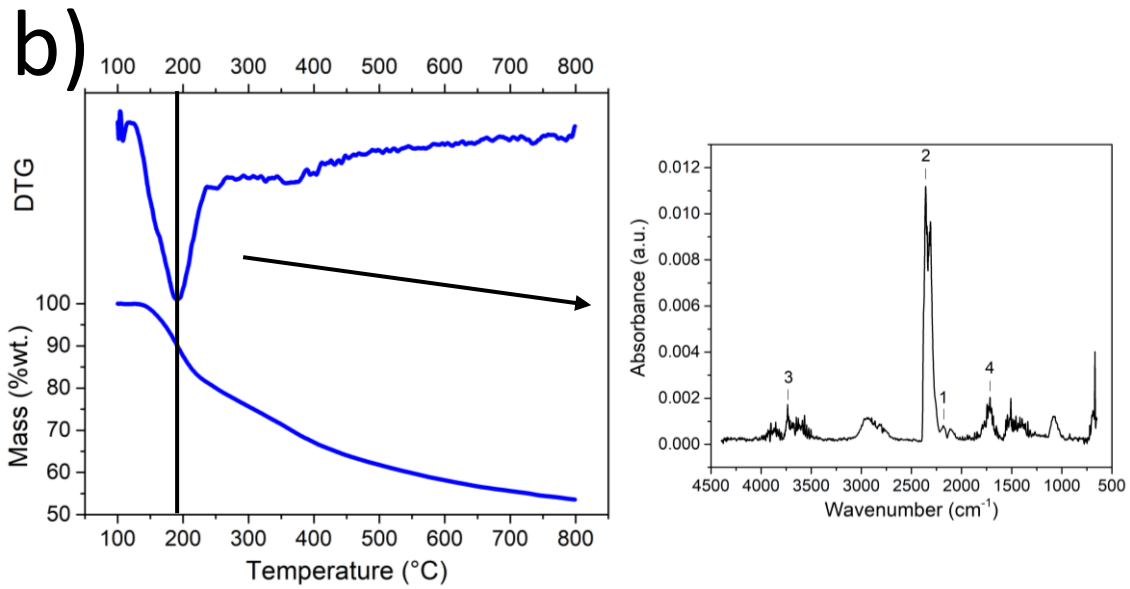

Fig. 35: TGA of fGO-Step I. a) 3D IR adsorption as a function of temperature. In the inset, maximum adsorption for evaluated molecules compared with DTG: CO 2179 cm^{-1}, CO_2 2349 cm^{-1}, H_2O 3735 cm^{-1}, DMF 1716 cm^{-1}. b) On the left, weight vs temperature (%wt. vs °C) and differential weight vs temperature (d%wt./d°C vs °C). On the right, FTIR of gasses developed at 190 ° C.

The thermogravimetric analysis of fGO-Step II (Fig. 36) shows two main degradation peaks at 190 °C and at 308 °C. The weight losses are about 20% wt. each. fGO-Step II lost 10% wt. from 500 °C to 800 °C, the final residue is about 50% wt. with a difference respect to GO of about 15% wt. on dry bases.

Infrared analysis of the evolved gasses shows that the main products during the first degradation process are similar to the ones obtained with fGO-Step I with the formation of DMF. During the second degradation process the presence of Hydrochloric acid, trimethylamine and acrylate formed from the depolymerisation of the [2-(Acryloyloxy)ethyl]trimethylammonium chloride is evident (Fig. 36b).

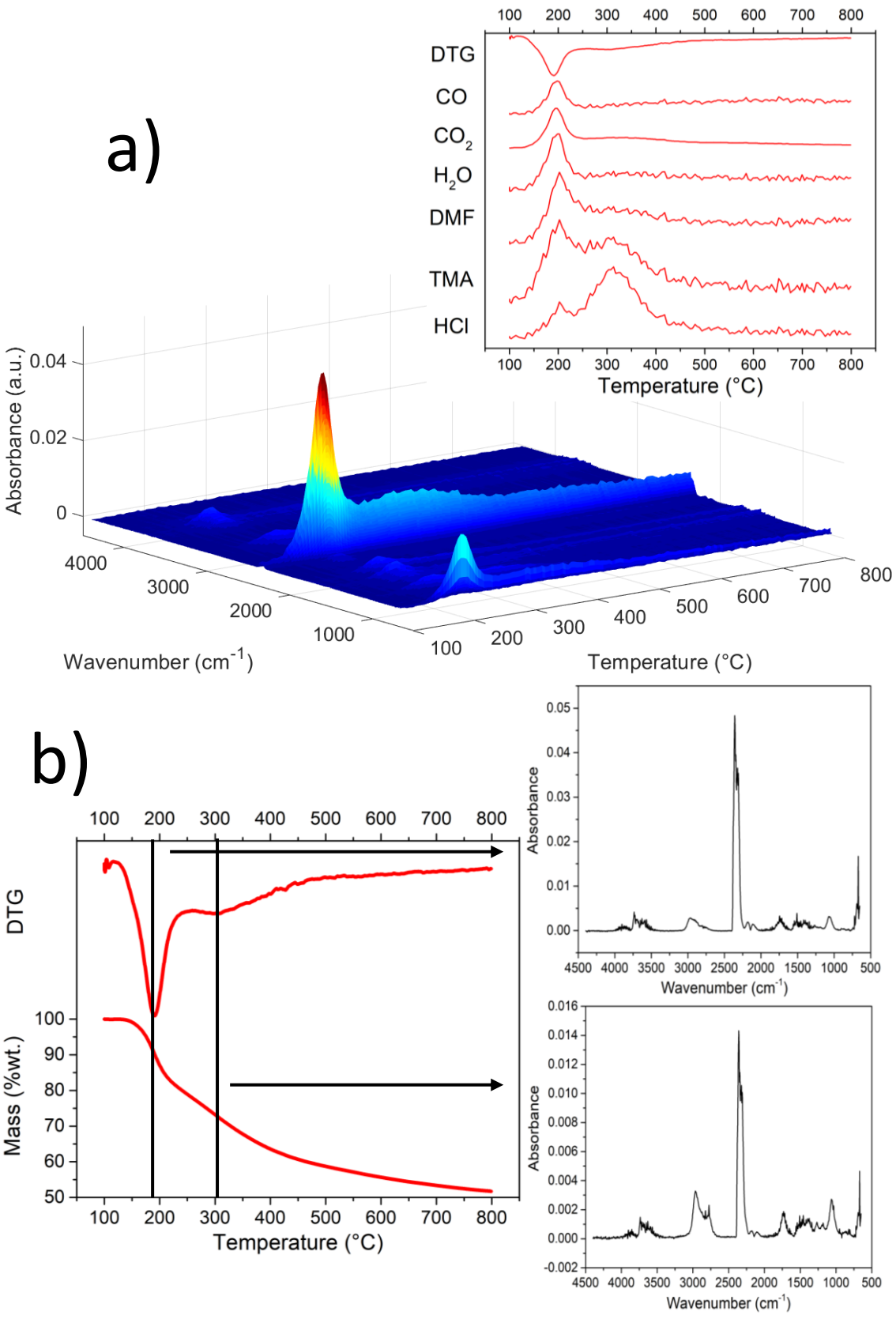

Fig. 36: TGA of fGO-Step II. a) 3D IR adsorption as a function of temperature. In the inset, maximum adsorption for many evaluated molecules compared with DTG. b) On the left, weight vs temperature (%wt. vs °C) and differential weight vs temperature (d%wt./d°C vs °C). On the right, FTIR of gasses developed at 190 ° C and 308 °C.

EDX analysis performed of fGO-step II confirmed the presence of the monomer on the flakes. From Fig. 37 it is possible to observe the presence of nitrogen, totally absent in GO flakes.

a)

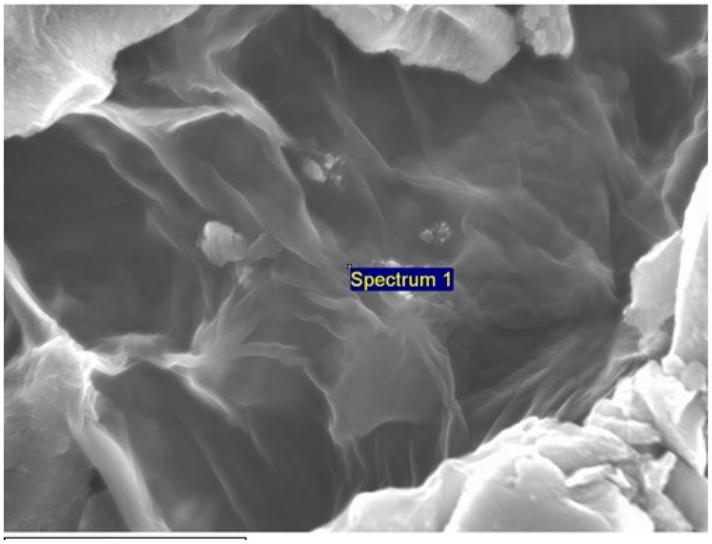

b)

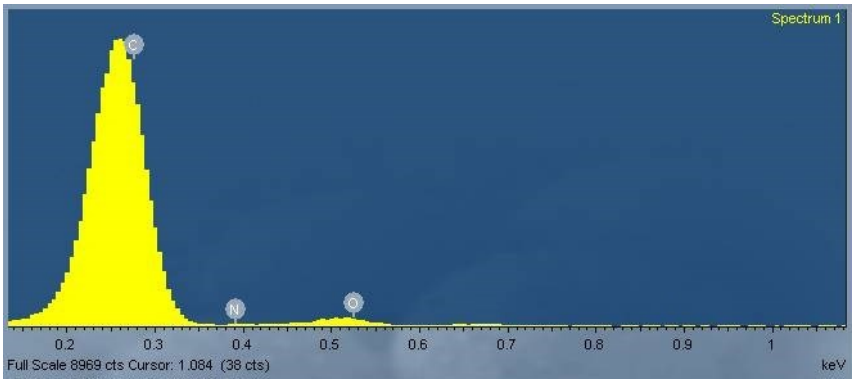

c)

Element	Weight %	Atomic %
C	87.5	89.7
N	7.7	6.7
O	4.8	3.6

Fig. 37: EDX on fGO-step II. a) FESEM image of the sample. b) EDX spectrum. c) Element quantification.

Z-potential measurements, performed on the GO and the fGO-Step II samples, confirmed the success of the two-step functionalization procedure. In Fig. 38 it is possible to appreciate the shift of the peak related to the surface charge of GO flakes.

Indeed, starting from -37 mV for the native GO, two peaks are obtained. The positive one, around 64 mV, is due to the presence of positive charges on the fGO, while the neutral one, centered in 0 mV, is marking the presence of rGO flakes, reduced during the process but not functionalized. Indeed, the peak of the pristine GO at negative potential is absent or overshadowed by the rGO one, meaning that the process was able to convert the nearly totality of GO flakes.

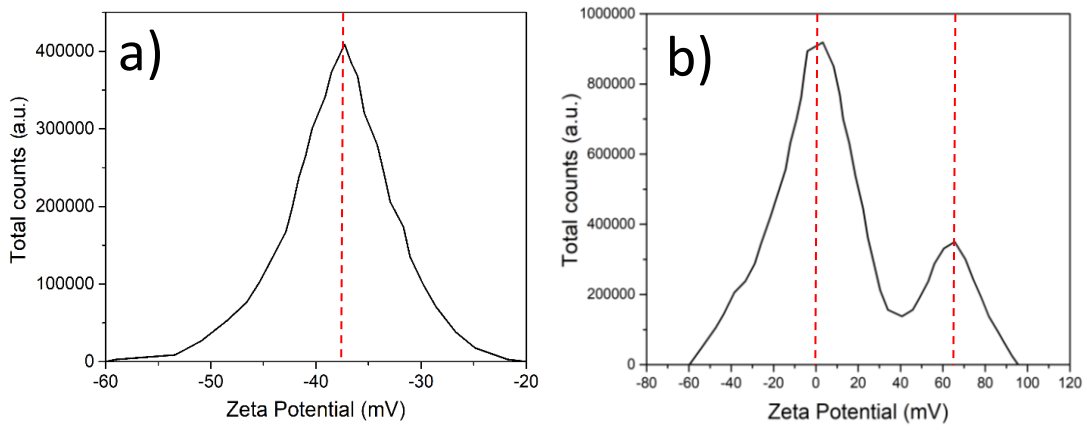

Fig. 38: a) Z-potential of GO as it is. The typical negative peak is clearly represented. b) Z-potential of fGO-Step II. Two peaks are present. The positive one is linked to the functionalized flakes (amine). The neutral one, more intense, is related to GO flakes which have been reduced during the process, but not functionalized.

Z-potential measurements were run also on GO functionalized with 3-sulfopropyl acrylate potassium salt (simply called fGO^-K^+ from now on) and 2-Acrylamido-2-methyl-1-propanesulfonic acid (called fGO^-). Since these materials were prepared a couple of years later with respect to one previously described, z-potential measurement was repeated also on GO, since this material is renown to be unstable over a large time scale.

The results are reported in Fig. 39, in which is clearly visible the effect of aging on the pristine GO and the potential shift as a consequence of functionalization. The peak of the functionalized materials is shifted towards negative values, proving that the functionalization worked as intended. The most negative z-potential value has been obtained with the fGO^-.

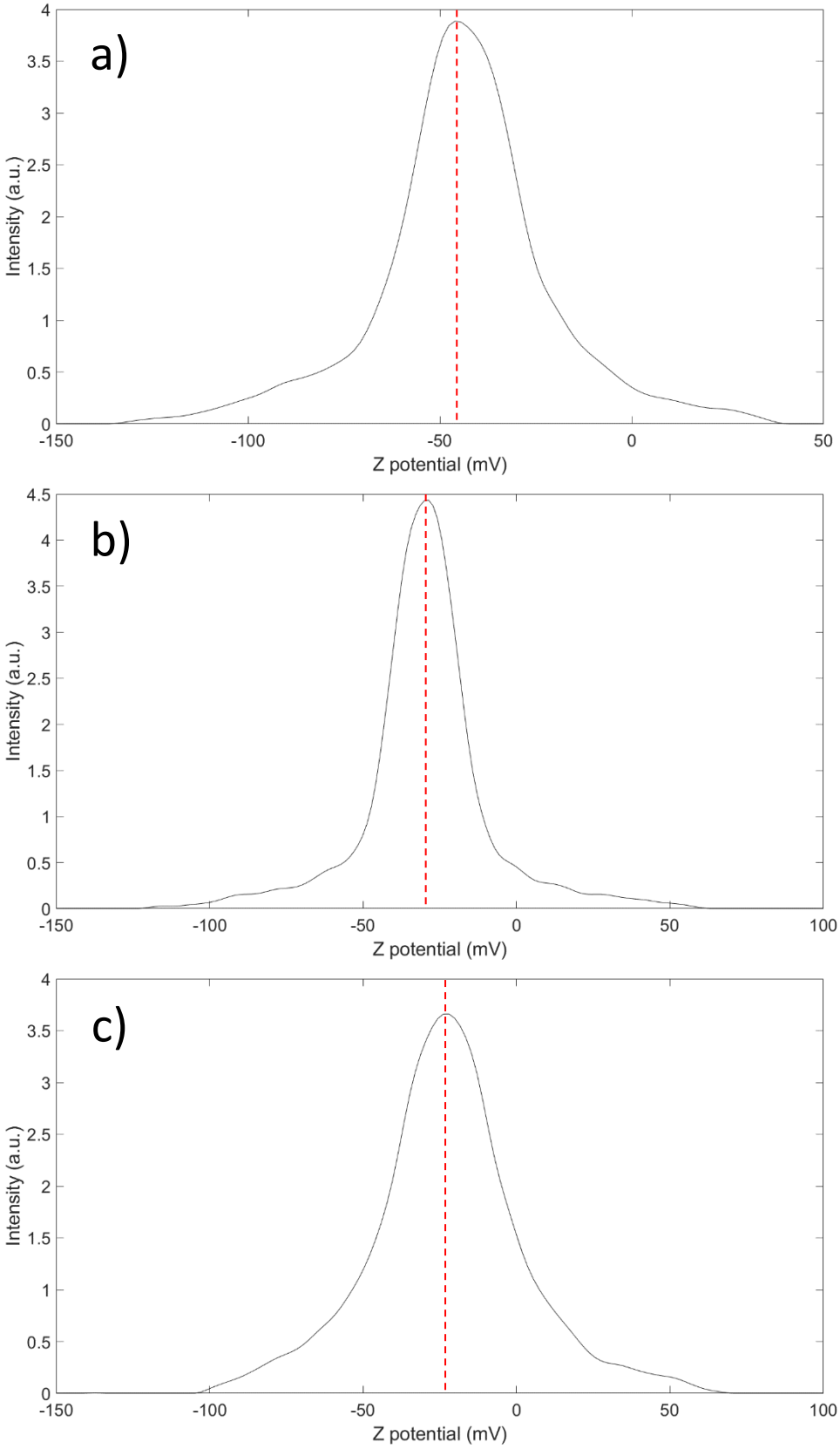

Fig. 39: a) Z-potential of fGO^-. The negative peak is centred at -46 mV. b) Z-potential of fGO^-K^+, showing a sharp peak at -30 mV. c) Z-potential of the pristine GO. The aging moved the peak from -37 mV to -23 mV.

To summarize, in Fig. 40 are illustrated the three molecules used in this thesis activity. From this moment on, the three functionalization are called respectively $GONH_3$, fGO^-K^+, fGO^-. In particular, in the results section, this terminology refers also to the active materials containing the activated carbon, the binder and functionalized graphene oxide.

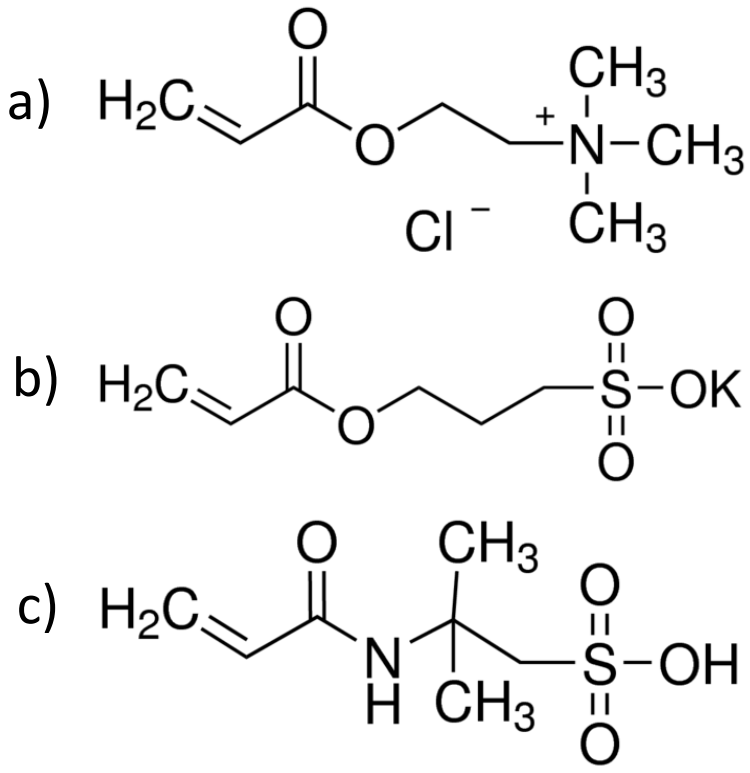

Fig. 40: The three acrylates used to functionalize the GO flakes.
a) [2-(Acryloyloxy)ethyl]trimethylammonium chloride.
b) 3-sulfopropyl acrylate potassium salt.
c) 2-Acrylamido-2-methyl-1-propanesulfonic acid.

5.1.2.2 Morphological investigation

Following the procedure described in chapter 4.1.1.2, electrodes made of titanium coated with active material have been obtained. Electron microscopy was employed to study the morphology of the as prepared samples, in order to check the uniformity of the active material. Fig. 41 reports a comparison between two active materials tested, the bare AC and the AC mixed with GO.

The branched structure of this kind of samples is evident. The GO flakes (Fig. 41, right column) are perfectly integrated inside the AC and PVDF network. In both cases, the absence of aggregation of the polymer clearly indicates the effectiveness of the preparation procedure.

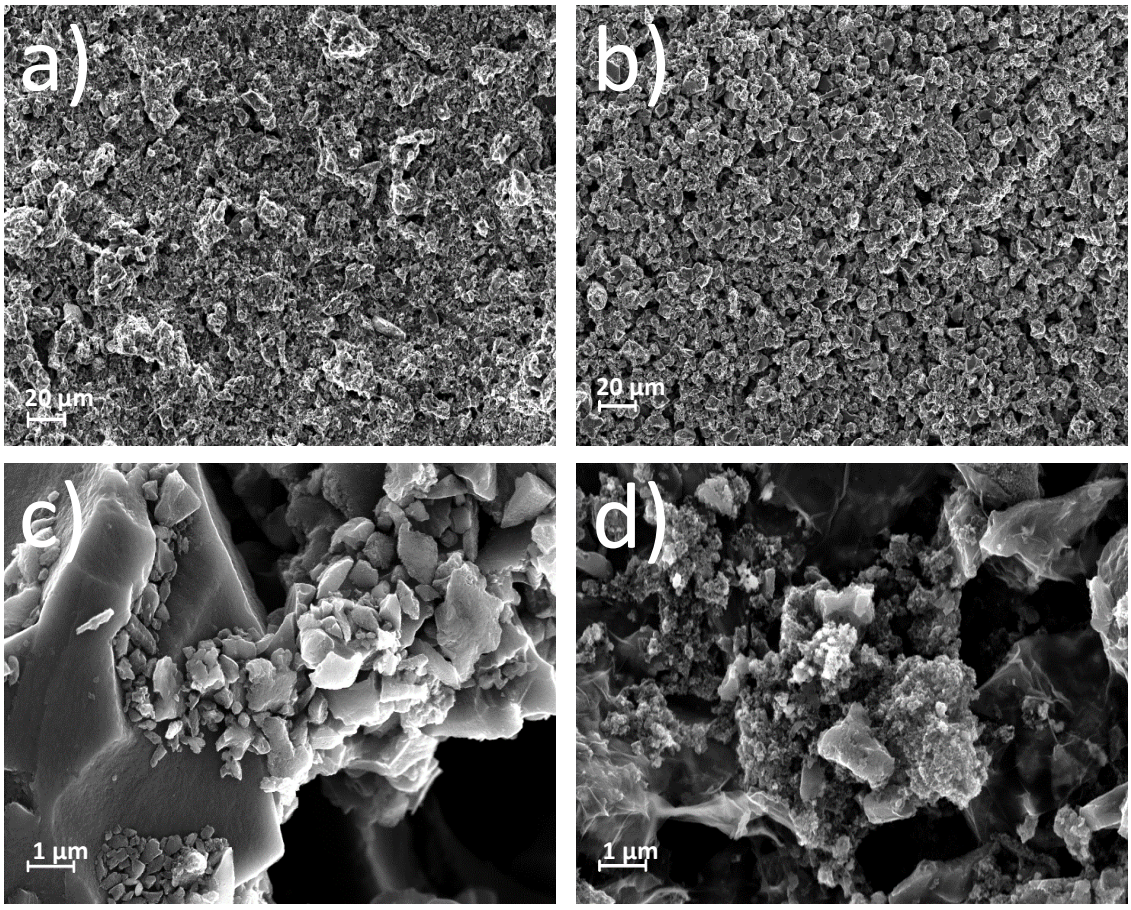

Fig. 41: On the left, AC and PVDF network. Magnification: a) 1000x, c) 25000x. On the right, AC, GO and PVDF network. Magnification: b) 1000x, d) 25000x.

Another material which has been investigated using the electron microscopy is the MXene. In Fig. 42 is shown the typical laminated structure of this material. All around the central stacked structure, it is possible see exfoliated flakes obtained through sonication.

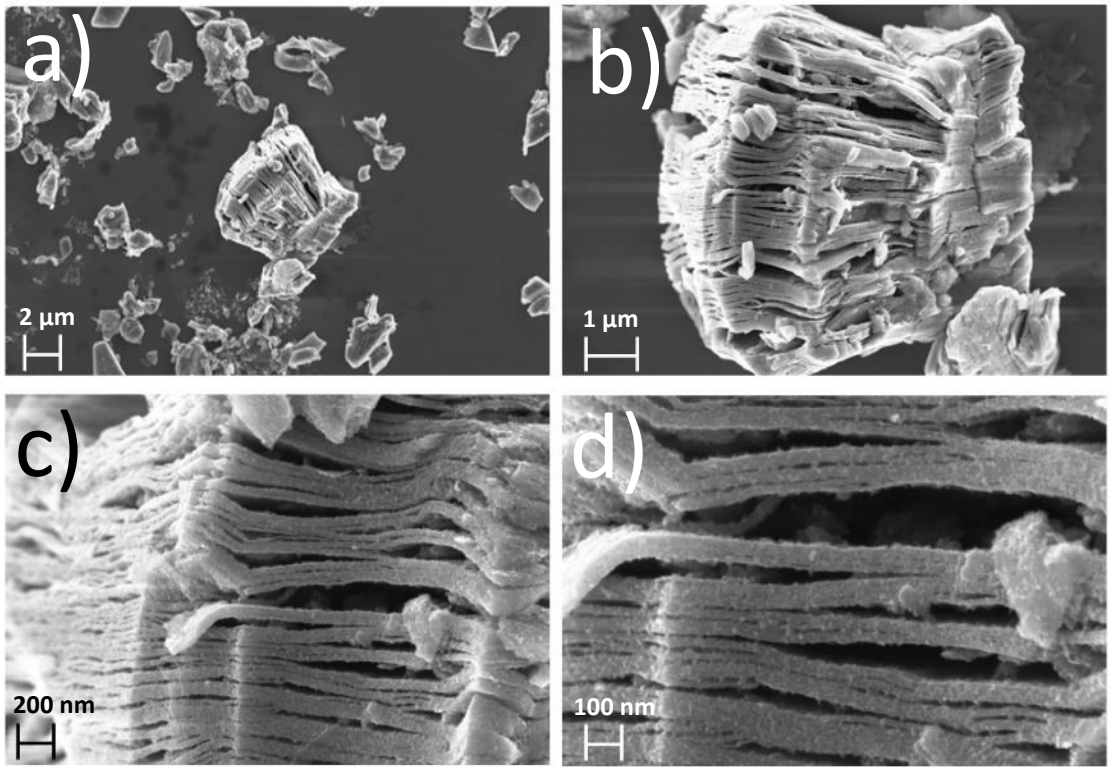

Fig. 42: MXene flakes. Magnification: a) 10000x, b) 30000x, c) 100000x, d) 200000x.

5.1.2.3 Electrochemical characterization

To determine the specific capacitance of each couple of materials, cyclic voltammetry measurements have been run on a voltage window of 1.2 V, setting the parameters as described in chapter 4.3.2.1.

In Fig. 43 is reported a comparison of the results obtained for each couple of materials tested for CDI. It is interesting to note if Fig. 43c the presence of a small redox peak around 0.9 V, which is not disappearing increasing the number of cycles. Such peak is probably linked to the presence of the PSS, which contains sulfonated groups.

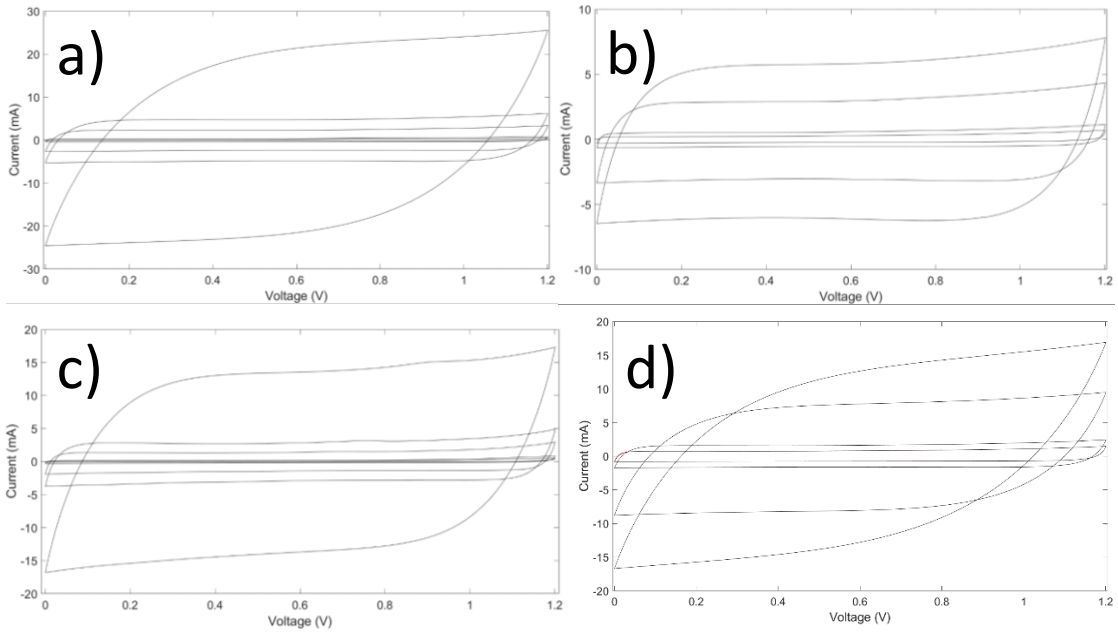

Fig. 43: CV performed on different couple of materials. a) bare AC. b) GO-GONH$_3$. c) GOPSS-GONH$_3$. d) MX-GONH$_3$.

The specific capacitance values calculated through CV measurements are collected in Fig. 44. The capacitance values are obtained in a 2-electrodes configuration, with a distance between the electrodes that is exactly the same of the CDI cell. Despite of the low values, which were expected with such a large working distance and a 2-electrodes configuration (always ~ 4 times lower than a 3-electrodes configuration), the overall behavior of the materials is quite similar. GOPSS-$GONH_3$ shows a lower specific capacitance, especially at low scan rates. The MX-$GONH_3$ shows a dramatical drop in capacitance when increasing the scan rate. This can be linked to the presence of MXenes, whose nanometric structure may require longer time for the ions to diffuse through it.

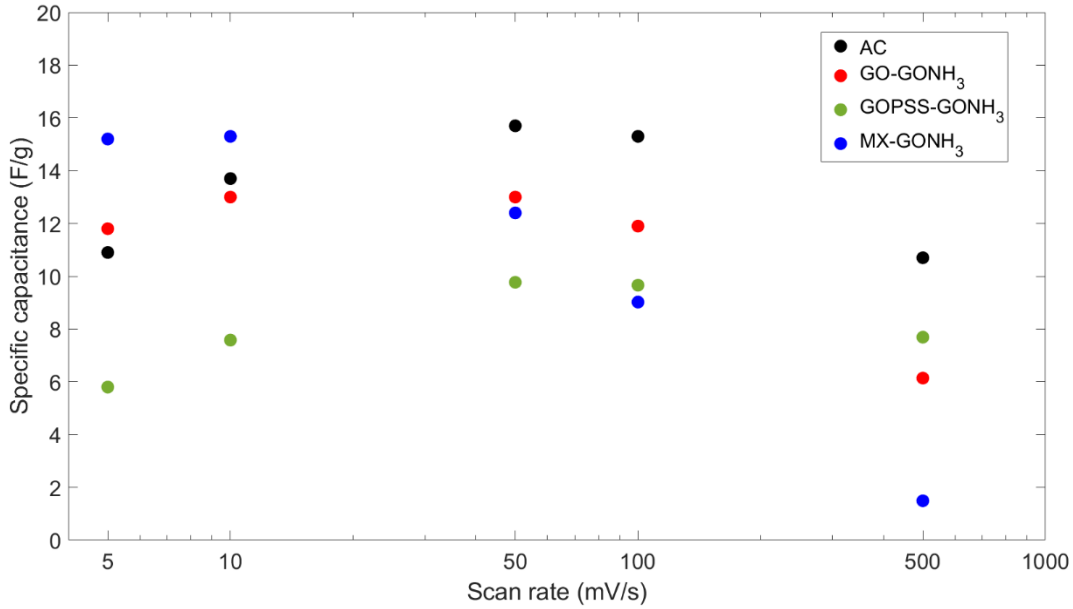

Fig. 44: Specific capacitance as a function of scan rate for the different couples of materials tested in CDI.

5.1.3 Desalination results

From CDI experiments, two kinds of data are collected: the values of the solution conductivity over time and the variation of current and voltage. Fig. 45 shows an example of this kind of data. These graphs are reported to provide an overview of the measurements for purely illustrative purposes. For all below listed materials, only the amount of salt removal will be shown.

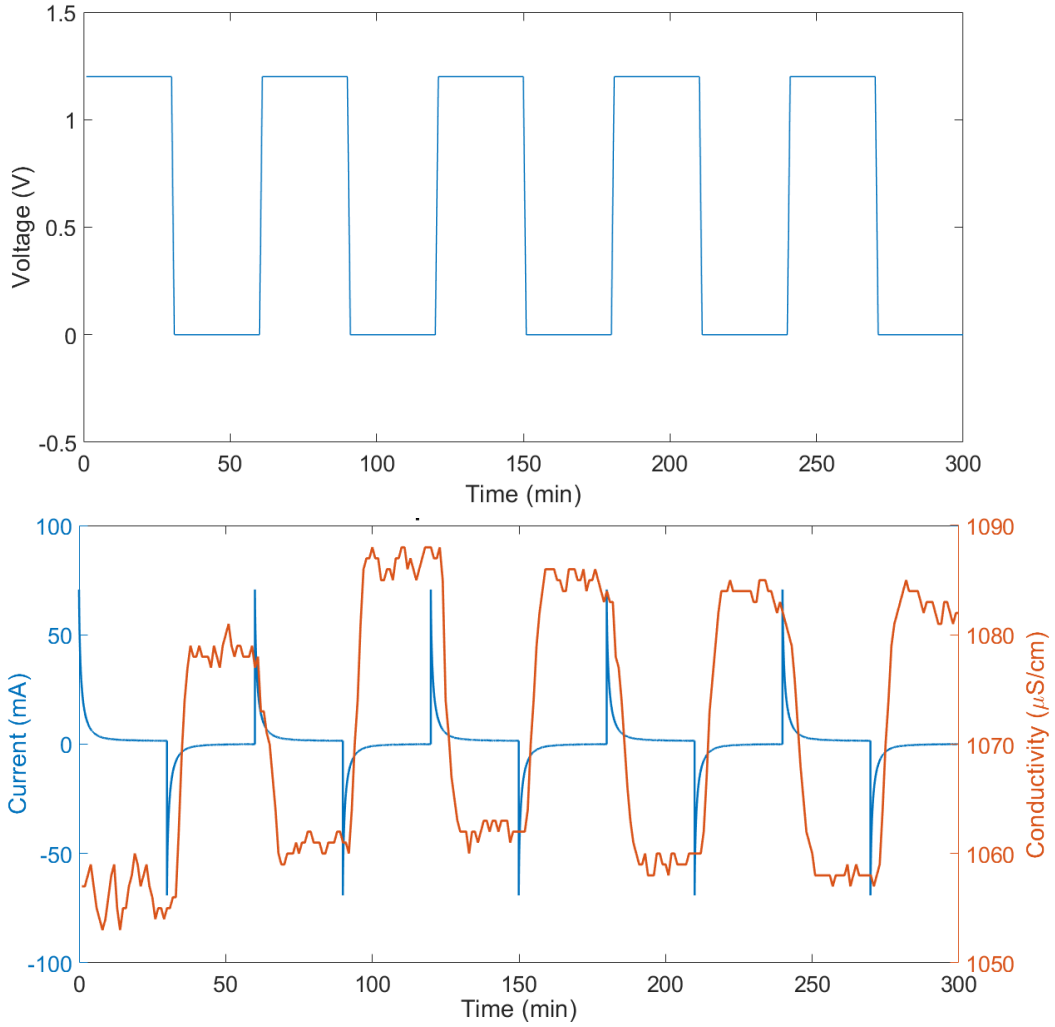

Fig. 45: On the top, voltage steps applied to the cell as a function of time. On the bottom, current and solution conductivity as functions of time.

The first set of CDI measurements was performed on a symmetric cell whose active material was bare activated carbon for both the electrodes. The results are reported in Fig. 46.

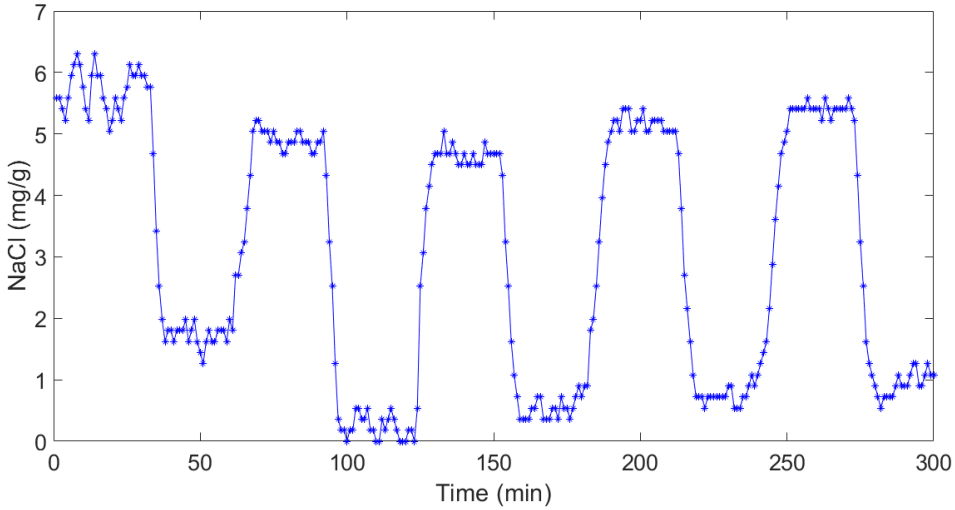

Fig. 46: Gravimetric salt adsorption capacitance of bare activated carbon.

The variation of conductivity recorded by the conductivity meter is of the order of 30 µS/cm between charge and discharge phases. While not being a large variation in percentage, taking into account the total volume of the solution and the mass of the electrodes, this value leads to an mSAC of approximately 5 mg/g. The ASAR is 0.46 mg g^{-1} min^{-1} and the Λ is 55 %.

The second set of measurements was performed on an asymmetric cell. The positive electrode was made of bare activated carbon, following the standard preparation. The negative electrode was made of activated carbon whose binder has been substituted with SPEEK. For simplicity, this configuration will be called AC-SPEEK. Taking a look at Fig. 47, it possible to observe a gradual shift of curve towards higher values. This phenomenon is linked to a loss in conductivity of the solution. It can be originated by the spontaneous absorption of the binder. Indeed, after the first two cycles, the salt adsorption reaches a stable value, with an mSAC of roughly 5 mg/g, like the standard activated carbon coating. The ASAR is a bit lower, reaching 0.38 mg g^{-1} min^{-1}. The Λ instead is a bit higher, with a value of 73 %.

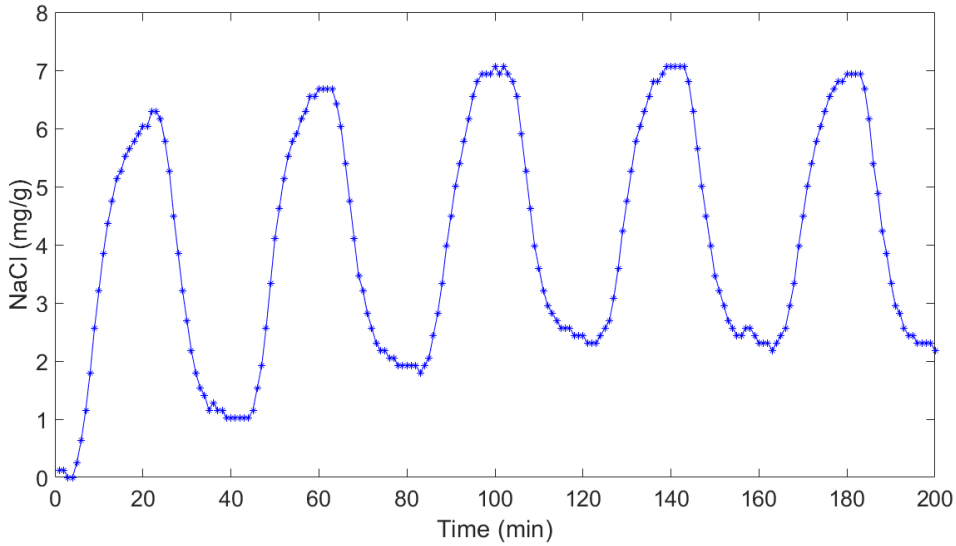

Fig. 47: Gravimetric salt adsorption capacitance of AC-SPEEK.

The third cell undergoing CDI measurements was an asymmetric one. The negative electrode was made of activated carbon and pristine graphene oxide. The positive one was made of activated carbon and graphene oxide functionalized with an amino-terminated monomer (see section 5.1.3 for further details). The final device is called GO-$GONH_3$. The results are reported in Fig. 48. In this case the mSAC is 9.0 mg/g, the ASAR is 0.64 mg g^{-1} min^{-1} and the Λ is 98 %.

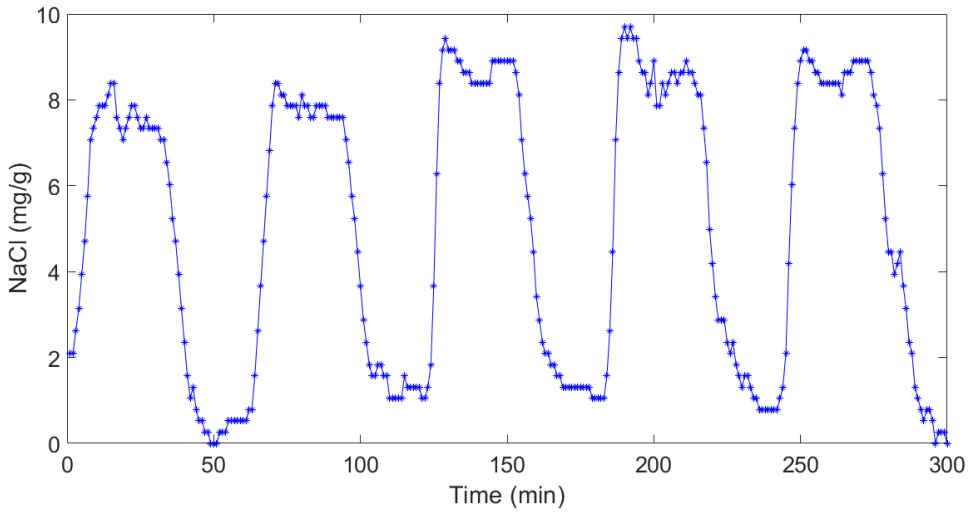

Fig. 48: Gravimetric salt adsorption capacitance of GO-$GONH_3$.

Trying to increase the performance of the GO-$GONH_3$, the pristine graphene oxide of the negative electrode has been mixed with PSS. Unfortunately, the results show a marked decrease in adsorption capacitance, with the mSAC reaching only 3 mg/g. Such a decrease can be addressed to the presence of the PSS, which is simply mixed with GO and can badly affect the porosity of the system. Moreover, as shown in Fig. 49, a decreasing trend is observed. Such a behaviour is due to the increase, over time, of the solution

conductivity which can be caused by the dissolution of the PSS. The ASAR is 0.30 mg g^{-1} min^{-1}, while the Λ is 91 %.

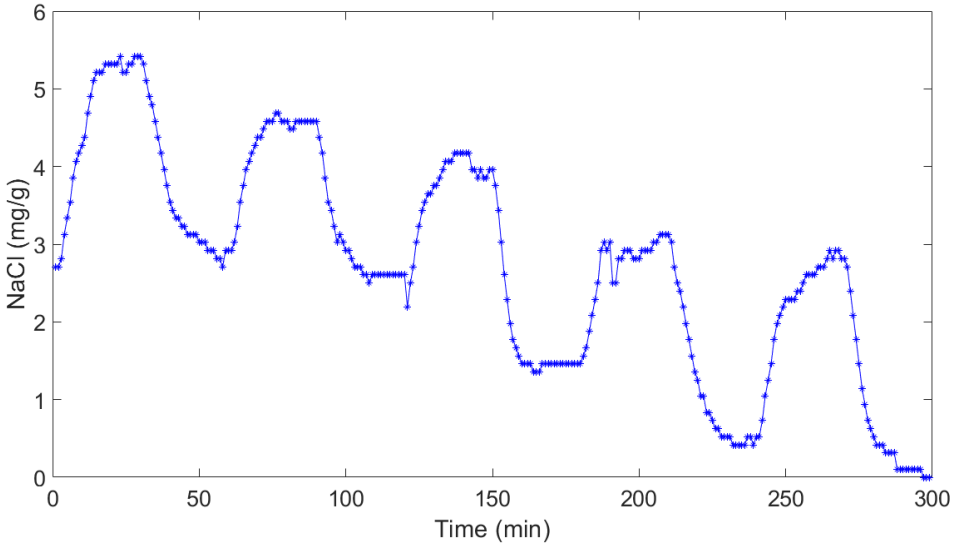

Fig. 49: Gravimetric salt adsorption capacitance of GOPSS-$GONH_3$.

Looking for a work-around for the negative electrode, a totally different class of material has been tested. The GO has been replaced with the MXenes. Despite their higher capacitance values, once tested for CDI the performance decreased a lot. The salt adsorbed for each cycle is 5 mg/g, fully comparable to the one of bare activated carbon. Moreover, a shift of the curve indicates that the MXenes are absorbing ions from the solution without been able to release them during the discharge step. In fact, having a look at Fig. 50, it is immediately clear that during the discharge this material is not able to reach a plateau. The ASAR is 0.42 mg g^{-1} min^{-1}, but only if considering the charging step. It cannot be computed for the discharge due to the absence of a steady value. The Λ is only 45 %, meaning that most of the active sites are not used or get permanently occupied by absorbed or intercalated ions.

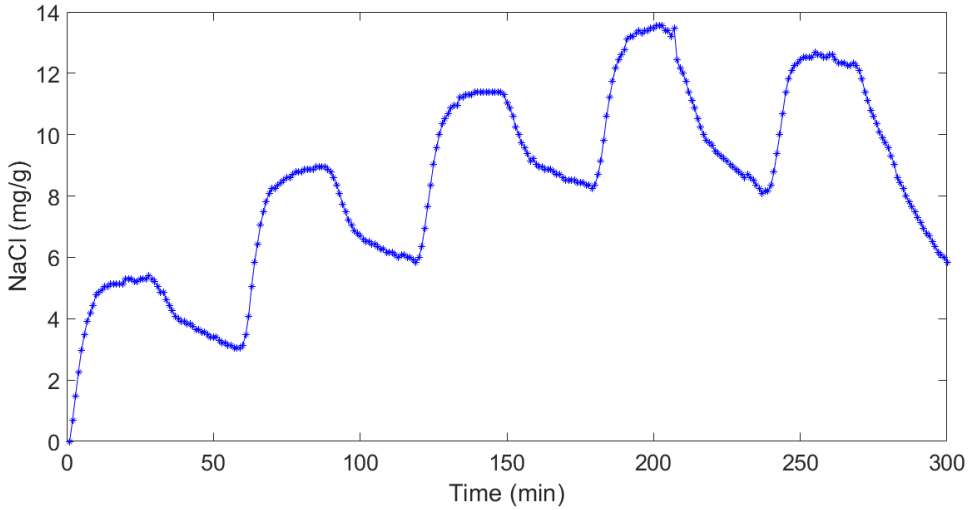

Fig. 50: Gravimetric salt adsorption capacitance of MX-$GONH_3$.

Finally, self-charge has been tested using the most promising material, the GO-GONH$_3$. In this test, the charge step at 1.2 V has been substituted with an open circuit condition. Everything else stayed the same. The results (Fig. 51) show a bad performance, with the mSAC being 1 order of magnitude lower than before. Moreover, the amount of adsorbed salt showed to be independent on the external charge/discharge switching. Being this test a complete failure, only 1 cycle was reported here.

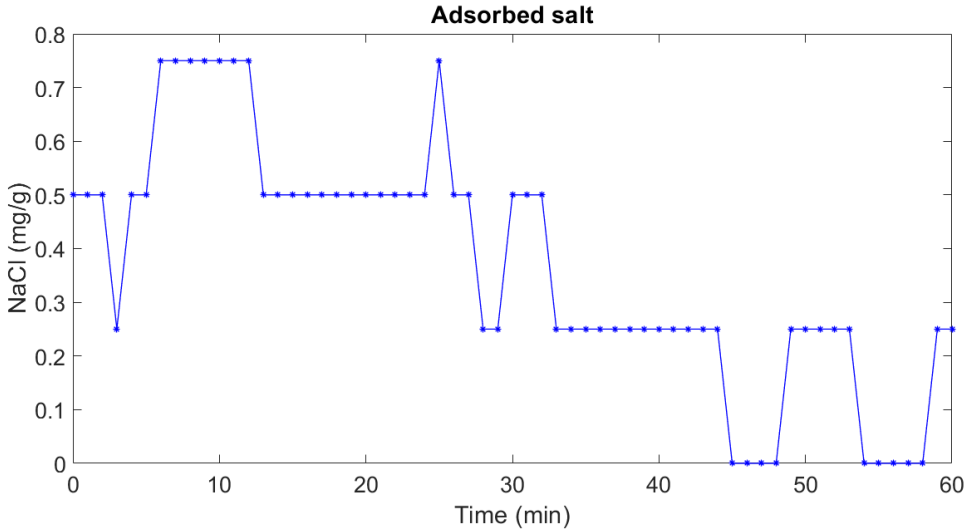

Fig. 51: Gravimetric salt adsorption capacitance of GO-GONH$_3$ in self-discharge condition. Only 1 cycle is here reported.

Having provided the performance of all these materials, for the sake of a wider perspective, it is necessary to compare each of these values to the state of the art. Porada et al. [5], Jia et al. [6], Oladunni et al. [154], Zhao et al. [167] all together provided a list of more than 200 works in their reviews. Looking at all these results, it is possible to see how many of the mSAC reported are below 5 mg/g, a part of them between 5 mg/g and 10 mg/g, while only few of them are above 10 mg/g. It is interesting to note how the top results have been obtained only in the very last years, mostly with costly 2D or nanostructured materials. Follows that, even if higher performances are reported in literature, a mSAC of 9 mg/g is a remarkable result, especially for a setup which has not been optimized to maximize the desalination performance. For what concerns the Λ, Suss et al. [7] analysed more than 100 works previously listed by Zhao et al. [168] and evaluated the Λ for each of them, highlighting how only membrane-based capacitive deionization was able to reach 90% and above. For GO-GONH3, instead, a Λ of 98% is obtained employing functionalized electrodes, without the need for membranes. The same material, without any functionalization, provided a Λ of only 55%, which is in line with what reported in literature.

From the comparison of such a large amount of papers found in literature, it comes evident that there is no standard at all. The approach and the procedures reported by one

paper are often very different from the ones reported in other papers. Starting from the basis, each experimental setup is different: the dimension and shape of the electrodes, the design of the cell and even the water flux are different.

Moreover, the method is not standardized. Some groups use the single-pass approach, consisting in fluxing the solution through the electrodes and measuring the change in conductivity over time, without reaching the equilibrium. The total amount of adsorbed salt is then evaluated by integrating the amount of adsorbed salt over time. Others use the batch mode, which consists in the evaluation of the adsorbed salt in equilibrium condition, like in this study.

Also, the experimental parameters are not standardized. The starting concentration of the solution is not univocally defined, ranging arbitrarily from 1 mM to 600 mM. Same situation for the applied potential: values ranging from 0.8 V to 2.0 V are commonly found. Even the time of the experiment is not the same, from few minutes to several hours.

Last but not least, the results are not reported in the same manner. It is possible to find the percentage of salt removed (meaningless most of the time, since it's not normalized), the mSAC (also called electrosorption capacity), the ASAR (strongly influenced by the experimental setup) and, finally, the Λ.

In conclusion, from CDI experiments, the most performing material proved to be the GO-$GONH_3$, even though the mSAC is not in the top of the leaderboard of the most adsorbing materials found in literature. However, its stunning charge efficiency makes it interesting for CDI applications.

Below is reported a table summarizing the results obtained for CDI. For the reason discussed above, only mSAC and Λ are reported in Tab. 3.

Material	mSAC (mg/g)	Λ	Stability
AC	5	55 %	Yes
AC-SPEEK	5	73 %	Yes
GO-$GONH_3$	9	98 %	Yes
GOPSS-$GONH_3$	3	91 %	No
MX-$GONH_3$	5	45 %	No

Tab. 3: Comparison of the results achieved through CDI. For each material, electrosorption capacity, charge efficiency and stability are reported.

5.2 Capacitive Mixing

In this section, the results of the CapMix measurements are reported, starting from the characterizations on the active materials and the passing to the energy harvesting results.

5.2.1 Active material

In this section is reported a series of characterizations performed on the materials employed for CapMix.

5.2.1.2 SPEEK coating

The availability of an ion exchange membrane moved the attention on the possibility of testing it for CapMix. A dedicated study was performed to design a procedure to obtain a uniform and repeatable SPEEK coating on the activated carbons. The goal was to obtain a very thin coating which does not increase too much the resistance of the electrode and contemporarily follows as best as possible to morphology of the active carbons to avoid a dramatical loss of capacitance.

Starting from the SPEEK solution described in chapter 4.1.1.1, many attempts have been done to obtain a uniform coating. The first attempt involved the use of a spin coater. However, trying different amounts of material and rotation speeds did not provide any result. The solution was always sliding on the AC. Therefore, a different approach was tested.

Drops of solution were directly casted on a hot AC substrate. This was done employing a hot plate and varying the temperature from 100 °C up to 200 °C, with the aim of forcing a fast evaporation of the solvent but without decomposing or modifying the polymer. In this case, a coating was obtained on the AC electrodes. Unfortunately, no matter the temperature and amount of solution, the final coating was never uniform. It was presenting as a translucid layer over the AC in the shape of coffee rings. On the edges stands a thick layer of polymer, while in the middle was none.

The turning point was reached when the procedure was implemented under vacuum condition. Indeed, dropping the solution on the AC substrate at room temperature and then applying a low vacuum to the system was enough to force the solution to permeate inside the AC structure. At naked eye, it was possible to see small bubbles of air coming out from the electrodes. Then, keeping the vacuum on, the electrode was heated up to 120 °C to force the evaporation of the solvent. By fixing a SPEEK mass load of 4 mg/cm^2, a uniform, thin coating was obtained. In Fig. 52 it is possible to appreciate the presence of the coating distributed all over the activated carbon matrix.

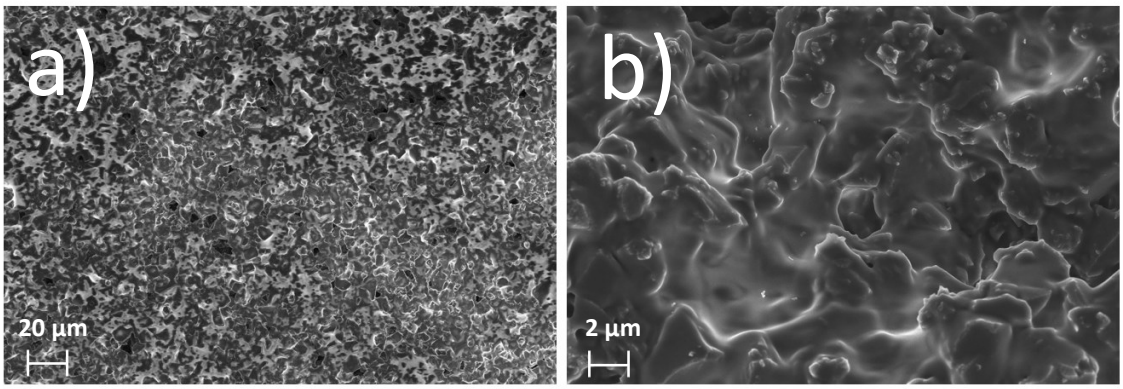

Fig. 52: AC coated with SPEEK. Magnification: a) 1000x, b) 10000x.

Impedance spectroscopy technique was used to check the effect of the SPEEK coating on the AC electrode. In Fig. 53 is reported a comparison of the two electrodes, the pristine and the coated one. It is possible to see how the presence of the thin membrane does not bring any significant shift to the resistance of the system.

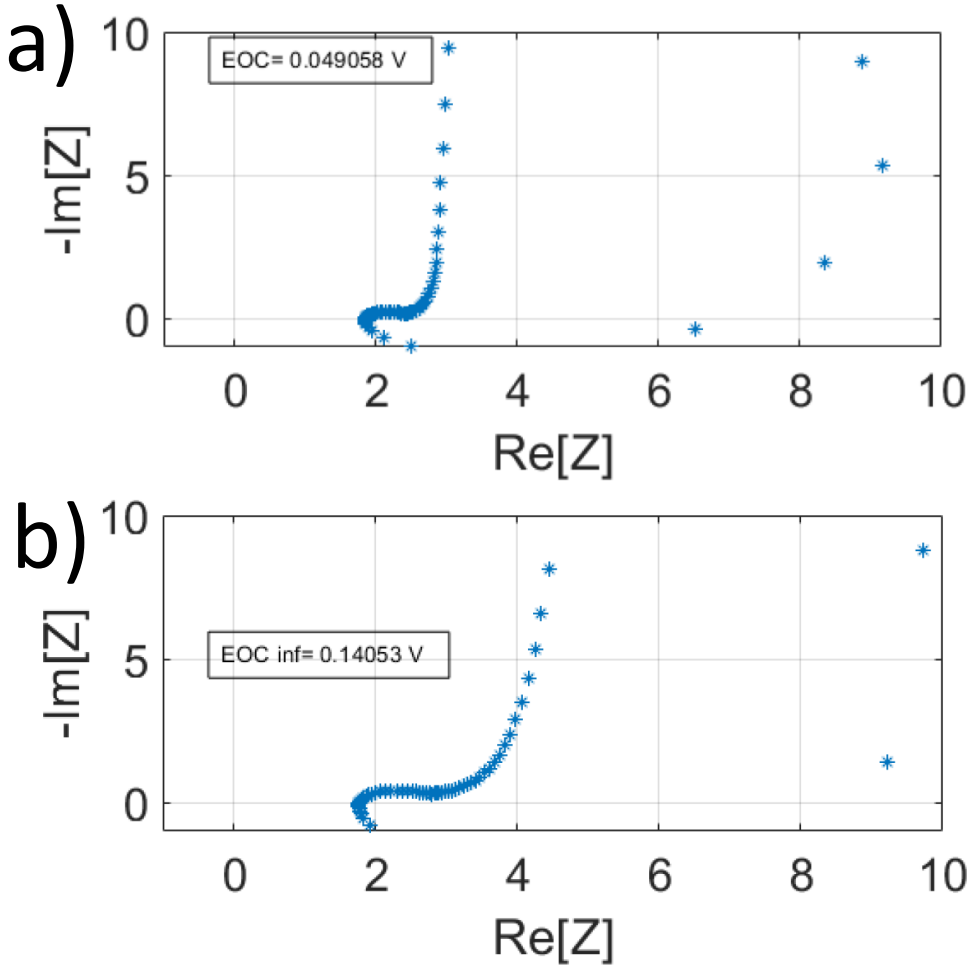

Fig. 53: Impedance spectroscopy results. a) AC. b) AC coated with SPEEK.

5.2.1.2 Electrochemical characterization

The first characterization performed on the materials employed for CapMix was the cyclic voltammetry. This is because not all the materials developed during the thesis activity had been already tested for capacitive deionization. The reason is that few of them arrived late in the activity and there was only time for CapMix testing.

Therefore, here are reported the CV performed at three electrodes. For the sake of conciseness, just an example of this kind of measurement is shown, here reported in Fig. 54.

There, it is possible to observe the anodic and cathodic CV for the $GONH_3$_20. This material is similar to the $GONH_3$, with just a different ratio of functionalized graphene oxide. The slurry composition was 75% in weight of AC, 5% of PVDF and 20% of $GONH_3$. This material was made with purpose of testing a higher concentration of functionalized graphene oxide to see if it was leading to a benefit in terms of electrochemical properties.

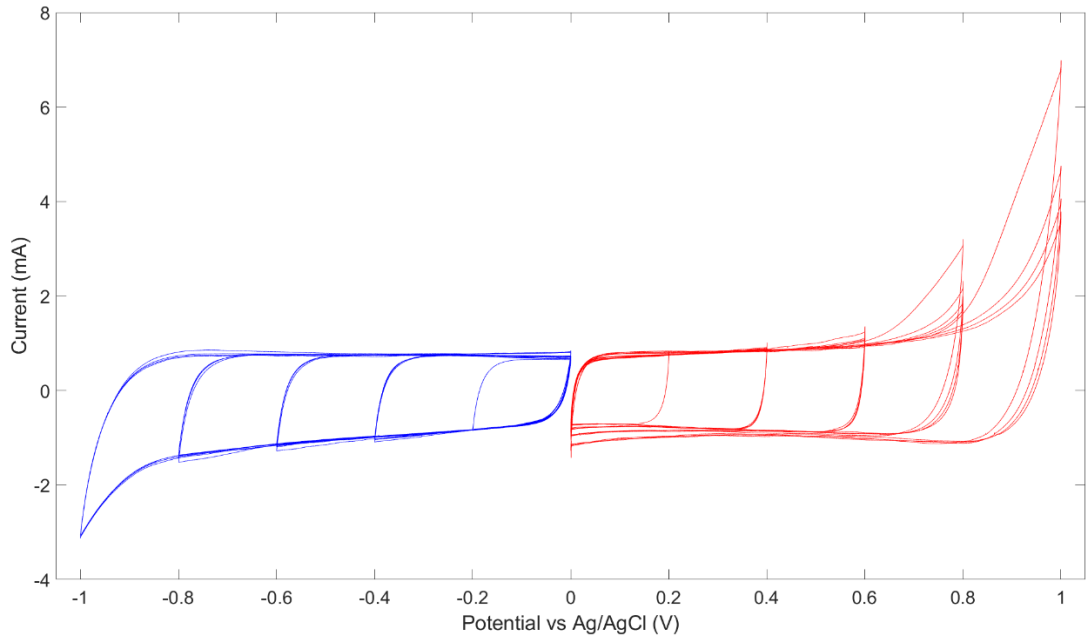

Fig. 54: CV of $GONH_3$_20. The potential is measured vs a standard Ag/AgCl electrode. Anodic and cathodic curves are reported on the same graph.

Together with the $GONH_3$_20, the new materials tested were fGO^- and fGO^-K^+. All the results (including the materials reported in chapter 5.1.2) are summarized in the following comparison charts.

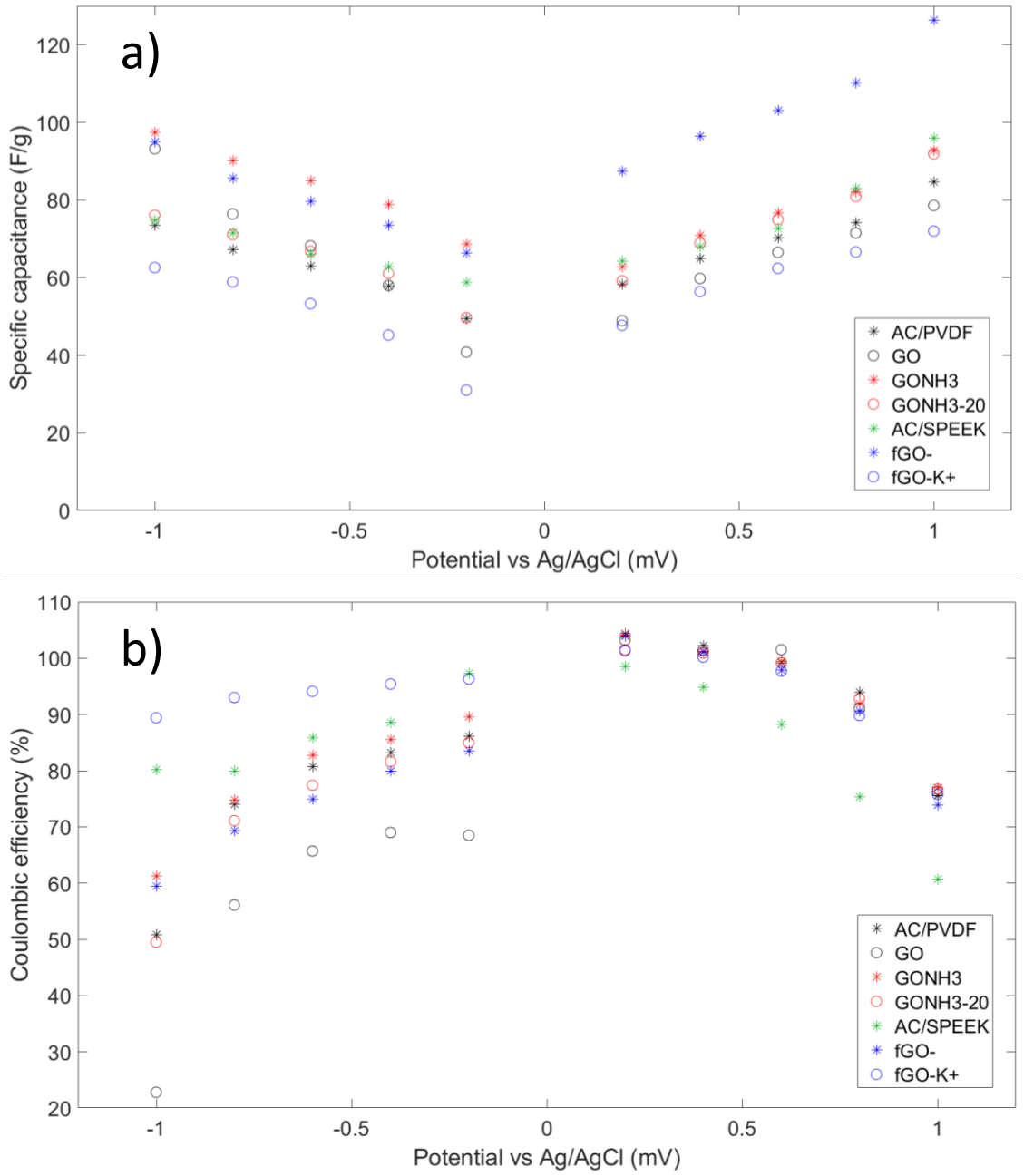

Fig. 55: a) Specific capacitance of different materials as function of the applied potential. b) Coulombic efficiency of the same materials as function of the applied potential.

Fig. 55a shows the capacitance values normalized by the mass of each material. Both anodic and cathodic windows are shown. The capacitance is evaluated every 200 mV. The potential is referred to a standard Ag/AgCl electrode. The material showing the lower specific capacitance is the $fGO^{-}K^{+}$. In the anodic, it shows values ranging from 48 F/g (200 mV) up to 72 F/g (1 V). In cathodic, the values go from 31 F/g (-200 mV) up to 63 F/g (-1 V). Interestingly, in the anodic window, the best performing material is the fGO^{-}, with values above 100 F/g. For the cathodic window, the fGO^{-} and the $GONH_3$ have similar behaviours, with values around 67 F/g at -200 mV, up to ~96 F/g at -1 V. The

base material (AC) is in the average for both anodic and cathodic windows. It is interesting to note how the AC/SPEEK in the cathodic window is showing the lowest dependence of the specific capacitance on the applied potential. Indeed, it ranges from 59 F/g at -200 mV to 75 F/g at -1 V. In the anodic window, all the materials show the same trend.

Fig. 55b shows the coulombic efficiency for all the materials as function of the applied potential. In the anodic window, almost all the materials perform the same. While being slightly above 100% at 200 mV, few of them are still above 99% at 600 mV, then drastically falling down after 800 mV. The only exception is the AC/SPEEK, having a poorer efficiency for all the positive potentials. It means that in the anodic window the activated carbon is doing most of the job in terms of efficiency, regardless of the functionalized material. The presence of SPEEK is worsening the performance, as expected. The SPEEK is a cation exchange polymer, thus it is not suited to work in anodic windows. Having a look at the cathodic window, instead, the scenario is totally different. The best performing material is the one showing the lowest specific capacitance, the fGO^-K^+. It is above 90% for all the potentials. A good result is also achieved by the AC/SPEEK, staying above 80%. The worst performance in the cathodic window is achieved by the GO, with a coulombic efficiency always below 70%.

The results here reported do not outline a clear pathway. Depending on the voltage applied, some materials perform better than others in terms of coulombic efficiency or specific capacitance. However, the specific capacitance does not play a key role in CapMix. In principle, any mismatch in capacitance between anode and cathode can be balanced by tuning the mass of the electrodes. The coulombic efficiency is a totally different story. Efficiency is the key point for CapMix, therefore materials showing high coulombic efficiency are to be preferred. For this reason, good candidates for positive electrode can be all of them, expect the AC/SPEEK. For the negative electrodes, fGO^-K^+ and AC/SPEEK are to be preferred.

However, the crossroads of capacitance and efficiency is not the only one found on the road to the CapMix measurements. The choice of the materials cannot be made simply on coulombic efficiency. More parameters are to be taken into account, and that's where other characterizations come in handy.

The first characterization that was strictly applied for CapMix is the OCV performed with 5 electrodes. The setup is described in chapter 4.3.2.3, together with the procedure.

The AC has been tested with both at positive and negative voltage applied. The results are shown in Fig. 56. By cycling freshwater and seawater while applying a potential to the cell, this measurement allows to predict the behaviour of the different materials as a function of the potential.

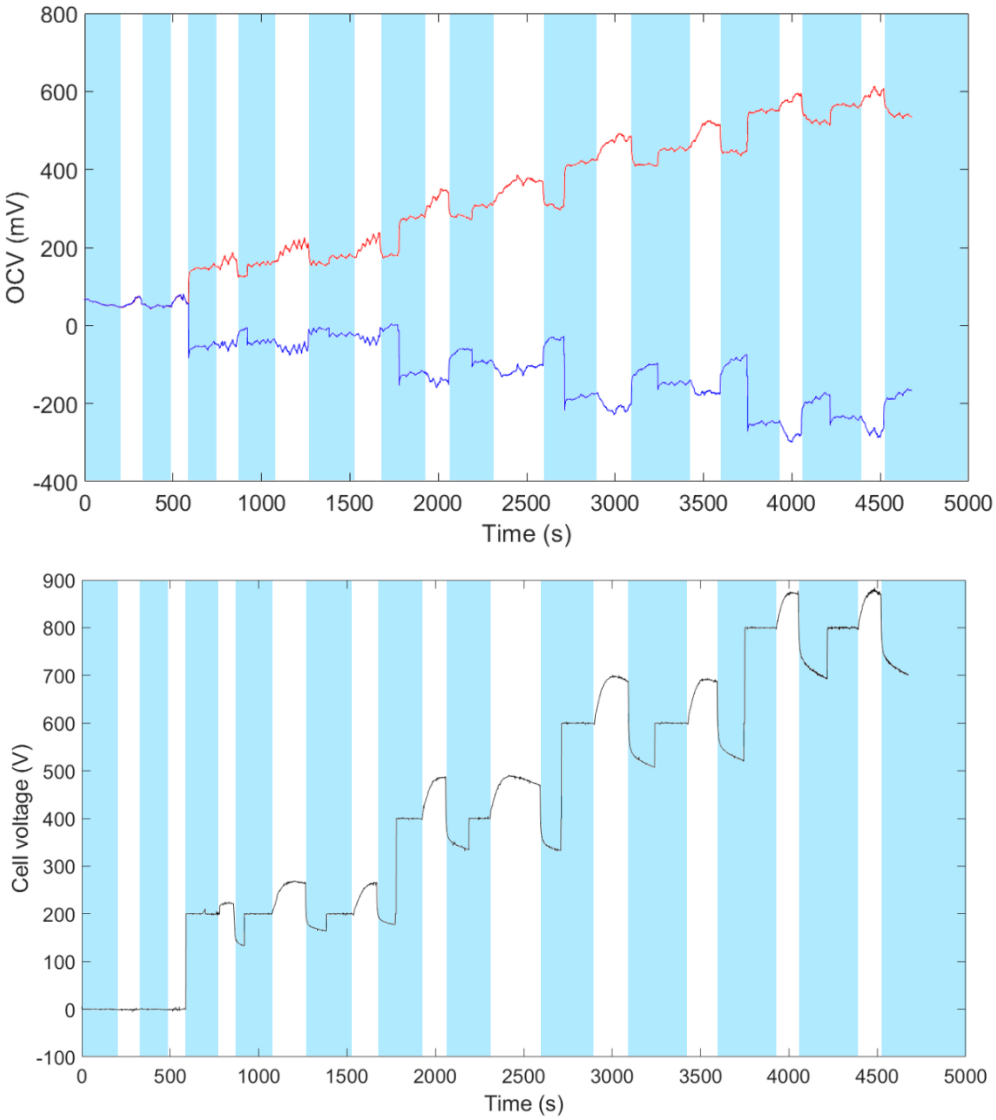

Fig. 56: OCV of bare AC. On the top, the potential measured vs Ag/AgCl. In red, the positive electrode. In blue, the negative one. On the bottom, the cell voltage as a function of time. White bars refer to low salinity solution, blue bars to high salinity one.

The initial part of the measurement is performed without applying any external voltage to the cell. This is done with the purpose of studying the behaviour of the pristine electrodes. Indeed, when switching the salinity of the solutions, each electrode can both rise or decrease its potential, depending on its nature. Then, the measurement goes on

applying an external bias to the cell and switching the solutions. The maximum voltage rise/decrease is recorded as a function of the potential.

In Fig. 57 is reported the same measurement, performed with two different electrodes. The positive one, $GONH_3$, shows high stability over time and remarkable voltage rise. In particular, for all the measurements performed, the $GONH_3$ showed the best stability and lowest self-discharge among all the materials tested. The negative material here shown is the fGO^-K^+.

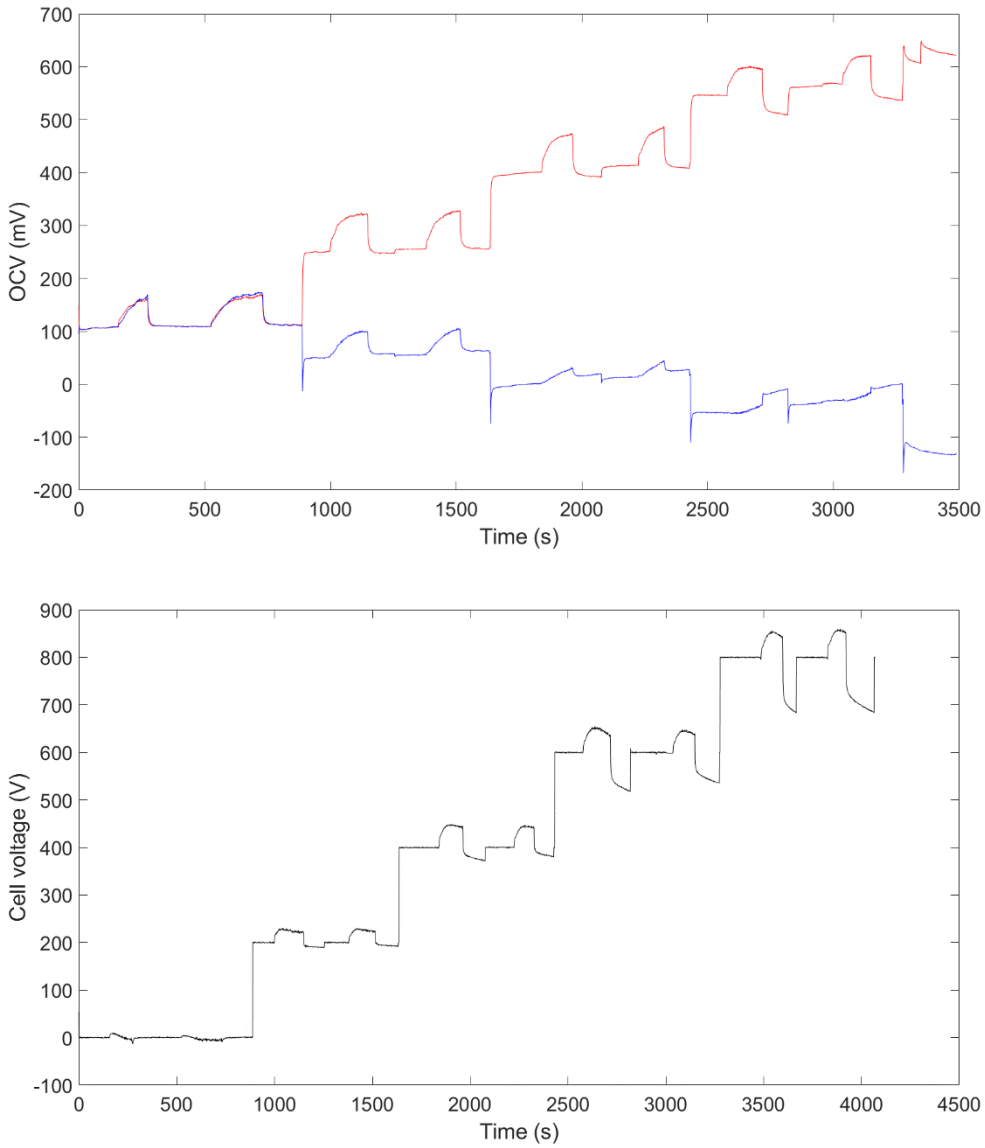

Fig. 57: OCV of $fGO^-K^+/GONH_3$. On the top, the potential measured vs Ag/AgCl. In red, the positive electrode. In blue, the negative one. On the bottom, the cell voltage as a function of time.

Collecting all these kind of measurements, here not shown, the graph presented in Fig. 58 can be obtained.

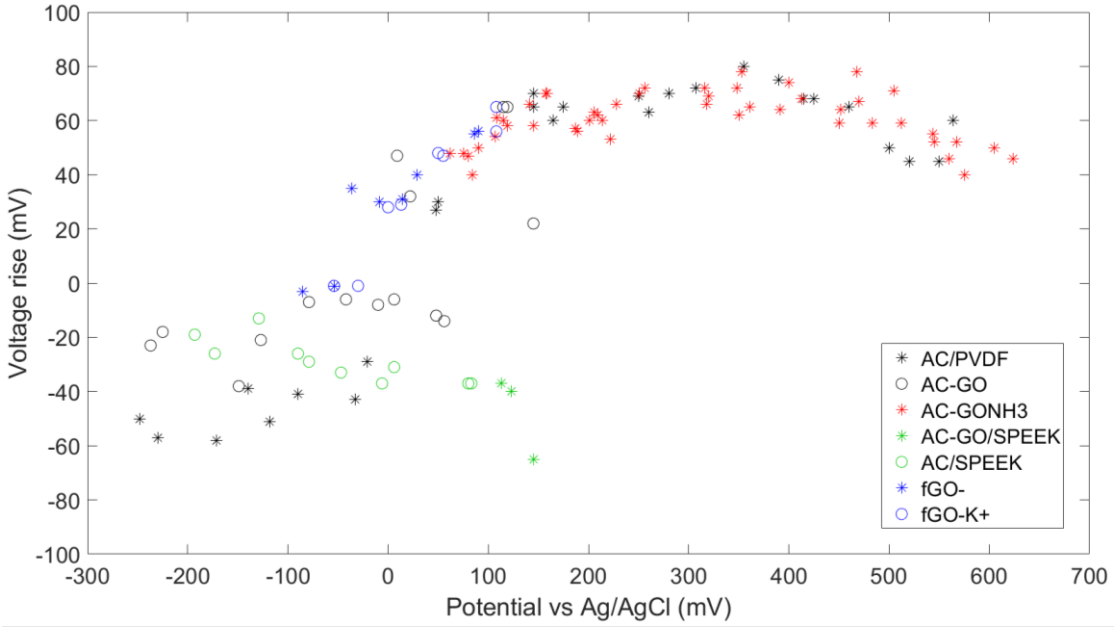

Fig. 58: Voltage rise as a function of the potential for all the investigated materials.

The graph is a comparison of all the materials investigated during the thesis activity. For positive potentials, the behaviour of AC and $GONH_3$ is similar. However, the latter showed a higher stability over time, thus making it promising for CapMix application. For the negative potentials, the functionalized materials showed poor performance, thus making the bare AC the best choice for the negative electrode. Interestingly, the AC mixed with SPEEK as a binder provided a negative voltage rise also for positive potential. Such a feature makes this material a good candidate for a CapMix cycle performed at 0 V bias, thus exploiting the spontaneous of this material without providing any external power.

As a last preliminary test before the CapMix measurements, the impact of self-discharge has been evaluated as described in chapter 4.3.2.4 for few couples of materials. In Fig. 59 is reported an example of such measurements.

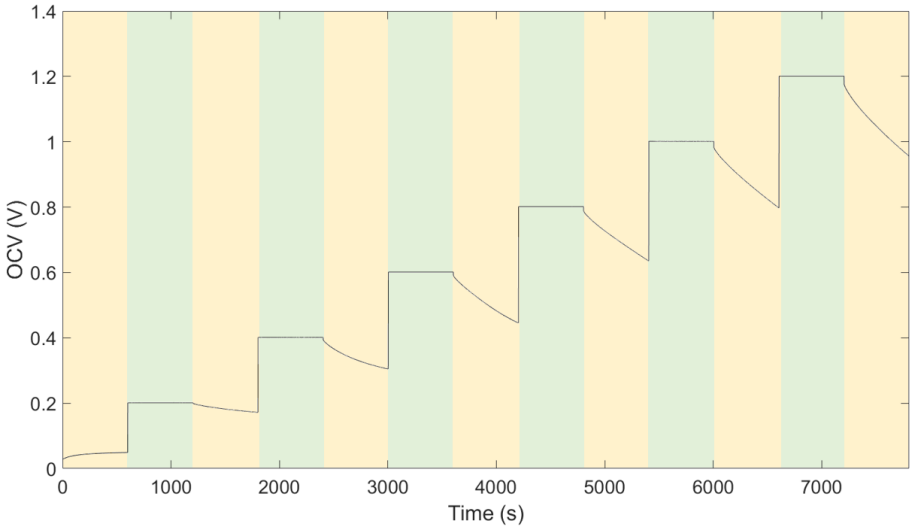

Fig. 59: Example of self-discharge evaluation. In yellow, the OCV phases. In green, the constant voltage steps.

After an initial OCV, the potential is set to 0.2 V for 10 min. Then, the device is let to rest in OCV condition for 10 min while measuring the voltage. This step is repeated every 200 mV up to 1.2 V. As expected, for all the materials, the self-discharge became more evident as the voltage was increased. In Tab. 4 is reported a summary of the evaluation of the self-discharge for different couple of materials.

Material	0.2 V	0.4 V	0.6 V	0.8 V	1.0 V	1.2 V
AC/AC	93%	93%	87%	83%	79%	75%
ACSPEEK/AC	88%	90%	88%	87%	86%	80%
GO/AC	91%	87%	84%	75%	74%	70%
AC/$GONH_3$	95%	92%	88%	82%	76%	73%
GO/$GONH_3$	97%	90%	85%	79%	74%	70%
$fGO^-K^+/GONH_3$	88%	83%	81%	79%	80%	79%
$fGO^-/GONH_3$	86%	76%	74%	79%	80%	80%
$fGO^-/GONH_3$_20	90%	83%	76%	80%	81%	80%
ACSPEEK/$GONH_3$	94%	93%	82%	83%	79%	78%
GOSPEEK/$GONH_3$	88%	83%	78%	73%	69%	66%

Tab. 4: Self-discharge for each couple of tested materials. The results are reported as percentage of preserved potential after 10 min. In green when above 90%, in red when below 80%, in yellow in between.

To be representative for the CapMix application, the self-discharge has been evaluated using a 10 mM solution, for which its presence has the real impact on the measurement. The time scale of these tests is larger than the one used for CapMix, but it's providing an overview of what we could expect to happen. For an applied voltage of 0.6 V and above, the self-discharge has a very high impact on the state of charge of the device. Therefore, independently on the materials, it will be recommended to work below 0.6 V.

Taking a look at each material, the ones containing fGO^- and fGO^-K^+ show a self-discharge less dependent on the applied voltage. On the other hand, the presence of $GONH_3$ seems to have a positive effect on the self-discharge. However, from these results it is not possible to infer which are the best performing materials. They need to be tested at least at 200 mV.

5.2.2 Energy harvesting results

The first set of CapMix measurements is a collection of constant current charge and discharge measurements performed from 0 V up to a maximum voltage. In Fig. 60 is shown an example of these measurements, in which bare AC is charged up to 0.6 V in 0.6 M NaCl. Then, the solution is switched, the voltage rises and the device is discharged.

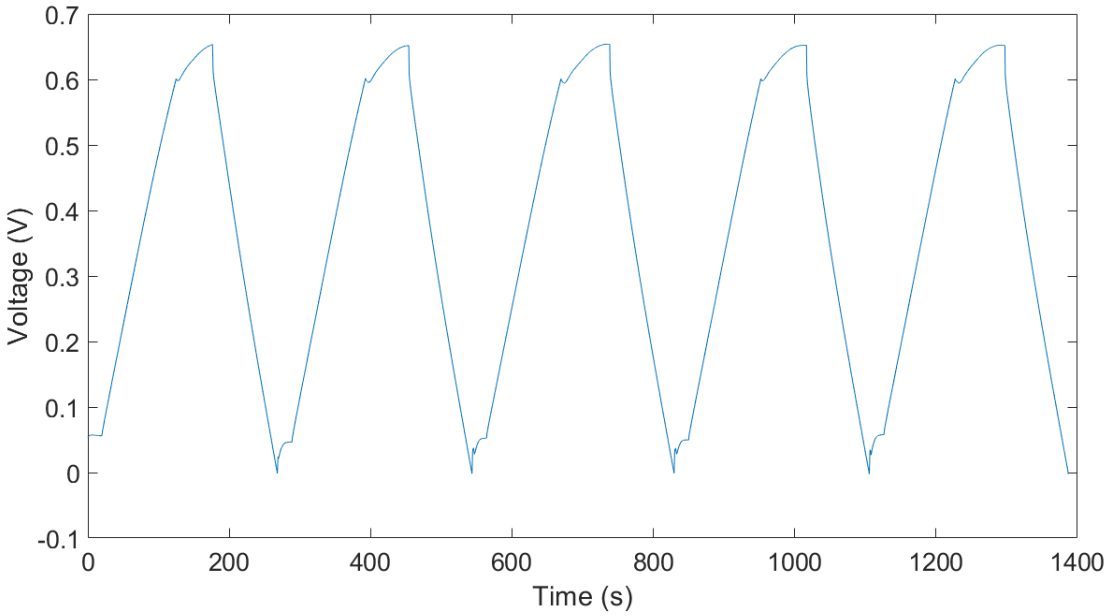

Fig. 60: CapMix on AC. The device is charged up to 600 mV and then fully discharged.

Taking a closer look at the graph, it is possible to recognize the 4 steps of CapMix. Referring to Fig. 61, the step 1 is the charging step at constant current. During the step 2, the solution is changed (passing from 0.6 M to 10 mM) in open circuit condition and the voltage rises. In step 3, the device is discharge at constant current. In step 4, in open circuit, the solution is switched again.

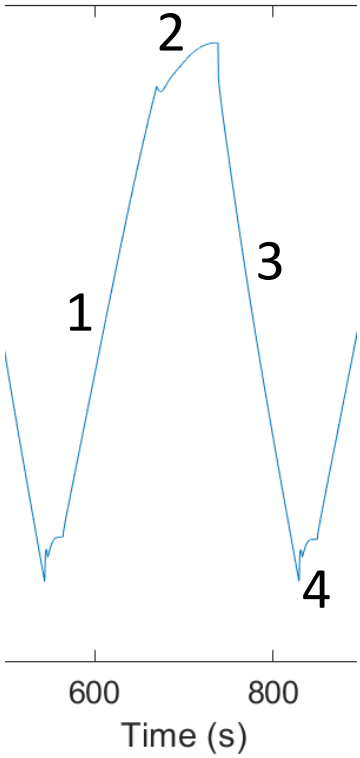

Fig. 61: Detail of Fig. 60, in which it is possible to see the 4 steps of CapMix.

The very first measurements were not fully standardized. They have been employed as a benchmark to verify the possibility of employing both the cell and the materials for CapMix application. Therefore, a criterion was not defined to choose the current intensity, the water flux and the time for the step 2. Initially, the current was set to a value such that the IR drop was not too large. The water flux was arbitrarily set to 4 ml/min. It was a compromise between a too fast flux which could create turbulence inside the cell and a too slow flux leading to a delay in the voltage rise. The time for the step 2 was manually adjusted at each cycle by moving to step 3 only when the voltage rise was reaching a plateau.

These measurements were repeated at different voltage windows and for different materials. An example of what obtained for bare AC is shown in Fig. 62. As expected, by increasing the voltage window, also the self-discharge is increasing, leading to no voltage rise at 1 V in the case of bare AC.

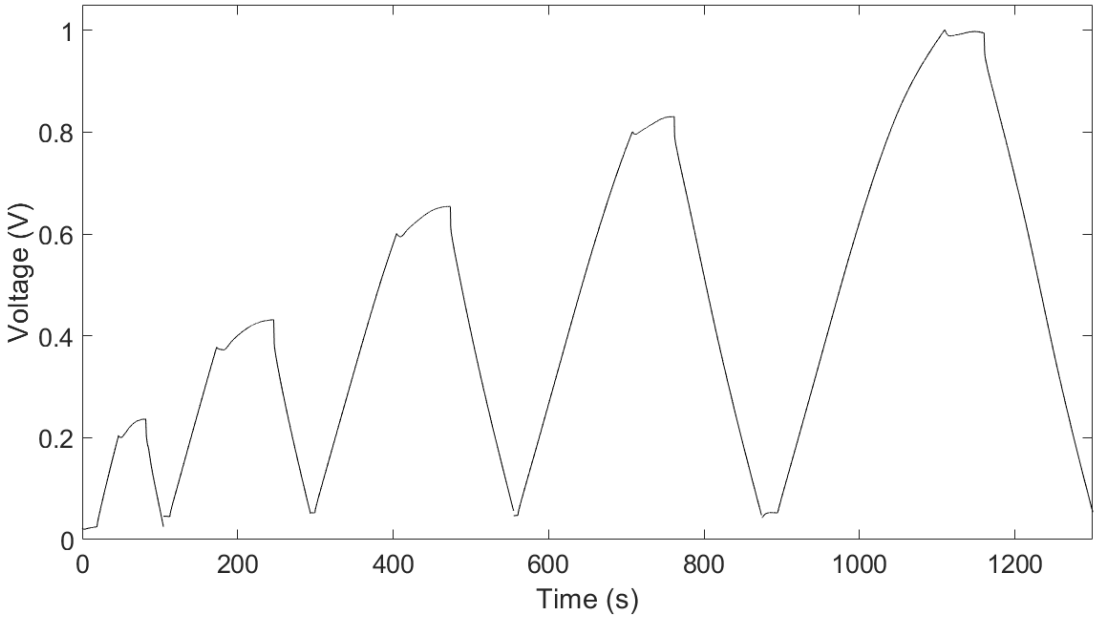

Fig. 62: CapMix on AC. Comparison of cycles performed with different voltage windows.

At a first look, it seems that the self-discharge is only lowering the voltage rise. If that was the case, the bare AC could be operated up to 0.8 V and it still could be possible to harvest energy thanks to the small voltage rise. However, that's not the case. Indeed, the self-discharge is not only affecting the voltage rise, but it also reduces the time of the discharge step, thus lowering the amount of energy recovered.

Referring to the theory described in chapter 3.3, follows that the condition $Q_{charge} \approx Q_{discharge}$ is never satisfied. Therefore, a direct evaluation of the energy first provided and then recovered is necessary to estimate the amount of harvested energy. By doing this computation, the Tab. 5 is obtained.

Material	Max voltage (mV)	Gain (mV)	Q_{charge} (mC/cm^2)	$Q_{discharge}$ (mC/cm^2)	Harvested energy per cycle (mJ/cm^2)
AC	200	40	11.2	9.2	0
AC	400	60	24.0	18.8	0
AC	600	50	42.0	36.8	0
AC	800	30	59.2	44.8	0
AC	1000	0	85.6	56.0	0
AC/SPEEK	200	60	28.4	19.2	0
AC/SPEEK	400	60	65.6	47.6	0
AC/SPEEK	600	60	108	84.4	0
AC/SPEEK	800	50	151	122	0
AC/SPEEK	1000	30	226	149	0
AC/SPEEK	1200	0	240	140	0
GO-$GONH_3$	200	40	24.8	20.8	0
GO-$GONH_3$	400	40	57.2	46.0	0
GO-$GONH_3$	600	30	76.0	63.6	0
GO-$GONH_3$	800	10	120	86.8	0

Tab. 5: CapMix results obtained charging and discharging from 0 V up to a maximum voltage. The harvested energy is always 0.

The table shows the results obtained for three couples of materials. They are the same that showed the best desalination performance. It is evident how, in a different context, the situation is totally different. For none of them has been possible to harvest energy. In the best cases, the efficiency was 100%, that means it was possible to recover all the electrical energy provided, but nothing more.

Failing to obtain a net energy income, a change in the procedure was mandatory. In principle, the idea of working in a wide voltage window (that is from 0 V up to a fixed V_{max}) would translate in a great energy income. However, exploiting such voltage range has the drawback of increasing the magnitude of the self-discharge. This is due to the fact that the materials are forced to work in a large dynamic, thus not promoting the stability of the system.

Therefore, the only choice was to work around a fixed potential. As extensively described in literature, the idea is to set a working potential and never charge above that value or discharge below. Practically speaking, it translates in charging the device at a certain voltage, switching the solutions to increase the potential, discharge to the same potential, switch again the solutions and charge back to the initial potential. Doing so, the materials will work in a much smaller voltage window.

To do so, many strategies can be adopted. For the charging step, the difference between constant current (CC) and constant voltage (CV) have been investigated. For the discharge, CC, CV and constant load (CL) have been investigated too. To minimize the variables at stake, the comparison has been performed on bare AC.

Starting from the charge, the aim was the evaluation of the energy (and power) provided with the two different methods. Here, the less energy-consuming method is desired. Starting from the CC, the device has been charged from 0 V up to 0.2 V with different current intensity. High current rates lead to significant voltage drop at 0.2 V. Low current rates would increase the time, thus reducing the output power of the whole CapMix cycle. A good compromise has been found for current density of 10~20 $\mu A/cm^2$, which translates in few mA/g if considering the mass of the active material.

To compare the CC with the CV, the device was charged at 0.2 V for the same time required by CC to reach 0.2 V. Then, the current was integrated over time to evaluate the energy provided to the system. Comparing the values obtained from CV with the ones coming from CC, it was immediately verified that CC charge was less energy consuming than CV. The reason is that forcing a voltage step to a capacitive system always leads to a current spike followed by an exponential decrease. Higher the voltage difference, higher the current intensity and, therefore, higher the energy/power spent. That being said, the exponential decrease cannot compensate the power spent in the initial spike, thus the CC method is always preferrable for the charging step of the device.

Moving to the discharge phase, CC, CV and CL have been compared in terms of energy and power extracted. Starting from CV, as for the charging step it was the most energy-consuming, here is the one allowing to collect the highest amount of energy. The reason is that it is the fastest discharge method and allows to strongly reduce the impact of the self-discharge. On the other end, this method can only be good to estimate the maximum energy that can be extracted. In fact, it fails to be reproducible in a real application, since to extract energy will be necessary to discharge the device on a load. In this method, the device is discharged by applying 0 V, thus simulating a short circuit, which, by definition, dissipate all the energy through the Joule effect.

For what concerns the CC and CL, they are both current-controlled methods. The difference is that in CC the current is kept constant, while in CL the current is instantly varied by the potentiostat to keep constant the voltage over current ratio, thus simulating a constant load. The latter is the most realistic one, of course. However, if the relative variation of the voltage is small, the two methods are equivalent.

In Fig. 63 is shown a comparison of all the methods cited above.

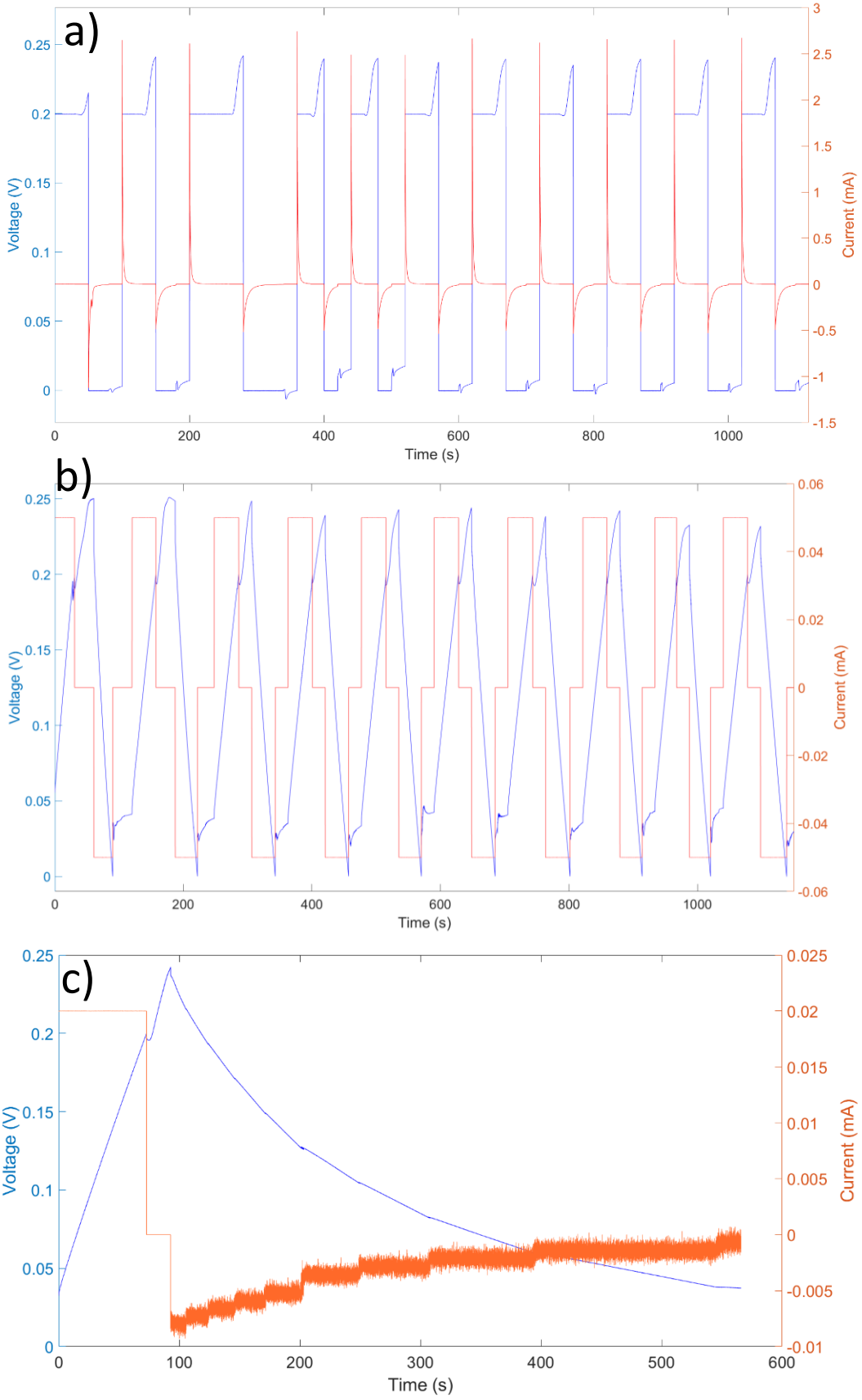

Fig. 63: Comparison of different charge and discharge methods. a) CV. b) CC. c) CC for the charge and CL for the discharge.

Having a look at Fig. 63c, it stands out that the impact of CL is huge. First of all, the decrease of the voltage is smoother, thus increasing the time required to discharge the device. Second, it is possible to see the noise and the discontinuities introduced by the instrument when modifying the current value.

This final consideration clearly lines out that working in a wide voltage window is not feasible. The impact of self-discharge and thinking about a possible future application in a pilot-scale prototype are leading to the conclusion that the only way to work efficiently with the CapMix is reducing the voltage window. To do so, it is mandatory to study all the materials at a fixed working point. This is done by charging the device up to a certain voltage and then discharge it up to the same voltage. In this way, the device is working around a fixed bias which, if properly chosen, can effectively reduce the impact of self-discharge.

Taking into account what already said, the final procedure for CapMix has been outlined. Both the charge and discharge steps will be performed in CC configuration. The bias will be varied and the energy and power harvested will be evaluated.

Many combinations of materials have been tested, focusing the attention on the materials which showed to be the most promising, as described in chapter 5.2.1. In Fig. 64 is reported a series of these measurements. The number of cycles displayed is reduced to provide a better overview to the reader about what has been done.

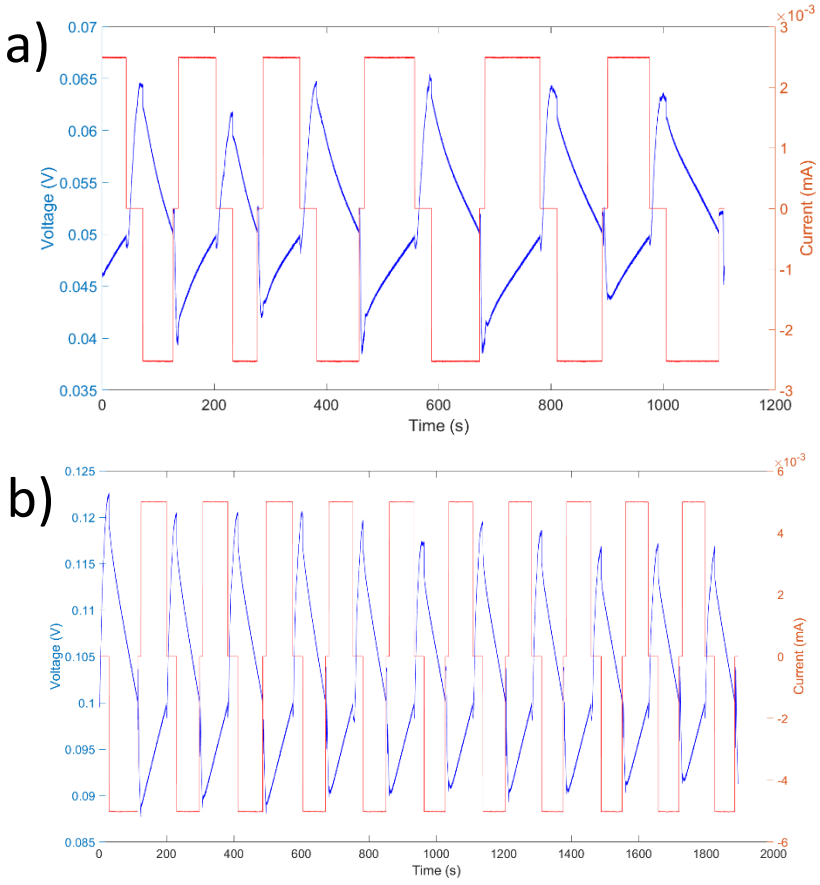

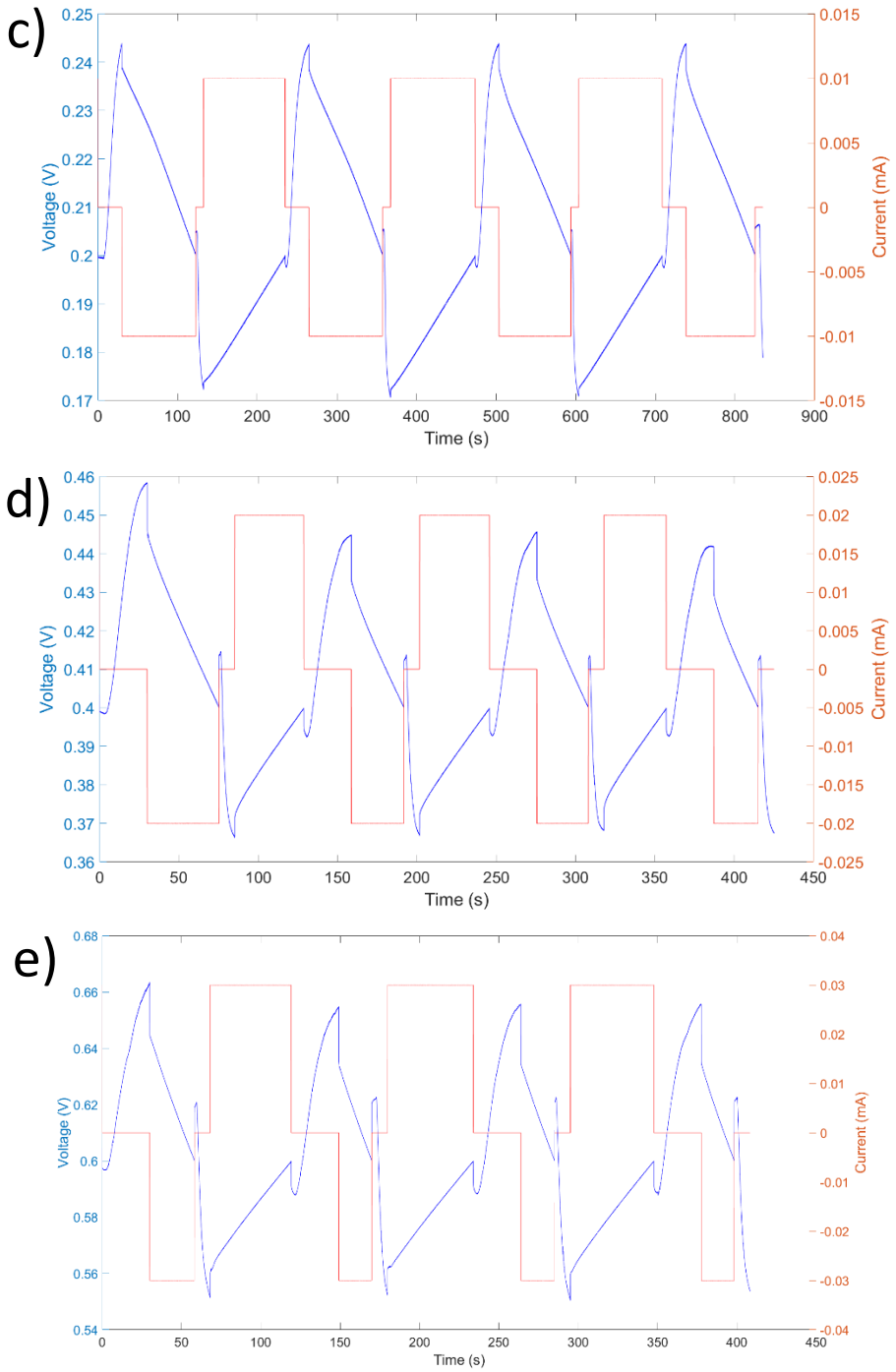

Fig. 64: Example of CapMix measurements. In blue the voltage of the cell, in red the current intensity. The material shown is AC-GONH$_3$. a) 50 mV. b) 100 mV. c) 200 mV. d) 400 mV. e) 600 mV.

Before testing each material, the impedance of the cell is estimated by means of impedance spectroscopy technique. Then, the load is set to maximize the output power. Therefore, by changing the working bias of the cell, the current is modified accordingly.

From Fig. 64d,e it is possible to appreciate the effect of the self-discharge when working at higher bias. The discharge time is much smaller than the charge one. There are also higher spikes when switching to open circuit.

The results for all the couples of materials tested is reported in Tab. 6.

Material	Bias (mV)	Gain (mV)	Harvested energy per cycle (mJ/m^2)	Harvested power per cycle (mW/m^2)
AC-AC	50	25	25 ± 5	0.10 ± 0.02
AC-AC	100	30	45 ± 10	0.22 ± 0.06
AC-AC	200	35	53 ± 15	0.60 ± 0.15
AC-AC	300	40	0	0
AC-$GONH_3$	50	15	59 ± 12	0.32 ± 0.07
AC-$GONH_3$	100	20	96 ± 20	0.51 ± 0.10
AC-$GONH_3$	200	42	255 ± 22	1.09 ± 0.12
AC-$GONH_3$	300	40	0	0
AC-$GONH_3$	400	45	0	0
AC-$GONH_3$	500	56	0	0
AC-$GONH_3$	600	60	0	0
fGO^--$GONH_3$	50	14	10 ± 2	0.06 ± 0.03
fGO^--$GONH_3$	100	10	0	0
fGO^-K^+-$GONH_3$	50	9	5 ± 2	0.03 ± 0.01
fGO^-K^+-$GONH_3$	100	18	3 ± 1	0.02 ± 0.01
fGO^-K^+-$GONH_3$	200	15	0	0
AC/SPEEK -$GONH_3$	50	21	64 ± 8	0.39 ± 0.04
AC/SPEEK -$GONH_3$	100	22	125 ± 15	1.93 ± 0.15
AC/SPEEK -$GONH_3$	200	25	0	0
AC/SPEEK -$GONH_3$	0	25	29 ± 8	0.12 ± 0.02

Tab. 6: CapMix results working at a fixed bias.

From these results it possible to see that working around a fix bias allowed to successfully achieve a net energy harvesting. However, the harvested power is very low. In the best case, the extracted power was slightly above 1 mW/m^2. Most of the time, it was few tens or hundreds of $\mu W/m^2$. Improvements are needed.

The first experimental parameter investigated was the water flux. It was varied from 1 ml/min up to 10 ml/min. Adjusting this parameter has a direct effect on the voltage rise. Too low flux (< 4 ml/min) is slowing the rise of the voltage when switching the solutions, thus increasing the overall time of the cycle, lowering the output power and providing more time to the self-discharge the act. On the other hand, high flux values (> 8 ml/min) create turbulent movement of the water inside the cell, flushing on the electrodes and creating instability on the system. The best configuration was found to be 8 ml/min, which is granting a faster voltage rise. Tab. 7 shows the effect of the water flux on the output power.

Material	Bias (mV)	Water flux (ml/min)	Gain (mV)	Time to reach the maximum gain (s)	Harvested power per cycle (mW/m^2)
AC-$GONH_3$	200	2	18	40	0.76
AC-$GONH_3$	200	4	20	30	1.09
AC-$GONH_3$	200	8	29	15	1.82
AC/SPEEK -$GONH_3$	100	2	19	30	1.54
AC/SPEEK -$GONH_3$	100	4	22	20	1.93
AC/SPEEK -$GONH_3$	100	8	30	10	2.51

Tab. 7: Effect of water flux on CapMix.

The second parameter under investigation was the mass load of the electrodes. By keeping fixed the area of the electrodes, the amount of active material was varied. From a thickness of 100 μm, it was increased up to a thickness of 400 μm. It was observed that an intermediate thickness provides the best performance in terms of output power. Higher thickness may lead to lower diffusion of ions inside the porous structure, thus increasing the resistance of the cell and the self-discharge. Lower thickness, on the other hand, do not maximize the capacitance per square meter. The results are summarized in Tab. 8.

Material	Bias (mV)	Coating thickness (μm)	Gain (mV)	Harvested energy per cycle (mJ/m^2)	Harvested power per cycle (mW/m^2)
AC-GONH$_3$	200	100	42	255	1.09
AC-GONH$_3$	200	200	50	317	2.34
AC-GONH$_3$	200	300	47	299	1.95
AC-GONH$_3$	200	400	40	210	0.88

Tab. 9: Effect of coating thickness on CapMix.

Combining all the optimization previously described, it was possible to achieve an output power of 4.6 mW/m^2 with AC-GONH$_3$, working with a bias of 200 mV, with a thickness of ~200 μm and a water flux of 8 ml/min.

Working with this experimental parameter, the possibility of harvesting energy from an artificial seawater source was investigated. It is well-known, indeed, that working with a mix of salts, both monovalent and divalent, usually lower the efficiency of any system, because of different diffusivity and chemical interaction of the various species. The composition of the artificial solution was selected to mimic the chemical composition of the Mediterranean Sea. The reference values are reported in Tab. 9.

Element/Ion	Concentration (M)	Source
Cl^-	$6.21 \cdot 10^{-1}$	[80]
Na^+	$4.70 \cdot 10^{-1}$	[80]
Mg^{2+}	$5.28 \cdot 10^{-2}$	[80]
SO_4^{2-}	$2.81 \cdot 10^{-2}$	[80]
Ca^{2+}	$1.03 \cdot 10^{-2}$	[80]
K^+	$1.02 \cdot 10^{-2}$	[80]
HCO_3^-	$2.38 \cdot 10^{-3}$	[80]
Br^-	$8.39 \cdot 10^{-4}$	[80]
B	$4.16 \cdot 10^{-4}$	[80]
I	$3.15 \cdot 10^{-4}$	[169]
Sr^{2+}	$7.60 \cdot 10^{-5}$	[170]
NO_3^-	$6.14 \cdot 10^{-5}$	[80]
F^-	$5.27 \cdot 10^{-5}$	[80]
SiO_2	$3.83 \cdot 10^{-5}$	[80]
Li^+	$2.45 \cdot 10^{-5}$	[171]
Fe	$5.80 \cdot 10^{-6}$	[80]
NH_4^+	$4.44 \cdot 10^{-6}$	[80]

Al	$4.90 \cdot 10^{-7}$	[170]
Ni	$3.34 \cdot 10^{-7}$	[170]
V	$1.04 \cdot 10^{-7}$	[170]
As	$9.40 \cdot 10^{-8}$	[170]
Cr	$7.80 \cdot 10^{-8}$	[170]
Mn	$4.70 \cdot 10^{-8}$	[170]
Ba	$4.2 \cdot 10^{-8}$	[170]
Zn	$3.10 \cdot 10^{-8}$	[170]
Cu	$1.40 \cdot 10^{-8}$	[170]
U	$1.00 \cdot 10^{-8}$	[170]
Hg	$5.00 \cdot 10^{-9}$	[170]
Se	$4.00 \cdot 10^{-9}$	[170]
Co	$4.00 \cdot 10^{-9}$	[170]
Cs	$2.00 \cdot 10^{-9}$	[170]
Cd	$5.00 \cdot 10^{-10}$	[170]
La	$2.69 \cdot 10^{-11}$	[81]
Nd	$2.58 \cdot 10^{-11}$	[81]
Ce	$1.84 \cdot 10^{-11}$	[81]
Dy	$1.01 \cdot 10^{-11}$	[81]
Er	$8.88 \cdot 10^{-12}$	[81]
Gd	$8.43 \cdot 10^{-12}$	[81]
Yb	$8.05 \cdot 10^{-12}$	[81]
Sm	$5.47 \cdot 10^{-12}$	[81]
Pr	$4.99 \cdot 10^{-12}$	[81]
Ho	$2.71 \cdot 10^{-12}$	[81]
Eu	$1.66 \cdot 10^{-12}$	[81]
Tb	$1.57 \cdot 10^{-12}$	[81]
Tm	$1.19 \cdot 10^{-12}$	[81]
Lu	$1.17 \cdot 10^{-12}$	[81]

Tab. 9: Mediterranean Sea water composition.

In Tab. 10, instead, is reported the composition of the artificial seawater prepared in the lab. Only species present in concentration above 10^{-5} M was considered. As representative for the freshwater, a dilution 60:1 of the same solution was employed.

Salt	Concentration (M)
LiCl	$2.45 \cdot 10^{-5}$
NaF	$5.25 \cdot 10^{-5}$
$SrBr_2$	$4.56 \cdot 10^{-5}$
Na_2SO_4	$1.07 \cdot 10^{-2}$
$CaCl_2$	$1.03 \cdot 10^{-2}$
K_2SO_4	$1.02 \cdot 10^{-2}$
$NaHCO_3$	$2.38 \cdot 10^{-3}$
$MgCl_2$	$3.17 \cdot 10^{-2}$
H_3BO_3	$4.16 \cdot 10^{-4}$
NaBr	$4.12 \cdot 10^{-4}$
NaI	$3.20 \cdot 10^{-4}$
$NaNO_3$	$3.68 \cdot 10^{-5}$
NaCl	$2.58 \cdot 10^{-1}$

Tab. 10: Artificial seawater composition.

The electrodes used for testing the artificial seawater are the AC-$GONH_3$. An example of this CapMix measurement in reported in Fig. 65, in which 10 full cycles are shown.

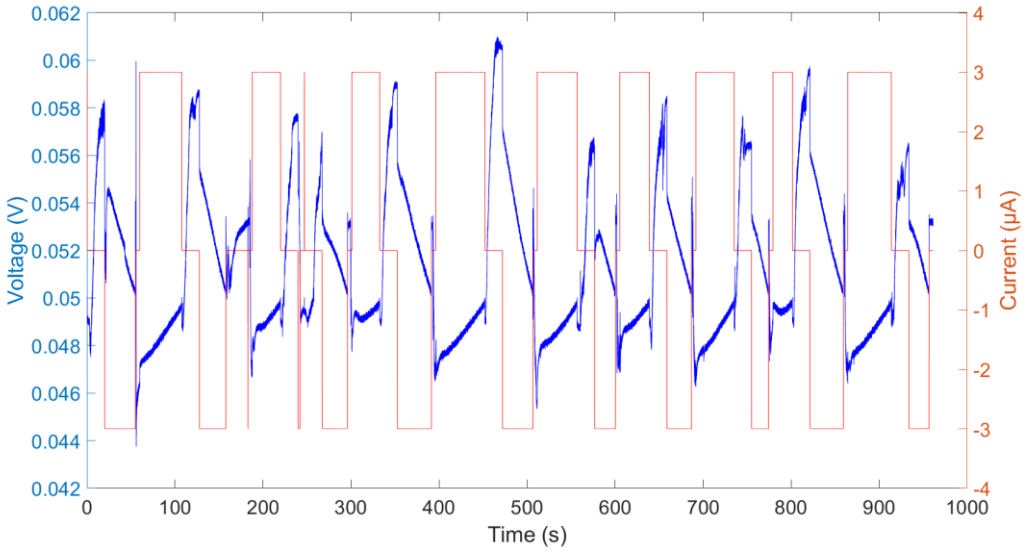

Fig. 65: Example of CapMix measurements on artificial seawater.

If comparing the voltage rise with the same bias in a pure solution of NaCl, it is immediately observed that with artificial seawater it's lower. Moreover, the cycles are very unstable. In Tab. 11 the results are reported.

Material	Bias (mV)	Gain (mV)	Harvested energy per cycle (mJ/m^2)	Harvested power per cycle (mW/m^2)
AC-$GONH_3$	50	9	29	0.31
AC-$GONH_3$	50	8	55	0.65
AC-$GONH_3$	100	14	0	0

Tab. 11: CapMix results with artificial seawater.

The power harvested is comparable to the one obtained with NaCl 0.6 M. However, due to the instability of the system, only 2 cycles over 10 provided a net amount of energy harvested. For all the others, there was no gain at all. Furthermore, going above a bias of 50 mV proved to be totally inefficient.

This last result shows how facing a real situation is always more complicated than a simplified, lab-scaled one. For this reason, it is first mandatory to find a solid and promising material before moving to study real-world applications.

6. Conclusions

This study showed how it is possible to design and characterize new materials for CDI and CapMix application starting from the very fundamentals. In particular, studies on the choice of the current collector and the type of the active material have been performed. Experimental procedures and details on the morphological, structural and electrochemical characterization have been provided.

For what concerns the CDI, the materials under tests showed a salt adsorption of 9 mg/g, in line with the literature, but not comparable to the state of the art. Actually, the best performing materials show an adsorption of tens of mg/g, thus being one order of magnitude higher than what reported in this study. However, the absence of a standardized method makes the comparison hard because many parameters come into play. The novelty of this study is linked to the investigation of materials that have never been reported in literature and to the high efficiency that has been obtained. Indeed, charge efficiency above 90% are usually obtained in presence of ion exchange membranes or small voltage windows. Improvement of the setup are required to achieve a salt adsorption comparable to the state of the art. However, it must be underlined that the top studies on this field describe active materials entirely made of 2D materials, thus being far from a large scale application, mainly due to the cost of the proposed materials.

For what concerns the CapMix, attempting to use a large voltage window to improve the output power proved to be unsuccessful. The presence of self-discharge was predominant and most of the effort has been spent to find a workaround for this issue. Following a path already proposed in literature by Brogioli et al., it was possible to reduce the impact of the this phenomenon, allowing to reach an output power of 4.6 mW/m^2. Comparing this value to what reported in literature, unfortunately this cannot be considered an advancement. This is mainly due to the absence of investigation on the spontaneous potential of these materials, which provides an instrument to minimize the energetic losses while strongly improve the yield of the electrochemical cycle. Initially planned following the studies of Brogioli et al., this step was not performed due to a lack of time. In this work, new materials have been tested and successfully employed for CapMix, proving that they can work. However, actually the best performing materials show an output power of tens of mW/m^2 for asymmetric devices working with a 0 V bias. Moving to the field of ion exchange membranes and mixing entropy batteries, hundreds of mW/m^2 has been reported. Therefore, further studies would be needed on the materials to achieve a result that can be comparable to the actual state of the art.

6.1 Future developments

The future developments will be in mainly two directions. On one side, keep looking for new active material to be tested, both for CDI and CapMix. The literature is an ever-growing scenario of new possibilities. Every year new and fancy materials are reported. Many of them would be good candidates for tests, from newly discovered 2D materials to more mature materials which are already undergoing the long road to large-scale production. In both cases, the aim would be finding materials offering high energetic efficiency, low losses and stability over time. Among them, depending on the application, would be selected the ones able to adsorb the highest amount of salt or the ones providing the higher voltage rise. Furthermore, the possibility of employing anion exchange membranes (totally absent in this study) will be investigated for both applications.

On the other side, this work laid the foundation for creating a performing device which can be used on large scale for CDI application to produce clean water, rather than CapMix application to harvest renewable energy. This thesis focused the attention only on finding performing active materials for the above-mentioned goals. From that moment on, it would be also necessary to investigate the setup.

For CDI, it would be mandatory to find a new geometry for the cell, to optimize the water flux among the electrodes while contemporarily reducing their distance. It is known, indeed, that shortening the distance between the electrodes can strongly improve the adsorption capability. This choice would also allow to lower the amount of water in the system and thus reducing the uncertainty on the salt adsorption calculation.

For CapMix, the main focus will be the investigation of the spontaneous potential of the materials here proposed. This investigation, together with the information collected during the thesis work, will allow to design a suitable electrochemical cycle exploiting the best performing materials and making them work the ideal situation, with all the parameters like bias, current, voltage rise, etc. been optimized. An improvement of at least one order of magnitude in the extracted power is expected, thus reaching the state of art of the CapMix. Another limitation to work was the absence of an automated system for the switching between freshwater and seawater. The scaling-up of the system would also benefit from increasing the area of the electrodes.

Finally, for both the technology, a new design of the electrodes will be investigated. Indeed, referring to the literature, the so-called wire/pillar architecture is attracting a lot of interest in the recent years. The wire-shaped electrodes seem to be very promising because of their increased surface area, compact design and reduced electrical resistance.

7. Acknowledgements

If you are now reading this chapter, I'm pretty sure you know I'm not the kind of man who likes manifesting his feelings. I'm more the kind of person who stands aside, watching everything from afar and talking only when asked to.

For this reason, I long debated if writing this section or not. As you can see, in the end I decided to do it, so here I am. However, I'll do it my own way. I won't make a list of names. I won't say thanks to each of you, listing what you've done for me. I think it's reductive. How can I thank a person for just one or few things?

During these years I've met a lot of people. Many just passed by, few remained. We all are the result of the equation that is combining the place we've visited, the people we've met and the choices we've taken.

There have been people who sustained me when I was discouraged, showing me that there is another way, even when everything seemed to go in the wrong direction.

There have been people who totally changed my life.

There have been people who taught me that alone I am strong, but together we are stronger.

There have been people whose journeys crossed mine for a short time, but left a permanent mark on my path.

There have been people who were with me when I was happy, making this happiness real.

There have been people who followed me, even when it seemed crazy, just because they trusted me.

There have been people who helped me out in my research activity, both making measurements or simply giving inputs for new ideas.

During these years, you had the possibility to face both my qualities and weaknesses. I don't pretend to be who I am not. But in the end, if I am who I am now, it's also thanks to you. Among the people I've mentioned above, you know who you are. I don't have to tell to anyone what you've done for me. It's just between you and me. If I am here and I've made it to the end, it's also because of you.

And you will know it, when passing by each other slowly, looking into the eyes without saying anything, but with a nod saying everything that needs to say.

This is for you.

Thank you.

8. References

[1] I. A. Shiklomanov, “World fresh water resources”, in *Water in Crisis: A Guide to the World's Fresh Water Resources*, New York, Peter Gleick, 1993, pp. 13-24.

[2] H. Zavadska, “CK-12 Foundation”, [Online]. Available: https://www.ck12.org/book/ck-12-earth-science-for-middle-school/section/13.1/. [Accessed 26 11 2020].

[3] M. A. Shannon, P. W. Bohn, M. Elimelech, J. G. Georgiadis, B. J. Marinas and A. M. Mayes, “Science and technology for water purification in the coming decades”, *Nature,* no. 452, pp. 301-310, 2008.

[4] M. R. Kebria and A. Rahimpour, “Membrane Distillation: Basics, Advances, and Applications”, in *Advances in Membrane Distillation*, 2020, p. 67.

[5] S. Porada, R. Zhao, A. van der Wal, V. Presser and P. M. Biesheuvel, “Review on the science and technology of water desalination by capacitive deionization”, *Progress in Material Science,* vol. 58, pp. 1388-1442, 2013.

[6] B. Jia and W. Zhang, “Preparation and Application of Electrodes in Capacitive Deionization (CDI): a State-of-Art Review”, *Nanoscale Research Letters,* no. 11, pp. 1-25, 2016.

[7] M. E. Suss, S. Porada, X. Sun, P. M. Biesheuvel, J. Yoon and V. Presser, “Water desalination via capacitive deionization: what is it and what can we expect from it?”, *Energy & Environmental Science,* no. 8, pp. 2296-2319, 2015.

[8] H. Cherif and J. Belhadji, “Environmental Life Cycle Analysis of Water Desalination Processes”, in *Sustainable Desalination Handbook*, 2018, pp. 527-559.

[9] S. Sorrell, “Reducing energy demand: A review of issues, challenges and approaches”, *Renewable and Sustainable Energy Reviews,* vol. 47, pp. 74-82, 2015.

[10] Z. Jia, B. Wang, S. Song and Y. Fan, “Blue energy: Current technologies for sustainable power generation from water salinity gradient”, *Renewable and Sustainable Energy Reviews,* vol. 31, pp. 91-100, 2014.

[11] A. Siria, M.-L. Bocquet and L. Bocquet, “New avenues for the large-scale harvesting of blue energy”, *Nature Reviews Chemistry,* vol. 1, p. 0091, 2017.

[12] BP p.l.c., “BP Statistical Review of World Energy”, 2019.

[13] H. Becker, “Low voltage electrolytic capacitor”. United States 23 07 1957.

[14] S. Kondrat, C. R. Perez, V. Presser, Y. Gogotsi and A. A. Kornyshev, “Effect of pore size and its dispersity on the energy storage in nanoporous supercapacitors”, *Energy & Environmental Science,* vol. 5, pp. 6474-6479, 2012.

[15] D. Ragone, “Review of Battery Systems for Electrically Powered Vehicles”, *SAE Technical Paper,* no. 680453, 1968.

[16] G. Z. Chen, “Supercapacitor and supercapattery as emerging electrochemical energy stores”, *International Materials Reviews,* vol. 62, pp. 173-202, 2016.

[17] J. O. Bockris, M. A. Devanathan and K. Muller, “On the structure of charged interfaces”, *Electrochemistry,* pp. 832-863, 1965.

[18] M. Okamura, Denki nijuso kyapashita to chikuden shisutemu, 2005.

[19] D. Brogioli, R. Ziano, R. A. Rica, D. Salerno and F. Mantegazza, “Capacitive mixing for the extraction of energy from salinity differences: Survey of experimental results and electrochemical models”, *Journal of Colloid and Interface Science,* vol. 407, pp. 457-466, 2013.

[20] T. Wu, G. Wang, F. Zhan, Q. Dong, Q. Ren, J. Wang and J. Qiu, “Surface-treated carbon electrodes with modified potential of zero charge for capacitive deionization”, *Water Research,* vol. 93, pp. 30-37, 2016.

[21] B. E. Conway, Electrochemical Supercapacitors: Scientific Fundamentals and Technological Applications, Springer, 2013.

[22] R. I. Kosheleva, A. C. Mitropoulos and G. Z. Kyzas, “Synthesis of activated carbon from food waste”, *Environmental Chemistry Letters,* vol. 17, pp. 429-438, 2019.

[23] A. Zabaniotou, D. Rovas, A. Libutti and M. Monteleone, “Boosting circular economy and closing the loop in agriculture: Case study of a small-scale pyrolysis–biochar based system integrated in an olive farm in symbiosis with an olive mill”, *Environmental Development,* vol. 14, pp. 22-36, 2015.

[24] F. Beck, M. Dolata, E. Grivei and N. Probst, “Electrochemical supercapacitors based on industrial carbon blacks in acqueous H2SO4”, *Journal of Applied Electrochemistry,* vol. 31, pp. 845-853, 2001.

[25] K. Yang, K. Cho and S. Kim, “Effect of carbon black addition on thermal stability and capacitive performances of supercapacitors”, *Scientific Reports,* vol. 8, p. 11989, 2018.

[26] F. Markoulidis, C. Lei, C. Lekakou, D. Duff, S. Khalil, B. Martorana and I. Cannavaro, “A method to increase the energy density of supercapacitor cells by the addition of multiwall carbon nanotubes into activated carbon electrodes”, *Carbon,* vol. 68, pp. 58-66, 2014.

[27] M. Toupin, D. Belanger, I. R. Hill and D. Quinn, “Performance of experimental carbon blacks in aqueous supercapacitors”, *Journal of Power Sources,* vol. 140, pp. 203-210, 2005.

[28] W. Yang and C. Wang, “Graphene and the related conductive inks for flexible electronics”, *Journal of Materials Chemistry C,* vol. 4, pp. 7193-7207, 2016.

[29] P. Sun, K. Wang and H. Zhu, “Recent Developments in Graphene-Based Membranes: Structure, Mass-Transport Mechanism and Potential Applications”, *Advanced Materials,* vol. 28, pp. 2287-2310, 2016.

[30] A. Gigot, M. Fontana, M. Serrapede, M. Castellino, S. Bianco, M. Armandi, B. Bonelli, C. F. Pirri, E. Tresso and P. Rivolo, “Mixed 1T–2H Phase MoS2/Reduced Graphene Oxide as Active Electrode for Enhanced Supercapacitive Performance”, *ACS Applied Materials & Interfaces,* vol. 8, pp. 32842-32852, 2016.

[31] J. Yan, C. E. Ren, K. Maleski, C. B. Hatter, B. Anasori, P. Urbankowski, A. Sarycheva and Y. Gogotsi, “Flexible MXene/Graphene Films for Ultrafast Supercapacitors with Outstanding Volumetric Capacitance”, *Advanced Funtional Materials,* vol. 27, p. 1701264, 2017.

[32] B. Zhao, P. Liu, Y. Jiang, D. Pan, H. Tao, J. Song, T. Fang and W. Xu, “Supercapacitor performances of thermally reduced graphene oxide”, *Journal of Power Sources,* vol. 198, pp. 423-427, 2012.

[33] B. Song, F. Wu, Y. Zhu, Z. Hou, K.-s. Moon and C.-P. Wong, “Effect of polymer binders on graphene-based free-standing electrodes for supercapacitors”, *Electrochimica Acta,* vol. 267, pp. 213-221, 2018.

[34] P. Meares, “Transport in ion exchange membranes”, in *Synthetic Membranes: Science, Engineering and Applications*, 1986, pp. 169-179.

[35] T. Xu, “Ion exchange membranes: State of their development and perspective”, *Journal of Membrane Science,* vol. 263, pp. 1-29, 2005.

[36] W. Ostwald, “Elektrische Eigenschaften halbdurchlässiger Scheidewände”, *Zeitschrift für Physikalische Chemie,* vol. 6, p. 17, 1890.

[37] F. G. Donnan, “Theorie der Membrangleichgewichte und Membranpotentiale bei Vorhandensein von nicht dialysierenden Elektrolyten. Ein Beitrag zur physikalisch-chemischen Physiologie”, *Zeitschrift für Elektrochemie und Angewandte Physikalische Chemie,* vol. 17, pp. 572-581, 1911.

[38] L. Michaelis and A. Fujita, “The electric phenomen and ion permeability of membranes II. Permeability of apple peel”, *Biochemistry Z,* vol. 158, pp. 28-37, 1925.

[39] W. Grot, “Laminates of support material and fluorinated polymer containing pendant side chains containing sulfonyl groups”. United States 11 06 1973.

[40] Z. Yang, J. Ran, B. Wu, L. Wu and T. Xu, “Stability challenge in anion exchange membrane for fuel cells”, *Current Opinion in Chemical Engineering,* vol. 12, pp. 22-30, 2016.

[41] D. V. Golubenko, R. R. Shaydullin and A. B. Yaroslavtsev, “Improving the conductivity and permselectivity of ion-exchange membranes by introduction of inorganic oxide nanoparticles: impact of acid–base properties”, *Colloid and Polymer Science,* vol. 297, pp. 741-748, 2019.

[42] M. Vaselbehagh, H. Karkhanechi, S. Mulyati, R. Takagi and H. Matsuyama, “Improved antifouling of anion-exchange membrane by polydopamine coating in electrodialysis process”, *Desalination,* vol. 332, pp. 126-133, 2014.

[43] R. S. Yee, R. A. Rozendal, K. Zhang and B. P. Ladewig, “Cost effective cation exchange membranes: A review”, *Chemical Engineering Research and Design,* vol. 90, pp. 950-959, 2012.

[44] K. A. Mauritz and R. B. Moore, “State of Understanding of Nafion”, *Chemical Reviews,* vol. 104, pp. 4535-4585, 2004.

[45] C. Heitner-Wirguin, “Recent advances in perfluorinated ionomer membranes: structure, properties and applications”, *Journal of Membrane Science,* vol. 120, pp. 1-33, 1996.

[46] R. S. Yee, K. Zhang and B. P. Ladewig, “The Effects of Sulfonated Poly(ether ether ketone) Ion Exchange Preparation Conditions on Membrane Properties”, *Membranes,* vol. 3, pp. 182-195, 2013.

[47] T. W. Kim, M. Sahimi and T. T. Tsotsis, “Preparation and Characterization of Hybrid Hydrotalcite-Sulfonated Polyetheretherketone (SPEEK) Cation-Exchange Membranes”, *Industrial & Engineering Chemistry Research,* vol. 48, pp. 9504-9513, 2009.

[48] M. Sharma, H. Sharma and S. Shannigrahi, “Tribology of advanced composites/biocomposites materials”, in *Biomedical Composites*, 2017, pp. 413-429.

[49] S. He, Y. Lin, H. Ma, H. Jia, X. Liu and J. Lin, “Preparation of sulfonated poly(ether ether ketone) (SPEEK) membrane using ethanol/water mixed solvent”, *Materials Letters,* vol. 169, pp. 69-72, 2016.

[50] G. M. Geise, H. J. Cassady, D. R. Paul, B. E. Logan and M. A. Hickner, “Specific ion effects on membrane potential and the permselectivity of ion exchange membranes”, *Physical chemistry chemical physics,* vol. 16, pp. 21673-21681, 2014.

[51] J. R. Varcoe, J. P. Kizewski, D. M. Halepoto, S. D. Poynton, R. C. Slade and F. Zhao, “FUEL CELLS - ALKALINE FUEL CELLS | Anion-Exchange Membranes”, *Encyclopedia of Electrochemical Power Sources,* pp. 329-343, 2009.

[52] J. S. Kim, C. S. Kim, H. S. Shin and J. W. Rhim, “Application of Synthesized Anion and Cation Exchange Polymers to Membrane Capacitive Deionization (MCDI)”, *Macromolecular Research,* vol. 23, pp. 360-366, 2015.

[53] S. S. Hosseiny and M. Wessling, “Ion exchange membranes for vanadium redox flow batteries”, in *Advanced Membrane Science and Technology for Sustainable Energy and Environmental Applications*, 2011, pp. 413-434.

[54] K. Sollner, “Uber mosaikmembranen”, *Biochemistry Z,* vol. 244, p. 390, 1932.

[55] G. Pourcelly, “Electrodialysis with Bipolar Membranes: Principles, Optimization, and Applications”, *Russian Journal of Electrochemistry,* vol. 38, pp. 919-926, 2002.

[56] J. N. Weinstein, B. W. Misra, D. Kalif and S. R. Caplan, “Transport properties of charge-mosaic membranes. II. Experimental studies”, *Desalination,* vol. 12, p. 1, 1973.

[57] F. Yan, P. Dejardin and A. Schmitt, “Electrochemical characterization of a hemodialysis membrane”, *The Journal of Physical Chemistry,* vol. 97, pp. 3824-3828, 1993.

[58] R. E. Pattle, “Production of Electric Power by mixing Fresh and Salt Water in the Hydroelectric Pile”, *Nature,* vol. 174, p. 660, 1954.

[59] R. S. Norman, “Water Salination: A Source of Energy”, *Science,* vol. 186, pp. 350-352, 1974.

[60] D. Brogioli, R. Ziano, R. A. Rica, D. Salerno, O. Kozynchenko, H. Hamelers and F. Mantegazza, “Exploiting the spontaneous potential of the electrodes used in capacitve mixing technique for the extraction of energy from salinity difference”, *Energy & Environmental Science,* vol. 5, pp. 9870-9880, 2012.

[61] S. Loeb, “Method and apparatus for generating power utilizing pressure-retarded-osmosis”. US Patent US3906250A, 3 7 1975.

[62] S. Loeb and R. S. Norman, “Osmotic Power Plants”, *Science,* vol. 189, pp. 654-655, 1975.

[63] S. E. Skilhagen, J. E. Dugstad and R. J. Aaberg, “Osmotic power — power production based on the osmotic pressure difference between waters with varying salt gradients”, *Desalination,* vol. 220, pp. 476-482, 2008.

[64] A. Staalstrom and J. Gitmark, “Environmental impacts by running an osmotic power plant”, 2012.

[65] G. Han, S. Zhang, X. Li and T.-S. Chung, “Progress in pressure retarded osmosis (PRO) membranes for osmotic power generation”, *Progress in Polymer Science,* vol. 51, pp. 1-27, 2015.

[66] B. E. Logan and M. Elimelech, “Membrane-based processes for sustainable power generation using water”, *Nature,* vol. 488, pp. 313-319, 2012.

[67] F. Helfer, C. Lemckert and Y. G. Anissimov, “Osmotic power with Pressure Retarded Osmosis: Theory, performance and trends – a review”, *Journal of Membrane Science,* vol. 453, pp. 337-358, 2014.

[68] F. Dinger, T. Trondle and U. Platt, “Optimization of the Energy Output of Osmotic Power Plants”, *Journal or Renewable Energy,* pp. 1-7, 2013.

[69] K. L. Lee, R. W. Baker and H. K. Lonsdale, “Membranes for power generation by pressure-retarded osmosis”, *Journal of Membrane Science,* vol. 8, pp. 141-171, 1981.

[70] X. Li, G. Han and T. S. Chung, “Membrane Development for Pressure-Retarded Osmosis”, in *Forward Osmosis*, 2015, pp. 465-490.

[71] M. M. Abu-Khader, “Viable engineering options to enhance the NaCl quality from the Dead Sea in Jordan”, *Journal of Cleaner Production,* vol. 14, pp. 80-86, 2006.

[72] J. Kleverud, S. E. Skilhagen and G. Brekke, “Experiences with the Tofte prototype plant”, in *3rd Osmosis Membrane Summit*, Barcelona, 2012.

[73] R. L. Stover, “Development of a fourth generation energy recovery device. A 'CTO's Notebook'“, *Desalination,* vol. 165, pp. 313-321, 2004.

[74] S. E. Skilhagen and R. J. Aaberg, “Power production based on the osmotic pressure difference between fresh water and sea water”, in *European Seminar on Offshore Wind and Other Marine Renewable Energies in Mediterranean and European Seas*, Civitavecchia, 2006.

[75] S. Loeb, “Method and apparatus for generating power utilizing reverse electrodialysis”. US Patent US4171409A, 25 2 1979.

[76] A. Cipollina, G. Micale, A. Tamburini, M. Tedesco, L. Gurreri, J. Veerman and S. Grasman, “Reverse electrodialysis: Applications”, in *Sustainable Energy from Salinity Gradients*, Elsevier, 2016, pp. 135-180.

[77] M. Tedesco, C. Scalici, D. Vaccari, A. Cipollina, A. Tamburini and G. Micale, “Performance of thefirst reverse electrodialysis pilot plant for power production from saline waters and concentrated brines”, *Journal of Membrane Science,* vol. 500, pp. 33-45, 2016.

[78] M. Tedesco, A. Cipollina, A. Tamburini and G. Micale, “Towards 1 kW power production in a reverse electrodialysis pilot plant with saline waters and concentrated brines”, *Journal of Membrane Science,* vol. 522, pp. 226-236, 2017.

[79] A. H. Avci, R. A. Tufa, E. Fontananova, G. Di Profio and E. Curcio, “Reverse Electrodialysis for energy production from natural river water and seawater”, *Energy,* vol. 165, pp. 512-521, 2018.

[80] M. M. Salama, S. K. El Ebaidi and D. P. Stickley, “WATER CHEMICAL ANALYSIS FOR DIFFERENT STAGES IN TOBRUK DESALINATION PLANT”, in *13th International Conference on Materials Science and its Applications in Oil and Gas Industries*, Benghazi, 2013.

[81] P. Censi, S. Mazzola, M. Sprovieri, A. Bonanno, B. Patti, R. Punturo, S. E. Spoto, F. Saiano and G. Alonzo, “Rare earth elements distribution in seawater and suspended particulate of the Central Mediterranean Sea”, *Chemistry and Ecology,* vol. 20, pp. 323-343, 2004.

[82] T. Chakrabarty, M. Kumar, K. P. Rajesh, V. K. Shahi and T. S. Natarajan, “Nano-fibrous sulfonated poly(ether ether ketone) membrane for selective electro-transport of ions”, *Separation and Purification Technology,* vol. 75, pp. 174-182, 2010.

[83] T. Rijnaarts, J. Moreno, M. Saakes, W. M. de Vos and K. Nijmeijer, “Role of anion exchange membrane fouling in reverse electrodialysis using natural feed waters”, *Colloids and Surfaces A: Physicochemical and Engineering Aspects,* vol. 560, pp. 198-204, 2019.

[84] J. L. Di Salvo, A. Cosenza, A. Tamburini, G. Micale and A. Cipollina, “Long-run operation of a reverse electrodialysis system fed with wastewaters”, *Journal of Environmental Management,* vol. 217, pp. 871-887, 2018.

[85] D.-E. Kim, Y. Oh, C.-H. Song, S. Chae and C.-S. Kim, “Fouling Behavior of Negatively Charged Natural Organic Matters to Anion Exchange Membranes in Reverse Electrodialysis”, in *ECS Meeting Abstracts*, 2016.

[86] D. A. Vermaas, D. Kunteng, M. Saakes and K. Nijmeijer, “Fouling in reverse electrodialysis under natural conditions”, *Water Research,* vol. 47, pp. 1289-1298, 2013.

[87] J. W. Post, *Blue energy: electricity production from salinity gradients by reverse electrodialysis,* 2009.

[88] J. W. Post, H. V. Hamelers and C. J. Buisman, “Influence of multivalent ions on power production from mixing salt and freshwater with a reverse electrodialysis system”, *Journal of Membrane Science,* vol. 330, pp. 65-72, 2008.

[89] J. Veerman, M. Saakes, S. J. Metz and G. J. Harmsen, “Reverse electrodialysis: evaluation of suitable electrode systems”, *Journal of Applied Electrochemistry,* vol. 40, pp. 1461-1474, 2010.

[90] Y. Fu, X. Guo, Y. Wang, X. Wang and J. Xue, “An atomically-thin graphene reverse electrodialysis system for efficient energy harvesting from salinity gradient”, *Nano Energy,* vol. 57, pp. 783-790, 2019.

[91] J. Feng, M. Graf, K. Liu, D. Ovchinnikov, D. Dumcenco, M. Heiranian, V. Nandigana, N. R. Aluru, A. Kis and A. Radenovic, “Single-layer MoS2 nanopores as nanopower generators”, *Nature,* vol. 536, pp. 197-200, 2016.

[92] J. Ji, Q. Kang, Y. Zhou, Y. Feng, X. Chen, J. Yuan, W. Guo, Y. Wei and L. Jiang, “Osmotic Power Generation with Positively and Negatively Charged 2D Nanofluidic Membrane Pairs”, *Advanced Funtional Materials,* vol. 27, p. 1603623, 2016.

[93] D. A. Vermaas, S. Bajracharya, B. B. Sales, M. Saakes, B. Hamelers and K. Nijmeijer, “Clean energy generation using capacitive electrodes in reverse electrodialysis”, *Energy & Environmental Science,* vol. 6, pp. 643-651, 2013.

[94] S. Kim, H. Wang and Y. M. Lee, “2D Nanosheets and Their Composite Membranes for Water, Gas, and Ion Separation”, *Angewandte Chemie Internation Edition,* vol. 58, pp. 17512-17527, 2019.

[95] T. Hyun, J. Jeong, A. Chae, Y. K. Kim and D.-Y. Koh, “2D-enabled membranes: materials and beyond”, *BMC Chemical Engineering,* vol. 1, p. 2418, 2019.

[96] M. Tedesco, E. Brauns, A. Cipollina, G. Micale, P. Modica, G. Russo and J. Helsen, “Reverse electrodialysis with saline waters and concentrated brines: A laboratory investigation towards technology scale-up”, *Journal of Membrane Science,* vol. 492, pp. 9-20, 2015.

[97] D. Brogioli, “Extracting Renewable Energy from a Salinity Difference Using a Capacitor”, *Physical review letters,* vol. 103, pp. 1-4, 2009.

[98] M. Faraday, Experimental Researches in Electricity, 1844.

[99] J. W. Gibbs, “A Method of Geometrical Representation of the Thermodynamic Properties of Substances by Means of Surfaces”, *ransactions of the Connecticut Academy of Arts and Sciences,* vol. 2, pp. 382-404, 1873.

[100] F. La Mantia, M. Pasta and D. Brogioli, “Capacitive Mixing and Mixing Entropy Battery”, in *Sustainable Energy from Salinity Gradients*, 2016, pp. 1-48.

[101] D. Brogioli, R. Zhao and P. M. Biesheuvel, “A prototype cell for extracting energy from a water salinity difference by means of double layer expansion in nanoporous carbon electrdes”, *Energy & Environmental Science,* vol. 4, pp. 772-777, 2011.

[102] S. Ahualli, M. L. Jiménez, M. M. Fernandez, G. Iglesias, D. Brogioli and A. V. Delgado, “Polyelectrolyte-coated carbons used in the generation of blue energy from salinity differences”, *Physical Chemistry Chemical Physics,* vol. 16, pp. 25241-25246, 2014.

[103] O. Burheim, B. B. Sales, O. Schaetzle, F. Liu and H. V. Hamelers, “Auto Generative Capacitive Mixing for Power Conversion of Sea and River Water by the Use of Membranes”, *Journal of Energy Resources Technology,* vol. 135, p. 011610, 2012.

[104] B. B. Sales, M. Saakes, J. W. Post, C. J. Buisman, P. M. Biesheuvel and H. V. Hamelers, “Direct Power Production from a Water Salinity Difference in a Membrane-Modified Supercapacitor Flow Cell”, *Environmental Science & Technology,* vol. 44, pp. 5661-5665, 2010.

[105] S. Porada, D. Weingarth, H. V. Hamelers, M. Bryjak, V. Presser and P. M. Biesheuvel, “Carbon flow electrodes for continuous operation of capacitive deionization and capacitive mixing energy generation”, *Journal of Material Chemistry A,* vol. 2, pp. 9313-9321, 2014.

[106] M. Janssen, A. Hartel and R. Roij, “Boosting Capacitive Blue-Energy and Desalination Devices with Waste Heat”, *Physical Review Letters,* vol. 113, p. 269501, 2014.

[107] F. La Mantia, M. Pasta, H. D. Deshazer, B. E. Logan and Y. Cui, “Batteries for Efficient Energy Extraction from a Water Salinity Difference”, *Nano letters,* vol. 11, pp. 1810-1813, 2011.

[108] M. Ye, M. Pasta, X. Xie, Y. Cui and C. S. Criddle, “Performance of a mixing entropy battery alternately flushed with wastewater effluent and seawater for recovery of salinity-gradient energy”, *Energy & Environmental Science,* vol. 7, pp. 2295-2300, 2014.

[109] Z. Jia, B. Wang, S. Song and Y. Fan, “A membrane-less Na ion battery-based CAPMIX cell for energy extraction using water salinity gradients”, *RSC Advances,* vol. 3, pp. 26205-26209, 2013.

[110] S. H. Tehrani, S. A. Seyedsadjadi and A. Ghaffarinejad, “Application of electrodeposited cobalt hexacyanoferrate film to extract energy from water salinity gradients”, *RSC Advances,* vol. 5, pp. 30032-30037, 2015.

[111] W. J. Gomes, C. d. Oliveira and F. Huguenin, “Energy Harvesting by Nickel Prussian Blue Analogue Electrode in Neutralization and Mixing Entropy Batteries”, *Langmuir,* vol. 31, pp. 8710-8717, 2015.

[112] M. Ye, M. Pasta, X. Xie, K. L. Dubrawski, J. Xu, C. Liu, Y. Cui and C. S. Criddle, “Charge-Free Mixing Entropy Battery Enabled by Low-Cost Electrode Materials”, *ACS Omega,* vol. 4, pp. 11785-11790, 2019.

[113] J. W. Blair and G. W. Murphy, “Electrochemical Demineralization of Water with Porous Electrodes of Large Surface Area”, *Saline Water Conversion,* vol. 27, p. 206, 1960.

[114] G. W. Murphy and D. D. Caudle, “Mathematical theory of electrochemical demineralization in flowing systems”, *Electrochimica Acta,* vol. 12, p. 1655, 1967.

[115] G. W. Reid, “Field operation of a 20 gallons per day pilot plant unit for electrochemical desalination of brackish water”, *Washington D.C.: U.S. Dept. of the Interior,* vol. 239, pp. 1-38, 1968.

[116] S. Evans, M. A. Accomazzo and J. E. Accomazzo, “Electrochemically Controlled Ion Exchange”, *Journal of the Electrochemical Society,* vol. 116, p. 307, 1969.

[117] A. M. Johnson and J. Newman, “Desalting by Means of Porous Carbon Electrodes”, *Journal of the Electrochemical Society,* vol. 118, p. 510, 1971.

[118] Y. Oren and A. Soffer, “Electrochemical Parametric Pumping”, *Journal of the Electrochemical Society,* vol. 125, p. 869, 1978.

[119] C.-L. Yeh, H.-C. Hsi, K.-C. Li and C.-H. Hou, “Improved performance in capacitive deionization of activated carbon electrodes with a tunable mesopore and microscope ratio”, *Desalination,* vol. 367, pp. 60-68, 2015.

[120] J. C. Farmer, D. V. Fix, G. V. Mack, R. W. Pekala and J. F. Poco, “The Use of Capacitive Deionization with Carbon Aerogel Electrodes to Remove Inorganic Contaminants from Water”, in *Low Level Waste Conference*, Orlando, 1995.

[121] M. Bhadra, S. Roy and S. Mitra, “Enhanced desalination using carboxylated carbon nanotube immobilized membranes”, *Separation and Purification Technology,* vol. 120, pp. 373-377, 2013.

[122] D. J. Johnson and N. Hilal, “Can graphene and graphene oxide materials revolutionise desalination processes?”, *Desalination,* vol. 500, p. 114852, 2021.

[123] T. Wajima, T. Shimizu, T. Yamato and Y. Ikegami, “Removal of NaCl from seawater using natural zeolite”, *Toxicological & Environmental Chemistry,* vol. 92, pp. 21-26, 2009.

[124] R. McNair, G. Szekely and R. A. Dryfe, “Ion-Exchange Materials for Membrane Capacitive Deionization”, *ACS ES&T Water,* 2020.

[125] Jedykstra, “Wikipedia”, 2 August 2013. [Online]. Available: https://en.wikipedia.org/wiki/Capacitive_deionization. [Accessed 10 January 2021].

[126] M. A. Ahmed and S. Tewari, “Capacitive deionization: Process, materials and state of the technology”, *Journal of Electroanalytical Chemistry,* vol. 813, pp. 178-192, 2018.

[127] J.-H. Choi, “Comparison of constant voltage (CV) and constant current (CC) operation in the membrane capacitive deionisation process”, *Desalination and Water Treatment,* vol. 56, pp. 921-928, 2015.

[128] Y. Zhao, Y. Wang, R. Wang, Y. Wu, S. Xu and J. Wang, “Performance comparison and energy consumption analysis of capacitive deionization and membrane capacitive deionization processes”, *Desalination,* vol. 324, pp. 127-133, 2013.

[129] Y.-J. Kim and J.-H. Choi, “Enhanced desalination efficiency in capacitive deionization with an ion-selective membrane”, *Separation and Purification Technology,* vol. 71, pp. 70-75, 2010.

[130] X. Zhang and D. Reible, “Exploring the Function of Ion-Exchange Membrane in Membrane Capacitive Deionization via a Fully Coupled Two-Dimensional Process Model”, *Processes,* vol. 8, p. 1312, 2020.

[131] M. E. Remillard, A. N. Shocron, J. Rahill, M. E. Suss and C. D. Vecitis, “A direct comparison of flow-by and flow-thruogh capacitive deionization”, *Desalination,* vol. 444, pp. 169-177, 2018.

[132] C. He, J. Ma, C. Zhang, J. Song and D. T. Waite, “Short-Circuited Closed-Cycle Operation of Flow-Electrode CDI for Brackish Water Softening”, *Environmental Science & Technology,* vol. 52, pp. 9350-9360, 2018.

[133] S.-i. Jeon, H.-r. Park, J.-g. Yeo, S. C. Yang, C. H. Cho, M. H. Han and D. K. Kim, “Desalination via a new membrane capacitive deionization process utilizing flow-electrodes”, *Energy & Environmental Science,* vol. 6, pp. 1471-1475, 2013.

[134] American Membrane Technology Association, “Membrane Desalination Power Usage Put in Perspective”, Stuart, Florida, 2016.

[135] M. A. Anderson, A. L. Cudero and J. Palma, “Capacitive deionization as an electrochemical means of saving energy and delivering clean water. Comparison to present desalination practices: Will it compete?”, *Electrochimica Acta,* vol. 55, pp. 3845-3856, 2010.

[136] P. Xu, J. E. Drewes, D. Heil and G. Wang, “Treatment of brackish produced water using carbon aerogel-based capacitive deionization technology”, *Water Research,* vol. 42, pp. 2605-2617, 2008.

[137] R. Borsani and S. Rebagliati, “Fundamentals and costing of MSF desalination plants and comparison with other technologies”, *Desalination,* vol. 182, pp. 29-37, 2005.

[138] J. C. Farmer, “Method and apparatus for capacitive deionization and electrochemical purification and regeneration of electrodes”. United States Patent US5954937A, 20 5 1994.

[139] J. P. Sullivan, “Method of operating a capacitive deionization cell using gentle charge”. Europe Patent EP2373587B1, 11 9 2009.

[140] C.-H. Kim, H.-r. Kang, H.-J. Yang and H.-s. Kim, “Capacitive deionization device”. United States Patent US8557098B2, 13 8 2010.

[141] S. Porada, L. Zhang and J. E. Dykstra, “Energy consumption in membrane capacitive deionization and comparison with reverse osmosis”, *Desalination,* vol. 488, p. 114383, 2020.

[142] Y.-Y. Shen, S.-H. Sun, S.-W. Tsai, T.-H. Chen and C.-H. Hou, “Development of a membrane capacitive deionization stack for domestic wastewater reclamation: A pilot-scale feasibility study”, *Desalination,* vol. 500, p. 114851, 2021.

[143] W. D. Schepper, C. Vanschepdael, H. Huynh and J. Helsen, “Membrane Capacitive Deionization for Cooling Water Intake Reduction in Thermal Power Plants: Lab to Pilot Scale Evaluation”, *Energies,* vol. 13, p. 1305, 2020.

[144] C. Huyskens, J. Helsen, W. J. Groot and A. B. Haan, “Cost evaluation of large-scale membrane capacitive deionization for biomass hydrolysate desalination”, *Separation and Purification Technology,* vol. 146, pp. 294-300, 2015.

[145] J. Nordstrand and J. Dutta, “Design principles for enhanced up-scaling of flow-through capacitive deionization for water desalination”, *Desalination,* vol. 500, p. 114842, 2021.

[146] F. Ahmad, S. J. Khan, Y. Jamal, H. Kamran, A. Ahsan, M. Ahmad and A. Khan, “Desalination of brackish water using capacitive deionization (CDI) technology”, *Desalination and Water Treatment,* vol. 57, pp. 7659-7666, 2016.

[147] D. I. Kim, P. Dorji, G. Gwak, S. Phuntsho, S. Hong and H. Shon, “Reuse of municipal wastewater via membrane capacitive deionization using ion-selective polymer-coated carbon electrodes in pilot-scale”, *Chemical Engineering Journal,* vol. 372, pp. 241-250, 2019.

[148] C. Tan, C. He, W. Tang, P. Kovalsky, J. Fletcher and D. T. Waite, “Integration of photovoltaic energy supply with membrane capacitive deionization (MCDI) for salt removal from brackish waters”, *Water Research,* vol. 147, pp. 276-286, 2018.

[149] J. J. Lado, C. Santos, E. G. Quismondo, M. A. Anderson, B. Gutierrez, F. Huertas, A. Ordonez and A. d. Miguel, “Singular Applications of Capacitive Deionization: Reduction of the Brine Volume from Brackish Water Reverse Osmosis Plants”, in *Frontiers in Water-Energy-Nexus—Nature-Based Solutions, Advanced Technologies and Best Practices for Environmental Sustainability*, Springer, 2018, pp. 429-431.

[150] V. Flexer, C. F. Baspineiro and C. I. Galli, “Lithium recovery from brines: A vital raw material for green energies with a potential environmental impact in its mining and processing”, *Science of The Total Environment,* vol. 639, pp. 1188-1204, 2018.

[151] E. G. Quismondo, C. Santos, J. Soria, J. Palma and M. A. Anderson, “New Operational Modes to Increase Energy Efficiency in Capacitive Deionization Systems”, *Environmental Science & Technology,* vol. 50, pp. 6053-6060, 2016.

[152] C. Santos, J. J. Lado, E. G. Quasimodo, I. V. Rodriguez, D. H. Benito, J. Palma, M. A. Anderson and J. J. Vilatela, “Interconnected metal oxide CNT fibre hybrid networks for current collector-free asymmetric capacitive deionization”, *Journal of Materials Chemistry A,* vol. 6, pp. 10898-10908, 2018.

[153] C. Santos, I. V. Rodriguez, J. J. Lado, M. Vila, E. G. Quasimodo, M. A. Anderson, J. Palma and J. J. Vilatela, “Low-energy consumption, free-form capacitive deionisation through nanostructured networks”, *Carbon,* 2021.

[154] J. Oladunni, J. H. Zain, A. Hai, F. Banat, G. Bharath and E. Alhseinat, “A comprehensive review on recently developed carbon based nanocomposites for capacitive deionization: From theory to practice”, *Separation and Purification Technology,* vol. 207, pp. 291-320, 2018.

[155] M. A. Luciano, H. Ribeiro, G. E. Bruch and G. G. Silva, “Efficiency of capacitive deionization using carbon materials based electrodes for water desalination”, *Journal of Electroanalytical Chemistry,* vol. 859, p. 113840, 2020.

[156] S. A. Hawks, A. Ramachandran, S. Porada, P. G. Campbell, M. E. Suss, P. M. Biesheuvel, J. G. Santiago and M. Stadermann, “Performance metrics for the objective assessment of capacitive deionization systems”, *Water Research,* vol. 152, pp. 126-137, 2019.

[157] J. Ge, H.-B. Yao, W. Hu, X.-F. Yu, Y.-X. Yan, L.-B. Mao, H.-H. Li, S.-S. Li and S.-H. Yu, “Facile dip coating processed graphene/MnO2 nanostructured sponges as high performance supercapacitor electrodes”, *Nano Energy,* vol. 2, pp. 505-513, 2013.

[158] Y. Guo, W. Li, H. Yu, D. Perepichka and H. Meng, “Flexible Asymmetric Supercapacitors via Spray Coating of a New Electrochromic Donor-Acceptor Polymer”, *Advanced Energy Material,* vol. 7, pp. 1-7, 2016.

[159] K. M. Ajay, M. N. Dinesh, K. A. Murthy, C. R. Ravikumar and H. P. Nagaswarupa, “Deposition & Electrochemical characterization of Multilayer coated electrode material for super capacitor application”, *materialstoday: PROCEEDINGS,* vol. 5, pp. 21452-21457, 2018.

[160] T. Cheng, Y.-Z. Zhang, J.-D. Zhang, W.-L. Lai and W. Huang, “High-performance free-standing PEDOT:PSS electrodes for flexible and transparent all-solid-state supercapacitors”, *Journal of Materials Chemistry A,* vol. 4, pp. 10493-10499, 2016.

[161] Y. Xu, M. G. Schwab, A. J. Strudwick, I. Hennig, X. Feng, Z. Wu and K. Mullen, “Screen-Printable Thin Film Supercapacitor Device Utilizing Graphene/Polyaniline Inks”, *Advanced Energy Materials,* vol. 3, pp. 1035-1040, 2013.

[162] I. Roppolo, A. Chiappone, K. Bejtka, E. Celasco, A. Chiodoni, F. Giorgis, M. Sangermano and S. Porro, “A powerful tool for graphene functionalization: Benzophenone mediated UV-grafting”, *Carbon,* no. 77, pp. 226-235, 2014.

[163] M. Naguib, O. Mashtalir, J. Carle, V. Presser, J. Lu, L. Hultman, Y. Gogotsi and M. W. Barsoum, “Two-Dimensional Transition Metal Carbides”, *ACS Nano,* vol. 6, pp. 1322-1331, 2012.

[164] Y. Deng, E. Peng, Y. Shao, Z. Xiao, Q. Dong and J. Huang, “Scalable fabrication of efficient organolead trihalide perovskite solar cells with doctor-bladed active layers”, *Energy & Environmental Science,* vol. 8, pp. 1544-1550, 2015.

[165] A. Sacco, D. Pugliese, A. Lamberti, M. Castellino, A. Chiodoni, A. Virga and S. Bianco, “A long-term analysisof Pt counter electrodes for Dye-sensitized Solar Cells exploiting a microfluidic housing system”, *Materials Chemistry and Physics,* vol. 161, pp. 74-83, 2015.

[166] A. Gholampour, M. V. Kiamahalleh, D. N. H. Tran, T. Ozbakkaloglu and D. Losic, “From Graphene Oxide to Reduced Graphene Oxide: Impact on the Physiochemical and Mechanical Properties of Graphene–Cement Composites”, *ACS Applied Materials & Interfaces,* vol. 49, no. 9, pp. 43275-43286, 2017.

[167] X. Zhao, H. Wei, H. Zhao, Y. Wang and N. Tang, “Electrode materials for capacitive deionization: A review”, *Journal of Electroanalytical Chemistry,* vol. 873, p. 114416, 2020.

[168] R. Zhao, P. M. Biesheuvel and A. van der Wal, “Energy consumption and constant current operation in membrane capacitive deionization”, *Energy & Environmental Science,* vol. 5, pp. 9520-9527, 2012.

[169] T. I. Shaw and L. H. Cooper, “State of Iodine in Sea Water”, *Nature,* vol. 180, p. 250, 1957.

[170] N. Koron, J. Faganeli, I. Falnoga, D. Mazej, K. Klun and N. Kovac, “Association of macroaggregates and metals in coastal waters”, *Marine Chemistry,* vol. 157, pp. 185-193, 2013.

[171] F. Scholz, C. Hensen, G. J. De Lange, M. Haeckel, V. Liebetrau, A. Meixner, A. Reitz and R. L. Romer, “Lithium isotope geochemistry of marine pore waters - Insights from cold seep fluids”, *Geochimica et Cosmochimica Acta,* vol. 74, pp. 3459-3475, 2010.